DEVELOPMENT OF AN AUTOMATED MICROFLUIDIC DEVICE FOR HIGH-THROUGHPUT SINGLE CELL KINASE ANALYSIS

Amy Diane Hargis

A dissertation submitted to the faculty of the University of North Carolina at Chapel Hill in partial fulfillment of the requirements for the degree of Doctor of Philosophy in the Department of Chemistry

Chapel Hill
2010

Approved by:

Professor J. Michael Ramsey (Advisor)

Professor N.L. Allbritton (Chair)

Professor Gary Glish

Professor Matthew Redinbo

Professor Joseph Templeton

ABSTRACT

Amy D. Hargis

DEVELOPMENT OF AN AUTOMATED MICROFLUIDIC DEVICE FOR HIGH-THROUGHPUT SINGLE CELL KINASE ANALYSIS
(Under the direction of J. Michael Ramsey)

In this work, development of a microfluidic device to perform high-throughput single cell analysis is described. The objective is to be able to separate and detect the intracellular contents of hundreds of individual mammalian cells in a short time period. The current biological target is to assess kinase enzyme activity within single cells to study the role these enzymes play in intracellular signaling transduction pathways. Microfluidic devices are well-suited to address this type of high-throughput assay because of their ability to precisely manipulate the sub-picoliter volume contained within a mammalian cell and to achieve rapid electrophoretic separation of the cellular contents.

This dissertation describes continued development of a microfluidic network in which a constant stream of cells is pulled through an electric field. Once cells enter the electric field region, electrical cell lysis occurs and the resulting cell lysate is electrokinetically injected into a perpendicular separation channel. Electrophoretic separation of the intracellular contents then occurs. The development of this microfluidic device includes investigations into channel surface coatings to reduce cell adhesion and cellular debris buildup on the glass microfluidic channels, development of electrophoretic separation conditions for kinase substrate and product peptides, control of the cell flow through the lysis intersection to improve the lysate injection efficiency, assessment of the hydrodynamic flow

on the separation conditions and modifications to the channel network to increase the sample throughput.

A significant portion of this research also involved development of a new microfluidic network for high-throughput single cell analysis. The new device design utilizes a modified patch-clamp trapping method and is capable of rapidly trapping and lysing individual cells in succession. Development, unique fabrication aspects and implementation of automation to control cell flow on this device is described. Additionally, demonstration of data collection on both the new and older designs is demonstrated.

This work is dedicated to my parents,
Jackson and Kaye Hargis, for all of their love and support

ACKNOWLEDGEMENTS

There are many people to thank for their support and assistance in performing the work described. First of all, I would like to thank my advisor, Dr. Ramsey, for allowing me to work in his research group. Dr. Ramsey has been very supportive of trying new things and much of the progress was a result of this creative freedom. I also have to thank the entire Ramsey group, both current and former members, for all of their assistance in the laboratory. For the most part, I have worked on this project individually. Without the assistance, thoughtful discussions and guidance from my fellow group members, I would not have been able to accomplish much. Without a doubt, I have to thank J.P. Alarie for all of his help in pretty much every aspect of this project. J.P. helped keep all of the instruments running and helped me work through setting up experiments when I had no idea where to start.

I extend my gratitude to Dr. Nancy Allbritton, our collaborator on this project. Dr. Allbritton helped me understand the biological aspects of my project. She also was incredibly supportive and understanding of the difficulties associated with working with cells, which helped me get through some of the frustrating times. I also appreciate the help from members of Allbritton laboratory, especially Dr. Sumith Kottegoda and Dr. Chris Sims, for thoughtful discussions, materials and helpful information to guide my experiments.

Finally, I would like to thank all of my friends and family in Chapel Hill and beyond for supporting me during my time in graduate school. I could not have made it through

without the laughter and support. There is a world outside of this Chapman Hall basement laboratory and I am so grateful I had people to pull me out into it from time to time.

TABLE OF CONTENTS

LIST OF TABLES

LIST OF FIGURES

LIST OF ABBREVIATIONS AND SYMBOLS

A – analysis channel

AEPTMS - 3-[2-(2-Aminoethylamino)ethylamino]propyl-trimethoxysilane

APTES – aminopropyltriethoxysilane

BOE – buffered oxide etch

C-14 – 14 carbon chain

CF – cell flow channel

CMBA - chloromethylbenzoic acid

CMC – critical micelle concentration

CZE – capillary zone electrophoresis

DI – deionized

D_m – solute diffusion coefficient

E – electric field strength

e.g. – for example

ECB – extracellular buffer

EDTA – ethylenediaminetetraacetic acid

E-field – electric field

EOF- electroosmotic flow

EtOH – ethanol

F – focusing channel

FAM – carboxyfluorescein

FBS – fetal bovine serum, qualified

FIB – focused ion beam

GND - ground

HCl – hydrochloric acid

HEPES - 4-(2-hydroxyethyl)-1-piperazineethanesulfonic acid

HIV – human immunodeficiency virus

HV – high voltage

i.d. - inner diameter

i.e. – that is

kV – kilovolts

L_d – length of capillary to detector

LIF – laser induced fluorescence

LOD – limit of detection

LWD – long working distance

MEKC – micellar electrokinetic chromatography

MeOH – methanol

mm – micrometer

mM – millimolar

MOSFET – metal-oxide-semiconductor field-effect transistor

ms – microsecond

mW – milliwatt

Myr-SS-SPKC – myristoylated disulfide linked substrate for Protein Kinase C

N – theoretical plates

nA – nanoamperes

NaOH – sodium hydroxide

pA – picoamperes

PDMS – polydimethylsiloxane

PEG- polyethylene glycol

PEG-silane - 2-[methoxy(polyethyleneoxy)propyl]trimethoxysilane

PEG-SPA - polyethylene glycol succinimidylpropionate

PEG-urethane - N-(triethoxysilylpropyl)-O-poly(ethylene) oxide urethane

PKC – protein kinase C

psi – pound per square inch

PMT – photomultiplier tube

PSPKC – phosphorylated substrate peptide for protein kinase C

ROI - region of interest

RSD – relative standard deviation

S/N – signal-to-noise

S-1 – sphingosine

S-1-P – sphingosine-1-phosphate

SB – separation buffer channel

SDS – sodium dodecyl sulfate

SEM – scanning electron microscope

Ser – serine

SPKC – substrate peptide for protein kinase C

TAMRA – carboxytetramethylrhodamine, succinimidyl ester

TBE – 89 mM Tris, 89 mM boric acid, 2 mM EDTA buffer, pH 9.0

TCEP-HCl – Tris(2-carboxyethyl) phosphine hydrochloride

Tris/BA – 50 mM Tris, 10 mM boric acid buffer containing 30 mM PEG, 1 mM TCEP-HCl and 1 mM spermine

μ_{ep} – electrophoretic mobility

μM – micromolar

UV – ultraviolet

W – waste channel

Chapter 1: Introduction to Single Cell Analysis: History and Methods

1.1 The importance of studying cells one at a time

Cells are the fundamental building blocks of life. They are extremely complex systems, but not well-understood. Looking at an individual mammalian cell, the typical volume is only around one picoliter. Within this picoliter volume is a mixture of water, inorganic ions, small organic molecules, DNA, RNA and proteins all working together to create a functioning, living mechanism.[1-3] At any given moment there can be 10^3 to 10^4 chemical reactions, or more, occurring within a single eukaryotic cell to control cellular functions such as metabolism, growth, reproduction and apoptosis.[4-6] In addition to these complex intracellular workings, cells also partake in highly organized *inter*cellular communication with surrounding cells through chemical release and uptake. These intra- and inter-cellular chemical signals trigger and coordinate events within and amongst the cells.[7] Thus, as each cell functions as an individual unit, it also works in conjunction with a large number of cells to create an entire organism. We must study these intra- and inter-cellular signaling networks in order to understand basic physiology. By understanding the smallest piece of the puzzle, i.e., the cell, we can potentially predict the function of the whole organism.[8] Through better knowledge of how cells function, we are also better positioned to understand how and why cells *mal*function. Elucidating the complexity of the cell is the key to understanding diseases, both from a prevention and treatment standpoint, as well as to determine methods for earlier diagnostics.[9]

Each cell has a unique molecular, metabolic and proteomic identity.[8] Amongst cells of the same type, it has been widely observed that significant biochemical heterogeneity exists.[10-13] Cells identical in genetic make-up and appearance can differ in numerous characteristics including the concentration of metabolites or other intracellular compounds, the extent of gene expression and the response to a given stimulus.[1,14-18] The heterogeneity in intracellular contents demonstrates not only the natural state of a cell population but also reflects the history of the cells as environmental factors can pose a significant influence on cellular functions.[19] Because biological membranes are dynamic systems in a constant state of flux, external factors such as pH, ionic strength and temperature lead to some of these variations in intracellular contents.[1] Additionally, heterogeneity can arise from a number of other factors including localized damage, mutations, stages in the cell cycle, cell age and exposure to various external stimuli.[10,20] The complexity introduced by this heterogeneity makes it challenging to study and fully understand cellular processes and cellular response to stimuli.[7]

Typical studies to quantify intercellular metabolites or to observe cellular response to stimuli are performed as ensemble averages. Ensemble averaging methods simultaneously analyze a large number of cells and the resulting parameter measured is an average value from all of the cells.[21-23] The methods for these pooled studies mostly utilize well-plate screenings[24] and western blot techniques.[22] Western blotting has been the work-horse method for screening cellular responses and identifying, or quantitating, specific proteins and other analytes within the pooled cell lysates.[22] Both of these methods have been recognized as sufficient for general screenings; however, the information supplied by these methods cannot be extrapolated down to the single cell level.[7] The measured cellular contents and/or

cellular response to stimuli using averaging methods rarely provides accurate information and can often be highly misleading as to what is happening within a single cell of the population.[12,14] It is well-understood that the optimal means to understand cell-based systems is to study cells individually.[12] Recently, the interest in single cell analysis techniques has spiked as various technologies to perform single cell level studies have advanced.

In addition to understanding the chemical heterogeneity, single cell level analysis is required for a number of other reasons. For instance, many cellular reactions occur on such short timescales such that they cannot be effectively studied using population averaging techniques.[7,9,12,14] Additionally, many diseases start with a single abnormal cell.[9] Irregularities within a few cells amongst a population of healthy cells will be obscured in a traditional ensemble average study.[25] Small increases in ensemble averaging results do not allow the researcher to conclude whether the result is a homogenous response of all the cells within the sample or due to a significant change in just a subset of the population being studied. It has been demonstrated that in certain cancers, such as breast cancer, diseased cells can circulate individually through the blood stream of the patient in concentrations as low as 1 to 10 cells per million healthy cells.[1,26] By screening cells individually, it may become possible to detect abnormalities, leading to earlier diagnosis for the patient.[14,27] Earlier detection capabilities generally lead to increased patient longevity post-diagnosis.[28] In addition to the aforementioned advantages, single cell analysis also allows for better understanding of biochemical processes such as carcinogenesis and embryogenesis.[4,10,29] It also provides a means for analysis of heterogeneous samples such as patient blood, liver or lymph node samples gathered in the clinic.[30]

1.2 History of single cell analysis methods

The progression of single cell analysis technology has taken place over the last 60 years and, today, there are numerous methods in which single cell data can be collected. As far back as the 1950s, proteins and lipids within an individual cell could be monitored using techniques such as X-ray microradiography[31] and nucleic acids could be semi-quantified using ultraviolet spectroscopy.[32] The ability to perform truly quantitative chemical cytometry, or single cell analysis, was first reported in 1953 by J.E. Edstrom.[33] In his experiments, RNA was studied through ribonuclease digestion of individual nerve cells followed by a paper chromatography separation. The separated RNA was then quantified using UV spectrometry. In 1965, Matioli and Niewisch separated hemoglobin variants from individual erythrocytes using an electrophoretic method.[34] Single cell gel electrophoresis, commonly referred to as a comet assay, eventually became the convention for studying DNA damage within single cells in the 1970s.[35] Since that time, several other techniques have also been implemented for single cell analysis. Some of these techniques include open tubular liquid chromatography (OTLC)[36], gel electrophoresis[37], mass spectrometry (MS)[38], micro-thin-layer chromatography[39-40], electron microscopy[41], enzymatic radiolabeling[42] and fluorescence microscopy.[43-44] The main challenges encountered with these techniques for single cell level analysis include poor detection limits, inability to distinguish multiple cellular components simultaneously and/or poor quantitative capabilities.[15] The invention and development of capillary electrophoresis (CE) in the 1980s overcame many of the limitations encountered with these other techniques.[45-46]

The first reports of single cell analysis by microcolumn separation were in the late 80s by Kennedy and Jorgenson.[47-48] In this work, neurotransmitter compounds from

individual snail neuronal cells were separated and quantified using electrochemical and laser induced fluorescence (LIF) detection. The first reported analysis of a single mammalian cell was by Yeung's group in 1992. In Yeung's work, hemoglobin and carbonic anhydrase from human erythrocytes were separated by capillary zone electrophoresis (CZE) and detected using LIF.[15] Currently, some research groups, such as Arriaga's, have even been able to analyze individual cell organelles using CE with LIF detection.[49] CE methods for single cell analysis have found many uses for detecting and quantitating cellular analytes and several recent reviews have been published on this work.[1-2,14,28,50-52]

The procedure for separating intracellular compounds by CE, also referred to as chemical cytometry[53-54], is performed using one of two methods. The first method involves injection of the whole cell into the capillary, followed by immediate lysis of that cell and electrophoretic separation of the contents.[29,52,55-56] Alternatively, the cell can be lysed just outside of the capillary with immediate injection of the lysate into the capillary for analysis.[12,14] Because of the small inner diameter of the capillary, CE techniques are capable of sampling the small volumes found within a cell and, depending on the injection technique, will not significantly dilute the cell volume post-lysis.[3] Many lysate analytes can be separated using CE owing to the high separation efficiency that can be achieved.[2,19,57] The ability to separate multiple analytes can provide more information compared to microscopy methods. Finally, the development of highly sensitive detection techniques, such as LIF and electrochemical methods, has allowed for the quantification of many low-copy number intracellular analytes.[25,58] To date, there is extensive literature describing the analysis of single cells by CE.[2,12,50,59-60]

Although CE is an elegant technique for analyzing the contents of an individual cell, there are several drawbacks that limit its capabilities and the amount of data that can be collected. First, cell lysis and lysate injection techniques are problematic. The demonstrated techniques are not highly reproducible and can be time-consuming.[1-2,9,13-16,19,25,57-58] These labor intensive methods limit the throughput capabilities. Single cell experiments should ideally involve the analysis of a large number of cells (e.g., >1000) due to the inherent variability associated with biological samples. But, the collection of large data sets in a reasonable time frame is not feasible using CE-based methods.[1,17,19,56] The reported throughputs for CE analysis of cells range from 10-40 cells per day maximum.[1,16,52,56] Additionally, the long separation times frequently required by traditional CE systems also inhibit the throughput capabilities.[16-17,61-62] Although high-throughput single cell analysis by CE has been demonstrated for very simple systems, e.g., analysis of erythrocytes, it has not been well-established for complex mammalian cell analysis.[25]

Collection of high-throughput single cell data has been achieved using a technique called flow cytometry. Flow cytometry can be used to simultaneously quantify several cellular analytes from an intact cell.[59] The technique uses multiple fluorescent tags either loaded into the cell to label specific analytes or reacted on the outer membrane of the cell to target specific surface antigens. The prepared cells are then passed, single file, through a laser which excites the tags and allows for analyte detection. Because the cells are pulled rapidly through the laser beam, high-throughput analysis of individual cells can be achieved in a short period of time. Examples of recent single cell flow cytometry applications include determination of apoptosis, studying signaling transduction cascades and high-throughput

screening of stable cell lines.[63-67] Commercial flow cytometry instruments are available and are reported to provide throughputs of up to 70,000 cells per second.[64]

Although flow cytometry is highly sensitive and provides high-throughput analysis, there are limitations to the number of analytes that can be simultaneously detected from a single cell. First, each tag used must have unique spectral characteristics.[25,29] The limited availability of unique analyte tags is a major drawback to the technique.[63] Additionally, each tag that emits a unique wavelength requires a separate detector; thus, the equipment itself can become cumbersome if a large number of compounds are to be analyzed. Another disadvantage to the flow cytometry techniques is that inefficient reactions between the tag and the analyte provide questionable quantification accuracy.[17] It has been reported that flow cytometry analysis is generally used for total protein content or total DNA content rather than individual analyte detection.[19]

Because of the various disadvantages of each technique, neither flow cytometry nor capillary electrophoresis can provide a general method for simultaneous high-content, high-throughput chemical cytometry.

1.3 Microfluidics technology and single cell analysis

Microfluidics is a relatively new and advancing technology that has emerged with the potential to overcome the limitations associated with CE and flow cytometry for high-throughput single cell analysis.[9] The technology has been around since the 1980s[68] but has come of interest for biomedical applications since the 1990s.[13]

Microfluidic devices, also referred to as microchips or lab-on-chip devices, are being developed for a wide variety of applications. In general, they are used to manipulate chemicals, perform separations and conduct experiments within channels that are on the

micrometer regime.[69] In a typical device, channels range from 1 μm to 1 mm in dimension. More recent devices have features in the nanometer range as well.[70] The channels can be fabricated from a variety of materials to form the channel networks. Glass and polymers are the most common materials used for microdevice fabrication, although alternative materials such as plastics are also used.[71-72]

Microfluidic techniques have several advantages over traditional macroscale systems. Some of the initial motivations for microchip development include the low sample volume requirements for analysis and the high separation efficiencies that can be achieved.[24,48] The small channel dimensions result in low total volumes contained within the channels; therefore, smaller amounts of reagents and samples are required for analysis compared to macroscale techniques. This is highly advantageous for applications where only a small amount of sample is available, such as with DNA samples, or in instances where it is difficult to acquire large sample volumes.

Electrophoresis is the most common mode of separation performed on microfluidic devices. Because of the small channel dimensions and short channel lengths, extremely high electric fields can be applied using relatively safe voltage levels.[10] As shown in Equation 1, the efficiency of an electrophoretic separation varies linearly with electric field strength; therefore, highly efficient separations can be achieved on-chip.

Equation 1

$$N = \frac{\mu_{ep} E L_d}{2D_m}$$

Where: N = theoretical plates
E = Electric field strength
μ_{ep} = electrophoretic mobility
L_d = length of capillary to detector
D_m = solute diffusion coefficient

Because of the increased efficiency, separations within microchannels can be performed on a faster timescale compared to conventional CE systems.[9] Other advantages of microfluidic devices that have been cited include the ease of automation, portability, low power requirements, inexpensive fabrication and ability to manipulate precise fluid volumes.[7,9,24,56,68,73-74] The small channel volumes allow for highly sensitive analyte detection as well. Common detection methods, including electrochemical, mass spectrometry and fluorescence, have been interfaced for analyte detection on microchips. These combined separation and detection set-ups make it possible to develop total analysis systems that can control everything from sample preparation through detection and data collection.[24]

The application of microfluidic devices for high-throughput single cell analysis is feasible for many reasons. First, the small sample requirements give microchip analysis a distinct advantage over techniques that require much more sample for successful operation.[59] Often, the limited quantities of diseased cells that can be obtained from a patient are impossible to analyze using conventional techniques, such as flow cytometry, yet microfluidic devices can handle analysis of these smaller sample volumes. Next, because microfluidic channel dimensions are compatible with typical mammalian cell sizes[75], cells can be easily moved through the channel networks and multiple process steps can be incorporated onto a single device.[10,14,24] Retention and isolation of an individual cell and subsequent analysis of that cell's cellular content have also been demonstrated on microchips.[76-77] Because cells generally need to be moved through the device for analysis, microfluidics is the optimal technology for high-throughput analysis of *non-adherent* (i.e., circulatory) cells. Manipulation of adherent cells within a microfluidic channel network

would unfortunately cause too much stress on the cells and the resulting data from such an experiment would most likely be highly inaccurate. Because of this, conventional CE methods with modified lysate injection schemes still remain the best option for adherent cell analysis.[56]

Another advantage of microfluidic devices over conventional CE for non-adherent cell analysis is that fast buffer exchange can occur around the cell just prior to lysis.[1,78-79] It is known that buffers that are "cell-friendly", meaning buffers that maintain cell viability and place little stress on cells, are not usually optimal for performing electrophoretic separations.[80-81] Cell-friendly buffers generally contain high salt content to provide isotonic conditions for the cell. Even at low electric fields, this high salt content can lead to significant Joule heating and can result in bubble formation within the channels. Because fast buffer exchange can be achieved on a microfluidic device, cells can be maintained in a high salt content, cell-friendly buffer up until the time of lysis.

Besides the above mentioned reasons there are several other distinct advantages to using microfluidic devices for cell analysis. The small footprints of microfluidic channel networks make them amenable to parallelization that allows many cells to be observed simultaneously.[13,24,61,79] Highly sensitive detection techniques allow for detection of even the low copy number analytes that are often found within a single cell.[10] Injection of cell lysates can be achieved without significant dilution of the cellular contents.[10] Finally, the microenvironment around the cells can be carefully controlled within a microchannel, which reduces unnecessary stress on the cells.[7,13,74] Stress is known to invoke signaling transduction pathways, which can result in changes to the cellular analyte concentrations.

Although in theory microfluidic technology should be easily adapted for high-throughput single cell analysis applications, it has not yet been demonstrated in a practical manner.[6-7] However, many research groups have demonstrated novel ways to analyze single cells on microchips.

1.4 Application of microfluidics to high-throughput single cell analysis

Single cell analyses on microfluidic devices have been achieved through a variety of methods. In addition to chemical cytometry, on-chip methods have been developed to generate gradients for cell chemotaxis studies[82], to amplify DNA from a single cell using PCR[68], to monitor hormone secretions from live cells[83] and to screen cytotoxicity.[84]

One theory on how to achieve effective single cell analysis on microfluidic devices, either to perform chemical cytometry or simple microscopy experiments, is to first immobilize individual cells.[27,61,77,85] There are several methods for cell isolation, the majority of which involve dielectrophoresis, optical tweezers, mechanical trapping or cell trapping in a hydrogel.[4,76,86-87] Mechanical trapping is the simplest method to capture single cells and many groups have already demonstrated this type of cellular immobilization on microchips for single cell analysis. The first electropherogram of a single protein compound from an individual cell collected on a microfluidic device was in 2005 using an immobilization method.[85] In this case, a Sf9 insect cell was trapped using PDMS microstructures and then lysed using sodium dodecyl sulfate (SDS). In another example, an individual cell was docked at a "T" channel intersection where various solutions were then passed over the cell and the cellular response observed.[80] Additionally, Li's group has immobilized single cardiac myocytes in U-shaped retention chambers for fluorescence studies.[75,88] Di Carlo et al. have captured erythrocytes, HeLa and Chinese hamster ovary

(CHO) cells at a narrow channel, in a similar manner to patch clamping, to observed on-chip lysis using hydroxide generation.[89] Werdich et al. analyzed cardiac myocytes by gravity transport of an individual cell to a tapered channel where electrodes were used to monitor the calcium flux.[90] Zhang and coworkers immobilized CHO-K1 cells on a surface to observe the calcium release over time.[91] Many other examples of immobilization for single cell analysis can be found in the literature.[13,86,92]

Whether performing chemical cytometry experiments, where the cell is lysed and contents separated, or microscopy, where the cell behavior or response is observed over time, it is relatively simple to immobilize cells on microfluidic devices. Although most single cell analysis reports involve immobilization, the time required for cell trapping limits the throughput. The maximum reported throughput achieved using immobilization methods is 25 cells/hour.[1] Although these throughput rates are fast compared to traditional methods, maintaining these throughput rates for a significant period of time to collect a large data set has not been reported.

One strategy for analyzing a large number of cells on a microchip has been through parallelization of channels. Munce and co-workers performed parallel single cell analysis by trapping cells within an array of individual tapered channels. Cells were isolated and transported to the tapered channels using optical tweezers. The trapped cells were subsequently lysed and contents separated using electrophoresis.[61] Using this method, up to 24 cells per hour throughput was noted. Yun's group also developed fluidic chips for parallel cell trapping to observe the cellular response to drug compounds.[93] Zhong et al. achieved simultaneous processing of 20 cells using a multilayer PDMS device.[13]

High-throughput chemical cytometry experiments on microfluidic devices have not been easily achieved. The highest throughput rate for single cell chemical cytometry was published by Wang et al. They achieved analysis of calcein-loaded cells at a rate of 75 to 85 cells per minute by pulling the cells through a direct current (DC) field for lysis.[94] This throughput would be highly sufficient; however, the authors report significant peak overlap of the calcein dye peaks from one cell to the next. So, although the throughput rate was good, not enough time was allowed between cells for appropriate electrophoretic separation and detection of the lysate analytes for even a simplified system of dye-loaded cells. In another high-throughput example to quantify glutathione (GSH) levels in erythrocytes, gravity flow was used to transport a single cell to an analysis channel. Voltages were then switched on and off within the analysis channel to cause the cell to flow back and forth so that it eventually adhered to the channel surface. After adherence, the cell was subsequently lysed and analyzed. Using this method, 15 cells/hour throughput rate was reported.[95] Lin's group reported 10 cells/minute analysis rates for GSH in K562 cells using a simple cross chip design and approximately 100 cells per run could be analyzed. Yet, with their set-up, there was little control over the cell flow rate and the lysed cells were made to inject into the analysis channel. This method does not allow for adequate control over the separation of the intracellular analytes because the migration times will vary depending on where each cell lyses in the analysis channel.[96]

Other examples of high-throughput chemical cytometry experiments on microfluidic devices are sparse in the literature. Often the designed devices suffer from high-complexity and poor reproducibility.[84] One should note in the above mentioned examples, that although the throughput rate is relatively high compared to conventional techniques, collection of

large data sets was not demonstrated. Also, no reported devices have shown the ability to collect biologically relevant information from single cells in a high-throughput manner such that statistically significant conclusion can be made for biological experimentation.

1.5 Research goals and objectives

1.5.1 Main goals

The main objective of the research discussed in this dissertation is development of an automated microfluidic device to perform chemical cytometry analysis on individual cells in a high-throughput manner. The device should be capable of collecting large data sets from a sample of cells during a single operational run of the device. By automated, it is implied that the device should be capable of performing the following functions on-chip, with little to no user interaction required:

1. Preparation of the cell sample
2. Transport of the cells to a lysis region
3. Isolation of individual cells for analysis
4. Lysis of an isolated cell
5. Electrophoretic separation and detection of the analytes

As the term "high-throughput" is arbitrarily defined, the goal for this project is to achieve analysis of approximately 10 cells per minute. Additionally, "large data set" is also a relative term. Here, the goal is to obtain ≥ 100 data points (i.e., cells analyzed) per sample run. Consistent collection of large data sets (>100 cells) in a high-throughput manner has not yet been reported in the literature.

This project was started as a collaboration with Nancy L. Allbritton's laboratory. The goal was to develop the microfluidic device described above to replace the low-throughput

CE-based analysis method currently used for single cell analysis. This CE-based method is referred to as the Laser Micropipet System (LMS).[12,55,97-98] It is reported that only 8 to 10 cells per day can be analyzed using the LMS. Thus, development of the device described above would provide an approximate 1000-fold increase in throughput.

The device to be developed should be capable of analyzing any intracellular analytes, provided that the analytes can be separated without interference from other lysate components and can be measured on-chip through microchip-compatible detection methods. Although the device function will be universal for study of many cellular compounds, the initial objective of the device was to be able to measure kinase enzyme activity. Kinase enzymes and the methods to determine enzyme activity are discussed in later chapters.

Throughout development, each of the above listed functional steps for the device were addressed individually, in order of importance to device operation. Advancement of a channel network previously developed and published was achieved. Additionally, the proof-of-concept work for a completely new channel network to achieve some of the device goals is discussed. The advancements made for each process step are detailed in the following chapters with additional background information as needed.

1.5.2 Evaluation of a flow through device for high-throughput single cell analysis

The Ramsey group has already developed a microfluidic channel network for high-throughput single cell analysis. The device operation was demonstrated using Jurkat T-cells loaded with cytosolic dyes.[99] The channel network is shown in Figure 1.1. According to the proof of concept paper published in 2003, the device is capable of 7-12 cells per minute throughput. The device operates by hydrodynamically flowing cells through an electric field where subsequent electrical cell lysis occurs. The resulting cell lysate is electrokinetically

injected into the analysis channel for electrophoretic separation and LIF detection. To mark the on-set of the lysate separation, cells are focused into approximate single file just prior to the lysis intersection by constricting the cell flow path using a focusing channel. The focused cells pass through another detection point that provides a cytometric signal. This cytometric signal is used to provide a zero time point for the lysate separation.

At the start of this research, the channel network shown in Figure 1.1 was evaluated to determine what areas needed improvement to make the chip amenable to the collection of biologically relevant data. Several issues were immediately noted. These development areas included:

1. Reducing cellular adhesion along the cell flow channel and collection of cellular debris at the lysis intersection
2. Controlling the hydrodynamic cell flow through the chip and balancing it with the electromigration of cells down the analysis channel to achieve optimal lysate injection
3. Isolation of cells prior to lysis so that several cells do not enter the lysis intersection simultaneously
4. Automation of cell preparation

Each of these issues were addressed. Detailed explanation, results and discussion can be found in the subsequent chapters.

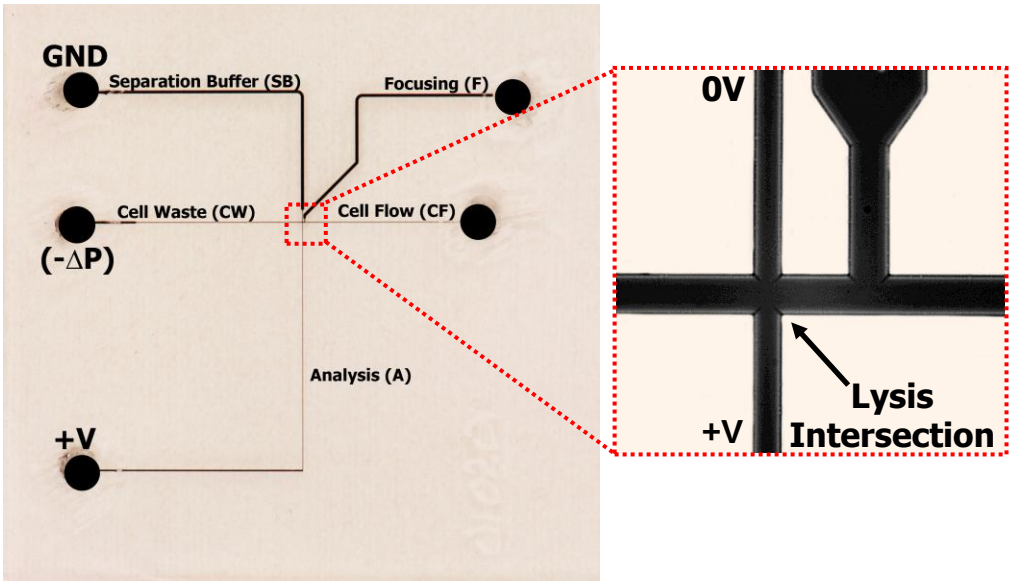

Figure 1.1 Image of the flow through microfluidic channel network with a close up image of the channel network and lysis intersection. Channels are filled with black ink for visualization. Cells are focused to single file, prior to entering the lysis intersection, by the focusing channel (F). At the lysis intersection cells encounter the applied DC electric field and dielectric breakdown of the cell membrane occurs. The cell lysate is electrokinetically injected into the analysis channel (A) and the cell membrane and uncharged debris flow to cell waste (CW) with the hydrodynamic flow.

1.6 References

(1) Sims, C. E.; Allbritton, N. L. *Lab on a Chip* **2007**, *7*, 423.

(2) Woods, L. A.; Roddy, T. P.; Ewing, A. G. *Electrophoresis* **2004**, *25*, 1181.

(3) Yeung, E. S. *Journal of Chromatography A* **1999**, *830*, 243.

(4) Andersson, H.; van den Berg, A. *Current Opinion in Biotechnology* **2004**, *15*, 44.

(5) Amiji, M.; Park, K. *Journal of Biomaterials Science-Polymer Edition* **1993**, *4*, 217.

(6) Yin, H. B.; Zhang, X. L.; Pattrick, N.; Klauke, N.; Cordingley, H. C.; Haswell, S. J.; Cooper, J. M. *Analytical Chemistry* **2007**, *79*, 7139.

(7) Breslauer, D. N.; Lee, P. J.; Lee, L. P. *Molecular Biosystems* **2006**, *2*, 97.

(8) Sweedler, J. V.; Arriaga, E. A. *Analytical and Bioanalytical Chemistry* **2007**, *387*, 1.

(9) Price, A. K.; Culbertson, C. T. *Analytical Chemistry* **2007**, *79*, 2614.

(10) Roman, G. T.; Chen, Y. L.; Viberg, P.; Culbertson, A. H.; Culbertson, C. T. *Analytical and Bioanalytical Chemistry* **2007**, *387*, 9.

(11) Sims, C. E.; Bachman, M.; Li, G. P.; Allbritton, N. L. *Analytical and Bioanalytical Chemistry* **2007**, *387*, 5.

(12) Meredith, G. D.; Sims, C. E.; Soughayer, J. S.; Allbritton, N. L. *Nature Biotechnology* **2000**, *18*, 309.

(13) Chao, T. C.; Ros, A. *Journal of the Royal Society Interface* **2008**, *5*, S139.

(14) Huang, W. H.; Ai, F.; Wang, Z. L.; Cheng, J. K. *Journal of Chromatography B-Analytical Technologies in the Biomedical and Life Sciences* **2008**, *866*, 104.

(15) Lee, T. T.; Yeung, E. S. *Analytical Chemistry* **1992**, *64*, 3045.

(16) Wong, K. S.; Yeung, E. S. *Mikrochimica Acta* **1995**, *120*, 321.

(17) McNamara, K. P.; Yeung, E. S.; Rosenzweig, N.; Rosenzweig, Z. *Analytica Chimica Acta* **1997**, *356*, 75.

(18) Huang, B.; Wu, H. K.; Bhaya, D.; Grossman, A.; Granier, S.; Kobilka, B. K.; Zare, R. N. *Science* **2007**, *315*, 81.

(19) Hogan, B. L.; Yeung, E. S. *Analytical Chemistry* **1992**, *64*, 2841.

(20) Mehrishi, J. N.; Bauer, J. *Electrophoresis* **2002**, *23*, 1984.

(21) Zabzdyr, J. L.; Lillard, S. J. *Trac-Trends in Analytical Chemistry* **2001**, *20*, 467.

(22) Li, P. C. H.; de Camprieu, L.; Cai, J.; Sangar, M. *Lab on a Chip* **2004**, *4*, 174.

(23) Ionescu-Zanetti, C.; Blatz, A.; Khine, M. *Biomedical Microdevices* **2008**, *10*, 113.

(24) Dittrich, P. S.; Manz, A. *Nature Reviews Drug Discovery* **2006**, *5*, 210.

(25) Chen, S. J.; Lillard, S. J. *Analytical Chemistry* **2001**, *73*, 111.

(26) Berthier, J.; Silberzan, P. *Microfluidics for biotechnology*; Artech House: Boston, 2006.

(27) Sun, Y.; Yin, X. F. *Journal of Chromatography A* **2006**, *1117*, 228.

(28) Xue, Q. F.; Yeung, E. S. *Journal of Chromatography B-Biomedical Applications* **1996**, *677*, 233.

(29) Krylov, S. N.; Dovichi, N. J. *Electrophoresis* **2000**, *21*, 767.

(30) Danna, E. A.; Nolan, G. P. *Current Opinion in Chemical Biology* **2006**, *10*, 20.

(31) Engstrom, A.; Lindstrom, B. *Biochimica Et Biophysica Acta* **1950**, *4*, 351.

(32) Caspersson, T. *Skand. Arch. Physiol.* **1936**, *73*.

(33) Edstrom, J. E. *Biochimica Et Biophysica Acta* **1953**, *12*, 361.

(34) Matioli, G. T.; Niewisch, H. B. *Science* **1965**, *150*, 1824.

(35) Rydberg, B.; Johanson, K. J. *DNA Repair Mechanisms*; Academic Press, 1978.

(36) Oates, M. D.; Cooper, B. R.; Jorgenson, J. W. *Analytical Chemistry* **1990**, *62*, 1573.

(37) Osborne, N. N. *Nature* **1977**, *270*, 622.

(38) Abramson, F. P.; Mccaman, M. W.; Mccaman, R. E. *Analytical Biochemistry* **1974**, *57*, 482.

(39) Briel, G.; Neuhoff, V.; Osborne, N. N. *International Journal of Neuroscience* **1971**, *2*, 125.

(40) Osborne, N. N.; Szczepan.Ac; Neuhoff, V. *International Journal of Neuroscience* **1973**, *5*, 125.

(41) Davis, D. *Micron* **1978**, *9*, 175.

(42) Mccaman, R. E.; Weinreic.D; Borys, H. *J Neurochem* **1973**, *21*, 473.

(43) Jongkind, J. F.; Ploem, J. S.; Reuser, A. J. J.; Galjaard, H. *Histochemistry* **1974**, *40*, 221.

(44) Reuser, A. J. J.; Jongkind, J. F.; Galjaard, H. *J Histochem Cytochem* **1976**, *24*, 578.

(45) Jorgenson, J. W. *Trac-Trends in Analytical Chemistry* **1984**, *3*, 51.

(46) Jorgenson, J. W.; Lukacs, K. D. *Analytical Chemistry* **1981**, *53*, 1298.

(47) Kennedy, R. T.; Stclaire, R. L.; White, J. G.; Jorgenson, J. W. *Mikrochimica Acta* **1987**, *2*, 37.

(48) Kennedy, R. T.; Oates, M. D.; Cooper, B. R.; Nickerson, B.; Jorgenson, J. W. *Science* **1989**, *246*, 57.

(49) Fuller, K. M.; Arriaga, E. A. *Analytical Chemistry* **2003**, *75*, 2123.

(50) Han, F. T.; Wang, Y.; Sims, C. E.; Bachman, M.; Chang, R. S.; Li, G. P.; Allbritton, N. L. *Analytical Chemistry* **2003**, *75*, 3688.

(51) Woods, L. A.; Ewing, A. G. *Analytical and Bioanalytical Chemistry* **2003**, *376*, 281.

(52) Stuart, J. N.; Sweedler, J. V. *Analytical and Bioanalytical Chemistry* **2003**, *375*, 28.

(53) Zhang, Z. R.; Krylov, S.; Arriaga, E. A.; Polakowski, R.; Dovichi, N. J. *Analytical Chemistry* **2000**, *72*, 318.

(54) Dovichi, N. J.; Hu, S. *Current Opinion in Chemical Biology* **2003**, *7*, 603.

(55) Sims, C. E.; Meredith, G. D.; Krasieva, T. B.; Berns, M. W.; Tromberg, B. J.; Allbritton, N. L. *Analytical Chemistry* **1998**, *70*, 4570.

(56) Borland, L. M.; Kottegoda, S.; Phillips, K. S.; Allbritton, N. L. *Annual Review of Analytical Chemistry* **2008**, *1*, 191.

(57) Gilman, S. D.; Ewing, A. G. *Analytical Chemistry* **1995**, *67*, 58.

(58) Gao, N.; Wang, W. L.; Zhang, X. L.; Jin, W. R.; Yin, X. F.; Fang, Z. L. *Analytical Chemistry* **2006**, *78*, 3213.

(59) Krutzik, P. O.; Nolan, G. P. *Nature Methods* **2006**, *3*, 361.

(60) Jankowski, J. A.; Tracht, S.; Sweedler, J. V. *Trac-Trends in Analytical Chemistry* **1995**, *14*, 170.

(61) Munce, N. R.; Li, J. Z.; Herman, P. R.; Lilge, L. *Analytical Chemistry* **2004**, *76*, 4983.

(62) Lillard, S. J.; Yeung, E. S.; McCloskey, M. A. *Analytical Chemistry* **1996**, *68*, 2897.

(63) Jayaraman, S. *Cytometry Part A* **2003**, *56A*, 104.

(64) Bonetta, L. *Nature Methods* **2005**, *2*, 785.

(65) Lecoeur, H.; Melki, M. T.; Saidi, H.; Gougeon, M. L. *Method Enzymol* **2008**, *442*, 51.

(66) Le, T. T.; Cheng, J. X. *Plos One* **2009**, *4*.

(67) Butts, C. L.; Shukair, S. A.; Duncan, K. M.; Harris, C. W.; Belyavskaya, E.; Sternberg, E. M. *Nuclear Receptor Signaling* **2007**, *5*, e007.

(68) Lee, C. Y.; Lee, G. B.; Lin, J. L.; Huang, F. C.; Liao, C. S. *Journal of Micromechanics and Microengineering* **2005**, *15*, 1215.

(69) Hadd, A. G.; Jacobson, S. C.; Ramsey, J. M. *Analytical Chemistry* **1999**, *71*, 5206.

(70) Kovarik, M. L.; Jacobson, S. C. *Analytical Chemistry* **2009**, *81*, 7133.

(71) Iles, A.; Oki, A.; Pamme, N. *Microfluidics and Nanofluidics* **2007**, *3*, 119.

(72) Sun, X. F.; Liu, J. K.; Lee, M. L. *Electrophoresis* **2008**, *29*, 2760.

(73) Hung, P. J.; Lee, P. J.; Sabounchi, P.; Lin, R.; Lee, L. P. *Biotechnology and Bioengineering* **2005**, *89*, 1.

(74) Nevill, J. T.; Cooper, R.; Dueck, M.; Breslauer, D. N.; Lee, L. P. *Lab on a Chip* **2007**, *7*, 1689.

(75) Li, X.; Huang, J.; Tibbits, G. F.; Li, P. C. H. *Electrophoresis* **2007**, *28*, 4723.

(76) Li, P. C. H. *Microfluidic lab-on-a-chip for chemical and biological analysis and discovery*; Taylor & Francis/CRC Press: Boca Raton, 2006.

(77) Ros, A.; Hellmich, W.; Regtmeier, J.; Duong, T. T.; Anselmetti, D. *Electrophoresis* **2006**, *27*, 2651.

(78) Lee, P. J.; Hung, P. J.; Lee, L. P. *Biotechnology and Bioengineering* **2007**, *97*, 1340.

(79) Taylor, R. J.; Falconnet, D.; Niemisto, A.; Ramsey, S. A.; Prinz, S.; Shmulevich, I.; Galitski, T.; Hansen, C. L. *Proceedings of the National Academy of Sciences of the United States of America* **2009**, *106*, 3758.

(80) Wheeler, A. R.; Throndset, W. R.; Whelan, R. J.; Leach, A. M.; Zare, R. N.; Liao, Y. H.; Farrell, K.; Manger, I. D.; Daridon, A. *Analytical Chemistry* **2003**, *75*, 3581.

(81) Li, H.; Wu, H. Y.; Wang, Y.; Sims, C. E.; Allbritton, N. L. *Journal of Chromatography B* **2001**, *757*, 79.

(82) Frevert, C. W.; Boggy, G.; Keenan, T. M.; Folch, A. *Lab on a Chip* **2006**, *6*, 849.

(83) Roper, M. G.; Shackman, J. G.; Dahlgren, G. M.; Kennedy, R. T. *Analytical Chemistry* **2003**, *75*, 4711.

(84) Brouzes, E.; Medkova, M.; Savenelli, N.; Marran, D.; Twardowski, M.; Hutchison, J. B.; Rothberg, J. M.; Link, D. R.; Perrimon, N.; Samuels, M. L. *Proceedings of the National Academy of Sciences of the United States of America* **2009**, *106*, 14195.

(85) Hellmich, W.; Pelargus, C.; Leffhalm, K.; Ros, A.; Anselmetti, D. *Electrophoresis* **2005**, *26*, 3689.

(86) Johann, R. M. *Analytical and Bioanalytical Chemistry* **2006**, *385*, 408.

(87) Huang, Y.; Ewalt, K. L.; Tirado, M.; Haigis, T. R.; Forster, A.; Ackley, D.; Heller, M. J.; O'Connell, J. P.; Krihak, M. *Analytical Chemistry* **2001**, *73*, 1549.

(88) Li, X. J.; Li, P. C. H. *Analytical Chemistry* **2005**, *77*, 4315.

(89) Di Carlo, D.; Ionescu-Zanetti, C.; Zhang, Y.; Hung, P.; Lee, L. P. *Lab on a Chip* **2005**, *5*, 171.

(90) Werdich, A. A.; Lima, E. A.; Ivanov, B.; Ges, I.; Anderson, M. E.; Wikswo, J. P.; Baudenbacher, F. J. *Lab on a Chip* **2004**, *4*, 357.

(91) Zhang, X. L.; Yin, H. B.; Cooper, J. M.; Haswell, S. J. *Electrophoresis* **2006**, *27*, 5093.

(92) Di Carlo, D.; Aghdam, N.; Lee, L. P. *Analytical Chemistry* **2006**, *78*, 4925.

(93) Yun, K. S.; Yoon, E. *Biomedical Microdevices* **2005**, *7*, 35.

(94) Wang, H. Y.; Lu, C. *Chem Commun* **2006**, 3528.

(95) Gao, J.; Yin, X. F.; Fang, Z. L. *Lab on a Chip* **2004**, *4*, 47.

(96) Yu, L. F.; Huang, H. Q.; Dong, X. L.; Wu, D. P.; Qin, J. H.; Lin, B. C. *Electrophoresis* **2008**, *29*, 5055.

(97) Li, H.; Sims, C. E.; Kaluzova, M.; Stanbridge, E. J.; Allbritton, N. L. *Biochemistry* **2004**, *43*, 1599.

(98) Li, H. N.; Sims, C. E.; Wu, H. Y.; Allbritton, N. L. *Analytical Chemistry* **2001**, *73*, 4625.

(99) McClain, M. A.; Culbertson, C. T.; Jacobson, S. C.; Allbritton, N. L.; Sims, C. E.; Ramsey, J. M. *Analytical Chemistry* **2003**, *75*, 5646.

Chapter 2: Prevention of cellular adhesion and cellular debris build-up on glass microchannels

2.1 Introduction

2.1.1 Cell adhesion and cellular debris build-up on the flow through device

Upon initial evaluation of the flow through device shown in Chapter 1, it was observed that the number of cells that could be analyzed in a single run of the chip was severely limited by cellular adhesion to the cell flow channel or by cellular debris collection at the lysis intersection. The collection of biomaterials to microchip channel surfaces is frequently referred to as biofouling. Examples of this biofouling can be seen in Figure 2.1. To reduce biofouling on the flow through device, several alternative coating procedures were investigated. Some of the coatings demonstrated an improvement over the original polydimethylsiloxane (PDMS)/Pluronic coating. These new procedures increased the number of cells that could be analyzed in a single run of the device without significant biofouling. In this chapter, the different surface coatings and channel pretreatments tested to reduce biofouling are discussed.

2.1.2 Cellular adhesion to microfluidic channel surfaces

It is well-documented that mammalian cells will strongly adhere to most of the materials used to fabricate microfluidic devices.[1-4] Although advantageous to some applications[2,5], cellular adhesion is especially problematic in devices that are being used to perform single cell analysis. Most high-throughput single cell analysis devices require that the cells flow through the device and that the intracellular analytes separate efficiently with

minimal biofouling.[3] Adhesion of a single cell to the surface often leads to agglomeration of cells within the channel.[1,6] This collection of cells hinders the ability of additional cells to flow and often causes complete clogging of the channel. Therefore, there is a great need to develop channel coatings that are biocompatible and resistant to biofouling.[7-8]

There are a number of reasons that cells adhere to channel surfaces. Low flow rates, such as those frequently required for on-chip chemical cytometry, allow the cells to interact with the channel surfaces and increases the probability that they will irreversibly adhere.[9-10] The proteins and glycoproteins present on cellular membranes give mammalian cells a net negative charge.[11-13] This surface charge creates electrostatic interaction between the cells and positive charges on the channel walls. Also, many transmembrane proteins are hydrophobic and allow for interaction between the cells and certain hydrophobic channel surfaces.[4,14-15]

2.1.3 Cellular debris build-up on channel surfaces

An additional consideration when performing chemical cytometry on a microfluidic device is that, once the cells are lysed, the intracellular contents are now exposed to the channel surface. Cells contain a mixture of biomolecules including proteins, carbohydrates, and lipids.[16] Thus, upon cell lysis, a mixture of hydrophobic and hydrophilic compounds is introduced within the channels that can interact with the surfaces through a variety of mechanisms.[14,17] The high surface area to volume ratio within a microfluidic channel increases the likelihood that these molecules will interact and adsorb, causing biofouling of the surface.[18] Nonspecific adsorption of biomolecules is cited as a common problem not only in microfluidic devices, but also biosensors and microarrays.[15,19-21]

Once biofouling begins on a microfluidic channel intended for biological data collection, a number of issues arise.[5] First, once sites of biomolecule adsorption are initiated, aggregation of biomaterial at those sites becomes even more favorable.[22] This debris aggregation can eventually cause complete blockage of the microfluidic channels.[23-24] After blockage, the device must be cleaned for reuse. To clean the biomaterials off the channel surfaces, harsh treatments are usually required. Rinses with 1% sodium dodecyl sulfate (SDS) or 1 N NaOH have been reported to clean some material from the surface.[24] For glass chips, heating to 500ºC for a period of time will oxidize the adsorbed biomaterial from the surface.[25] Sterilizing chips is also achieved using ethanol, bleach, UV radiation, or autoclaving.[25] Sterilization, however, does not necessarily remove the biomaterials from the channel surfaces. Many of the procedures for cleaning the channel surfaces will also remove channel coatings; therefore, the chip must also be recoated appropriately, which can cause significant delays in sample analysis.

For separation of biomolecules (e.g., proteins), adsorption of the analytes to the channel walls has been shown to cause peak broadening, changes in retention time and affect the electroosmotic flow (EOF) rate.[2,5,7,17,20,26-29] These effects are problematic for complex separations because resolution loss and retention time changes make it challenging to positively identify and quantify peaks. For analytes that are of low abundance within a single cell, adsorptive loss can critically affect the detection and quantification ability.[30]

The buildup of cellular debris has been cited in numerous studies as a major obstacle that hinders the ability to collect useful single cell data.[31-32] To avoid this biofouling, there are several options. Either a new chip can be used for each run or the channels can be coated in such a manner to reduce or prevent the biofouling.[6,33] Using a new chip for each run can

be time-consuming and may introduce additional experimental variability. For the collection of large single cell data sets, it is necessary that the cells be analyzed as quickly as possible. This is because signaling pathways can be initiated or inhibited as the cells await analysis. The intracellular analyte concentrations can also change on short timescales; therefore, a long analysis time will result in less accurate results. The optimal solution is to find a channel surface that will minimize the biofouling and allow a single device to be operated long enough for collection of large data sets (e.g., >100 cells analyzed).

2.1.4 Biofouling prevention

A variety of methods have been used to reduce biofouling within microfluidic channels. Surface modifications are the most commonly employed method and can create biocompatible surfaces for analysis. Other methods include adjustment of the buffer ionic strength within the channels[22], use of emulsification agents to try to wash the debris off the surface[17,25] and manipulations of buffer composition.[21] To date, surface coatings, whether applied dynamically or statically, have provided the best reduction in biofouling.

Hydrophobic surfaces are prone to cellular adhesion.[15,20,22,34] As mentioned above, it is believed that this adhesion is due to the hydrophobic nature of many transmembrane proteins.[4] On the other hand, it has been observed that protein adsorption is greatly reduced when using hydrophilic polymeric coatings, such as polyethyleneoxide (PEO).[35] Other coatings reported in the literature to reduce biofouling include: hydroxypropyl methylcellulose (HPMC)[3], zwitterionic materials[21], surface silanols that include neutral polymers[21], polydimethylacrylamide (PDMA)[21], poly(ethylene) glycol (PEG)[19,22,36], bovine serum albumin (BSA)[7,24], phosphatidylcholine (PC)[22], polyacrylamide films on acrylate-coated glass[37], hydrogels[38] and Pluronics.[3,35,39]

2.1.5 Channel coating investigations

In this chapter, the various surface coatings that were examined to prevent biofouling are discussed. Biofouling reduction focused mainly on surface modification with PEG and zwitterionic compounds due to the relatively simple channel coating procedures. Some alternative approaches, such as buffer additives and channel pretreatments, were also tested. Methods that were attempted but not discussed in this chapter due to poor results include the use of: phosphatidylcholine, starting block buffers and perfluorinated silanes. The best results for reduction in biofouling were obtained when the glass microfluidic channels were pretreated with 100% fetal bovine serum (FBS).

2.2 Experimental section

2.2.1 Chip fabrication

The microfluidic channel network layout is shown in Chapter 1, Figure 1.1. All microchips were fabricated from 50 mm x 50 mm, 0.9 mm thick B270 crown glass using traditional photolithography techniques and wet chemical etching methods.[40-42] The etchant used was a 10:1 buffered oxide etch (BOE) (Transene Company, Danvers, MA). Channel access holes were drilled through the substrate at the channel ends using aluminum oxide powder blasting (Microblaster, Comco Inc., Burbank, CA). The etched substrate was then fusion bonded to a 0.9 mm thick B270 cover slip to create a closed channel network.[40] Buffer and sample reservoirs were created by attaching cloning cylinders (Fisher Scientific, 4 mm i.d.) around the access holes using Norland 63 optical adhesive (Norland Products, Inc., Cranbury, NJ). Each reservoir holds a volume of approximately 100 μL. To connect a syringe pump to the chip, a 1/16″ barbed female Luer lock (Upchurch Scientific, Oak Harbor, WA) was altered by removing the barb and drilling an ~ 3 mm hole into the bottom using a

Dremel tool. The altered Luer lock was then epoxied onto the top of the cell waste reservoir and 1/16″ i.d. Tygon tubing was attached to the female Luer lock via a 1/16″ barbed male Luer lock (Upchurch Scientific, Oak Harbor, WA).

Several different microchips were used for this study. Channel depths and widths were determined using a stylus-based surface profiler (P-15; KLA-Tencor, Mountain View, CA). Widths are reported as the full channel width measured at the top of the channel. All channels were etched to a depth between 20 - 25 μm. The cell flow (CF) channel and the cell waste (CW) channel were 65-80 μm wide. The analysis (A) channel from the lysis intersection to the 90º turn and the narrow section of the separation buffer (SB) channel were 45-60 μm wide. The broad sections of all the channels were 255-270 μm wide. The analysis channel from the lysis intersection to the 90º turn was 20.0 mm long, and the distance between the tee intersection of the focusing (F) channel with the sample cell flow channel and the lysis intersection was approximately 105 μm.

For some coating studies, 25.4 mm x 50.8 mm chips were fabricated that had only three straight channels. For each chip, the channels were 19.5 μm deep and 110 μm wide. A maskless system (SF-100, Intelligent Micro Patterning, LLC, St. Petersburg, FL) was used to expose the photoresist on the substrates. All other photolithography, etching and bonding steps were the same as described above.

2.2.2 Cell culture and preparation

Jurkat Cells (ATCC TIB-152, American Type Culture Collection, Rockville, MD; obtained from the University of North Carolina Tissue Culture Facility) were used for all experiments. The cell cultures were maintained at 37ºC and 5% CO_2 in RPMI 1640 1X medium (Gibco BRL, Gaithersburg, MD) supplemented with 10% (v/v) FBS, 100 μg/mL

penicillin and 100 μg/mL streptomycin. The cells were grown in 25-mL polystyrene culture flasks (Nalge Nunc International, Rochester, NY) to densities of approximately $1x10^6$/mL before passage.

To load the cells with dye, ~5 x 10^5 cells were pelleted (1000g for 3 minutes) and the supernatant discarded. The cells were then re-suspended in a solution of 10 to 50 μM Oregon Green 488 carboxylic acid diacetate 6-isomer in extracellular buffer (ECB: 135 mM NaCl, 15 mM KCl, 2 mM $MgCl_2$, 2 mM $CaCl_2$, 10 mM HEPES, pH 7.4). Oregon Green in diacetate form is membrane permeable and cell loading was achieved through simple incubation (~20 minutes) in a centrifuge vial while maintaining the cells at 37ºC. The cells were then washed three to four times by pelleting with ECB and re-suspended in ECB containing 10 mM Glucose.

2.2.3 Channel coating procedures

2.2.3.1 PDMS/Pluronic coating

To coat the glass channels with PDMS, the channels were rinsed for approximately five minutes with 1 N NaOH followed by deionized (DI) water for five minutes. The channels were then thoroughly dried by pulling vacuum on one reservoir of the chip. A mixture of 1:10 PDMS (w/w, 1 part curing agent to 10 parts monomer, Sylgard, Dow Corning, Midland, MI) was prepared. A 20% mixture (v/v) of the PDMS in hexane was then prepared and pulled through the channels for approximately five minutes. Next, 100% hexane was pulled through the channels for 30 to 45 minutes to remove excess PDMS. The channels were dried by pulling air through the channels and the PDMS was cured in a vacuum oven at 100-110°C for 8 to 10 hours.

Pluronic F-127, a triblock copolymer of polypropylene oxide and polyethylene oxide, was coated onto the surface of the PDMS-coated channels. The PDMS-coated channels were prepared by first rinsing with methanol followed by DI water to ensure that the channels were free of air bubbles. The chip was cooled on an ice block and a solution of 30% (w/w) Pluronic F-127 in water was pulled through the channels for 20 minutes by applying vacuum to the waste reservoir. After 20 minutes, the reservoirs and channels were rinsed thoroughly with DI water. After the DI water rinse, the chip was ready for use.

2.2.3.2 Pluronic-only coating

To coat the channels with Pluronic F-127, the channels were prepared by rinsing with 1 N NaOH for approximately 1 hour followed by a DI water rinse. With the chip on an ice block to keep it cool, a solution of 30% Pluronic F-127 (w/w) was pulled through the channels for approximately 1 hour.

2.2.3.3 Poly(ethylene glycol) (PEG) coatings

2.2.3.3.1 Aminopropyltriethoxysilane (APTES) coating

Chip channels were rinsed with 1:1 (v/v) MeOH:HCl for approximately five minutes followed by a DI water rinse. The channels were then thoroughly dried under vacuum. To ensure complete dryness, the chip was placed in a 90°C oven for 20 minutes. Next, 3% (v/v) APTES in ethanol (EtOH) was pulled through the channels and allowed to react for 15 minutes. The channels were then flushed with EtOH to wash out the excess APTES and the chip was placed in a 120°C oven overnight.

2.2.3.3.2 PEG succinimidylpropionate (PEG-SPA)

Chip channels were first coated with APTES according to the above procedure. After APTES coating, a 1 mg/mL PEG-SPA solution in 20 mM sodium phosphate buffer (pH 8)

was pulled through the channels and reacted for 24 hours at 4°C. The channels were then flushed with DI water. The procedure was taken directly from Chuang et al.[43]

2.2.3.3.3 N-(triethoxysilylpropyl)-O-poly(ethylene) oxide urethane (PEG-Urethane)

Channels were rinsed with 1 N NaOH for 15 minutes followed by a 10 minute DI water rinse. Channels were flushed with anhydrous toluene for 10 minutes and dried by applying vacuum to the waste reservoir. A 6 mg/mL solution of N-(triethoxysilylpropyl)-O-poly(ethylene) oxide urethane (MW 400-500) (PEG-Urethane) in anhydrous toluene was pulled through the channels and allowed to react for 4 to 12 hours. After reaction, the channels were flushed with anhydrous toluene and the microchip placed in an 80°C oven for at least two hours.

2.2.3.3.4 2-[methoxy(polyethyleneoxy)propyl]trimethoxysilane (PEG-Silane)

Channels were rinsed with 1 N NaOH for approximately one hour followed by a DI water flush. The channels were dried by pulling vacuum on the waste channel. Channels were rinsed with concentrated HCl for 30 minutes and then rinsed again with DI water. A 100% solution of the PEG-silane was pulled through the channels and allowed to react for 30 minutes. After the reaction, the channels were rinsed with DI water and dried in a 95°C oven for 30 minutes.

2.2.3.3.5 Carboxytetramethylrhodamine, succinimidyl ester (TAMRA) Coating

Chip channels were first coated with APTES according to the above procedure. The APTES-coated channels were filled with a 1 mg/mL solution of 5(6)-TAMRA in 20 mM sodium phosphate buffer (pH 8). The TAMRA solution was allowed to react for 24 hours at 4°C. Channels were then flushed with DI water and filled with the appropriate buffers for analysis.

2.2.3.4 Fetal Bovine Serum (FBS) channel pretreatment

The channels were pre-rinsed with 2X Nanostrip (Cyantek, Fremont, CA) followed by DI water. Channels were then filled with 100% FBS (Invitrogen, Carlsbad, CA) and allowed to incubate for 15 to 30 minutes at room temperature. The reservoirs were refilled with fresh FBS and the fresh FBS was flushed through the channels.

2.3 Results and discussion

In the proof of concept publication for the flow through device, the channel coating used consisted of a layer of PDMS with a Pluronic F-127 overcoat.[44] The PDMS layer blocks the surface silanols to create a hydrophobic surface. The Pluronic layer then can diffuse into the PDMS layer and adhere to the PDMS surface. Pluronic is a triblock co-polymer of polypropylene oxide and polyethylene oxide; thus, the coating creates an effective PEG-like surface to reduce cell adhesion and cellular debris build-up. Additionally, to reduce debris adsorption around the lysis intersection, buffer containing Pluronic F-108 was placed in the focusing channel.

It was found here, however, that the PDMS/Pluronic coating was not optimal for achieving high-throughput analysis. The coating process was time-consuming, taking approximately one and a half days to complete. Additionally, it was found that the highly viscous PDMS and Pluronic-F127 solutions frequently clogged the channels. Generally, this clogging was found to be irreversible and required that the chip be placed in a furnace and incubated at 550°C to remove the blockage. Finally, the PDMS/Pluronic coating was not found to be very effective at preventing cell adhesion or preventing cellular debris build-up at the lysis intersection during prolonged chip operation. This problem was also noted in the proof of concept paper by McClain, et al.[44] Because Pluronic is slightly soluble in aqueous

solutions, over time the coating most likely washes off the channel surfaces and exposes the hydrophobic PDMS layer, which is prone to biofouling.

Collection of cellular debris on the chip channels was the main deterrent to collecting a large data set during a single run of the flow through device. Investigations were conducted to find an alternative coating that required less preparation time, was more stable and was effective at preventing cellular debris buildup within the channels.

2.3.1 Comparison of coating procedures

2.3.1.1 PDMS/Pluronic and Pluronic-only coatings

Initially, it was determined that a simple coating with Pluronic over the glass channel surface was sufficient to prevent most cellular adhesion. This reduced the coating time through elimination of the PDMS layer. Several studies using a Pluronic-only coating were performed including the lysate injection efficiency study detailed in Chapter 3. However, the 30% (v/v) Pluronic F-127 coating still posed the occasional problem of channel clogging during the coating procedure. Additionally, the Pluronic-only coating did not allow for the analysis of many cells before biofouling began to occur. It is believed that this is because the Pluronic washes off the channel surfaces over time. The Pluronic-only coating provided similar results as the PDMS/Pluronic-modified channel surfaces.

2.3.1.2 PEG-SPA coating

As an alternative to the Pluronic coating procedure, covalent bonding of PEG moieties onto the channel surfaces through a silanization reaction was studied. In general, silanization reactions with the surface silanols of glass microchannel surfaces are simple and fast.[4,27] The first silane used in these studies was a PEG-SPA. The PEG-SPA was reacted with the surface through a two step procedure. First, the surface silanols of the glass were

modified using APTES, which places amine groups on the surface. These amine groups are then reacted with the succinimidyl groups of the PEG-SPA (Figure 2.2).

To determine whether the anti-adhesive character of the PEG-SPA surface was an improvement over an uncoated channel, as well as over the PDMS/Pluronic coating or the Pluronic-only coating, a comparison study was performed to observe cell adhesion at the surfaces. Several flow through chips were coated, each with one of the listed procedures. A comparison was performed by pulling cells, loaded with Oregon Green cytosolic dye for visualization, through the coated cell flow channels for approximately 20 minutes. After the cells were pulled through, the number of cells adhering to the surface was counted. The number of adhered cells counted for each coating procedure is shown in Table 2.1. As can be seen from the data, the uncoated chip demonstrated the worst anti-adhesive character, indicating that a coating is necessary to allow for consistent cell flow through the glass microchannels. The PDMS/Pluronic and Pluronic-only coatings were about equal in terms of their ability to prevent cellular adhesion. The PEG-SPA coating was superior to both of the Pluronic-based coatings. No cells were observed to adhere to the PEG-SPA surface.

The PEG-SPA coating worked well to prevent cell adhesion; however, the procedure required two steps and was time consuming. Additionally, although cell adhesion was reduced with this coating, the cellular debris buildup post-lysis at the channel intersection was still problematic.

2.3.1.3 PEG-Urethane coating

Next, silanes that include a PEG moiety were tested in an attempt to directly couple the PEG groups to the glass surface through a one-step procedure. The goal was to reduce the coating time while maintaining the anti-adhesive character and potentially reduce the cell

debris adhesion. The first PEG-based silane tested is referred to as PEG-Urethane. This silane can be directly reacted to the glass surface. The coating procedure took approximately one day to complete. Because of the simplified coating procedure, this silane was used for some experiments to collect single cell data; however, this coating did not demonstrate improved anti-adhesive properties compared to the PEG-SPA coating.

2.3.1.4 TAMRA coating

During evaluation of the PEG-SPA coating, there was a question as to the degree of surface coverage achieved using the two part coating reaction. Inconsistencies in the anti-biofouling character were observed from chip-to-chip using the PEG-SPA coating procedure. It was hypothesized that the APTES reaction was not efficiently blocking the surface silanols of the glass during the first step. Also, the reaction of the PEG-SPA succinimidyl esters with the amine groups of the APTES may not be optimal. If unreacted amine groups are exposed to the bulk solution within the microchannel, it is likely that they will be positively charged at the near neutral pH levels of the separation buffers. These positive charges can interact with the negatively charged cells and cause irreversible cell adhesion through electrostatic interactions. In an attempt to determine the degree of surface silanol coverage by the APTES reaction, a fluorescent succinimidyl ester was reacted in place of the PEG-SPA. The goal of the experiment was to label the amine groups with something fluorescent so that the APTES surface coverage could be visualized. The fluorescent succinimidyl ester chosen was 5(and 6)-carboxytetramethylrhodamine, succinimidyl ester (5(6)-TAMRA) and was reacted with the APTES coated channel surfaces in the same manner as the PEG-SPA. The structure of 5(6)-TAMRA and final surface coating structure are shown in Figure 2.3. After the reaction with TAMRA, the channel surfaces were fluorescent, even after a thorough wash with DI

water to remove any unbound TAMRA molecules. Figure 2.4 shows an example of channel fluorescence after the APTES reaction with TAMRA.

The TAMRA coating was performed to visually observe the surface coverage of the APTES on the glass channel surfaces. However, it was found that the TAMRA-coated surfaces also demonstrated good anti-adhesive character when cells were pulled through the channels. This result was not expected. After the first observed success with the TAMRA coating, several additional flow through chips were coated in the same manner and displayed similar results. Additionally, it was observed that when cells were lysed on a chip coated with the APTES/TAMRA procedure, very little debris collected on the channel surfaces. This was a great improvement compared to the PEG-based coatings. In several instances, >100 cells could be lysed on a chip prior to any observed debris build-up. Figure 2.5 shows an example of a chip in which approximately 100 cells were lysed with no observed debris build up at the lysis intersection.

Several comparison studies of the TAMRA coating to PEG-based surfaces were conducted to determine whether the TAMRA coating was superior to the PEG surfaces. In one study, microchips were made that had only straight channels in order to compare cell adhesion. Each chip contained three separate straight channels and each of the three channels was prepared with the same coating procedure. A chip with uncoated channels was used as a control. The other two chips used in the study were coated with the PEG-Urethane and the APTES/TAMRA coating, respectively. To test the anti-biofouling character of the coatings, cells loaded with Oregon Green cytosolic dye were pulled through the channels for 30 minutes and cell adhesion to the surfaces was observed. The area of the channel where the most concentrated instances of adhered cells were observed was imaged using an

EMCCD camera. These images can be seen in Figure 2.6. As shown, the TAMRA and the PEG-Urethane coatings were equivalent at preventing cell adhesion to the surfaces. Both of these coatings were far superior to the uncoated channels.

In the next study performed, the number of cells that could be lysed on a flow through device prior to significant debris build up was tested. Three flow through chips were prepared with the following surface coatings: a) uncoated, b) PEG-Urethane coated and c) APTES/TAMRA coated. As can be seen in Figure 2.7, the top of the analysis channel on the uncoated chip was completely clogged after lysis of only 30 cells. The PEG-Urethane coated chip, in the best case observed, allowed lysis of up to 75 cells before significant clogging of the analysis channel. The APTES/TAMRA coated chip demonstrated lysis of 100 or more cells before the initiation of debris buildup was observed.

Based on the above results, it appeared that the TAMRA coating was superior at preventing cell adhesion and cellular debris buildup on the microfluidic channel surfaces. It was theorized that this reduced biofouling is a result of the zwitterionic character of the TAMRA moiety. At near neutral pHs, the carboxylic acid group on TAMRA is negatively charged and the amine carries a constant positive charge. Zwitterionic coatings such as phosphatidyl choline, sulfobetaines, poly CMBA and zwitterionic surfactants have been used to prevent cell adhesion and have been noted in the literature.[22,34,45-47] In some instances, the zwitterionic coatings are reported to resist biofouling better than PEG coated surfaces.[22,45]

Collection of some single cell kinase activity data was achieved using the APTES/TAMRA coating. It initially appeared that this coating would allow for collection of large data sets in a single run. However, the main issue encountered with this coating was the lack of consistency from chip-to-chip. Certain chips with the TAMRA coating were

excellent at preventing biofouling. Others did not exhibit the ability to prevent cell or cellular debris adhesion. Many attempts were made to adjust the coating procedure to achieve consistency without success. It is believed that the TAMRA coating does not provide enough surface coverage to completely block sites on the channel surface that favorably interact with cells and cellular debris. After an exhaustive study to determine the cause of the coating variability, it was decided to return to PEG-coated surfaces. Further investigations into zwitterionic coatings may provide improved resistance to biofouling.

2.3.1.5 PEG-Silane coating

The final PEG-based silane tested is referred to as the PEG-Silane. The procedure for coating the glass surfaces with this silane is simple and rapid compared to the other silanes tested. The entire coating procedure only took approximately one hour. A comparison of the cell adhesion at the channel inlet on a PEG-silane coated chip compared to PEG-SPA and TAMRA coated chips is shown in Figure 2.8. The channel inlet is a common place for significant cellular adhesion to occur. The new PEG-silane appeared to be superior to the PEG-SPA and comparable to the TAMRA coating. Because of the simplified coating procedure, the PEG-Silane was used for a large number of developmental experiments to collect single cell data.

The issues with cellular debris collection at the lysis intersection were not well-resolved using any of the above discussed coatings. Occasionally, certain coatings would allow for lysis of 100 or more cells before debris collection began. Yet, the inability to duplicate these results from chip-to-chip was a major deterrent in pursuing these coatings beyond initial evaluations. Other attempts to reduce cellular debris adhesion include using buffer additives such as SDS, Triton-X, Pluronics and low concentrations of bovine serum

albumin (BSA). None of these attempts provided significant improvement; therefore, experiments using these additives were not pursued.

2.3.2 FBS channel pretreatment

After some time working with the PEG-Silane coating to try to achieve high-throughput single cell data collection, another procedure was discovered that was far superior to any of the previously attempted coatings. It has been reported that cells in serum or plasma solutions will hover over a surface, whereas in aqueous-based buffers they will adhere strongly to the surface.[48] It was found that, using fetal bovine serum (FBS) to treat the glass channel surfaces prior to analysis, cellular adhesion was not observed and cellular debris build-up post-lysis was minimal. Additionally, filling the channels with FBS for the electrophoretic separation allowed for baseline resolution of cytosolic dyes, with excellent peak shape, from a large number of cells. The separation of cytosolic dyes using FBS as the separation solution is detailed in Chapter 4. To date, large data sets of single cell analyses (>100 cells each) have been collected in FBS-filled channels prior to any on-chip issues that required the operation to stop and the chip to be cleaned.

FBS is composed mainly of lipids, salts and proteins. Although FBS is not well-characterized, it is known that the main component of FBS is BSA.[49] It is believed that incubation of the glass channels with FBS allows the proteins and lipids to adsorb onto the surface. This adsorption creates a surface coating which blocks sites that are preferential for cell adhesion. Initially, 100% FBS was left in all channels of the chip and cells were suspended in extracellular buffer (ECB) containing 10 mM Glucose and 10% (v/v) FBS. After it was observed that cells did not adhere to the channel surfaces, an electric field was applied to the analysis channel to determine if the surface coverage also prevented adhesion

of the post-lysis cellular debris. Several attempts to lyse cells in this manner resulted in complete clogging of the analysis channels. An example of this clogging can be seen in Figure 2.9. FBS has a high salt content and is highly conductive. A result of this high conductivity is that, during application of high electric fields to FBS-filled channels, Joule heating occurs. The presence of Joule heating was confirmed by measuring the current through the analysis channel while increasing the applied voltage. The current-voltage curve collected is shown in Figure 2.10. The measured current deviates from linearity around 1500 volts, which corresponds to an electric field of ~480 V/cm. This Joule heating caused heat-induced gelation of the FBS proteins, which irreversibly clogged the chip channels and rendered the chips unusable.

To avoid Joule heating, and therefore the heat-induced gelation of the FBS proteins, it was determined that the applied voltage must be maintained within the linear range of the i-V curve. Using an electric field of approximately 480 V/cm, it was determined that the chip could be operated for an extended period of time before gelation was observed. During operation of several flow through chips, hundreds of cells were lysed and analyzed with little to no debris collection observed at the lysis intersection. Often, any debris that did adhere was easily dislodged from the surface by pulling high vacuum on the waste channel. The chip operation was most greatly affected by the gelation that began to occur at the corners of the lysis intersection. Images of a chip at the beginning and end of an analysis run can be seen in Figure 2.11. In the images shown, 413 cells were lysed prior to significant protein gelation that required chip cleaning. A little accumulation of protein gelation at the lysis corners did not affect cell lysis or other aspects of chip operation. However, as the gelation continued to accumulate, chip cleaning was required to prevent irreversible clogging of the

analysis channel. In other instances (not shown), up to 500 cells lysed in a single run was observed prior to necessary chip cleaning. As long as the voltage was kept low enough to prevent Joule heating, the chip could be operated for long periods of time, enough to allow for a large data set (>100 cells) to be collected.

2.4 Conclusion

Prevention of biofouling is key to achieving high-throughput single cell analysis on a microfluidic device. Several different coatings and buffer additives were tested in order to determine the optimal coating to prevent biofouling of the chip channel surfaces. Although there are many other coating methods that could also be investigated, the coatings used here focused on PEG-based surfaces. After testing several different methods to produce PEG-based channel coverage, it was found that the results are highly inconsistent from chip-to-chip and the procedures are generally time-consuming. It was determined that the reactions used to attach PEG moieties to glass surfaces do not provide enough surface coverage to eliminate sites of preferential adhesion.

The optimal method for preventing biofouling was found to be a channel pretreatment with FBS. This method required only ~30 minutes to prepare the microchip channels for analysis. With careful control of the applied electric field, it was found that hundreds of cells could be lysed on a chip prior to any issues arising from biofouling or heat-induced gelation of the FBS proteins.

2.5 Tables and figures

Table 2.1 Comparison of cell adhesion on various channel coatings

Coating	Number of adhered cells after 20 minutes
Uncoated	63
PDMS/Pluronic	14
Pluronic Only	13
PEG-SPA	0

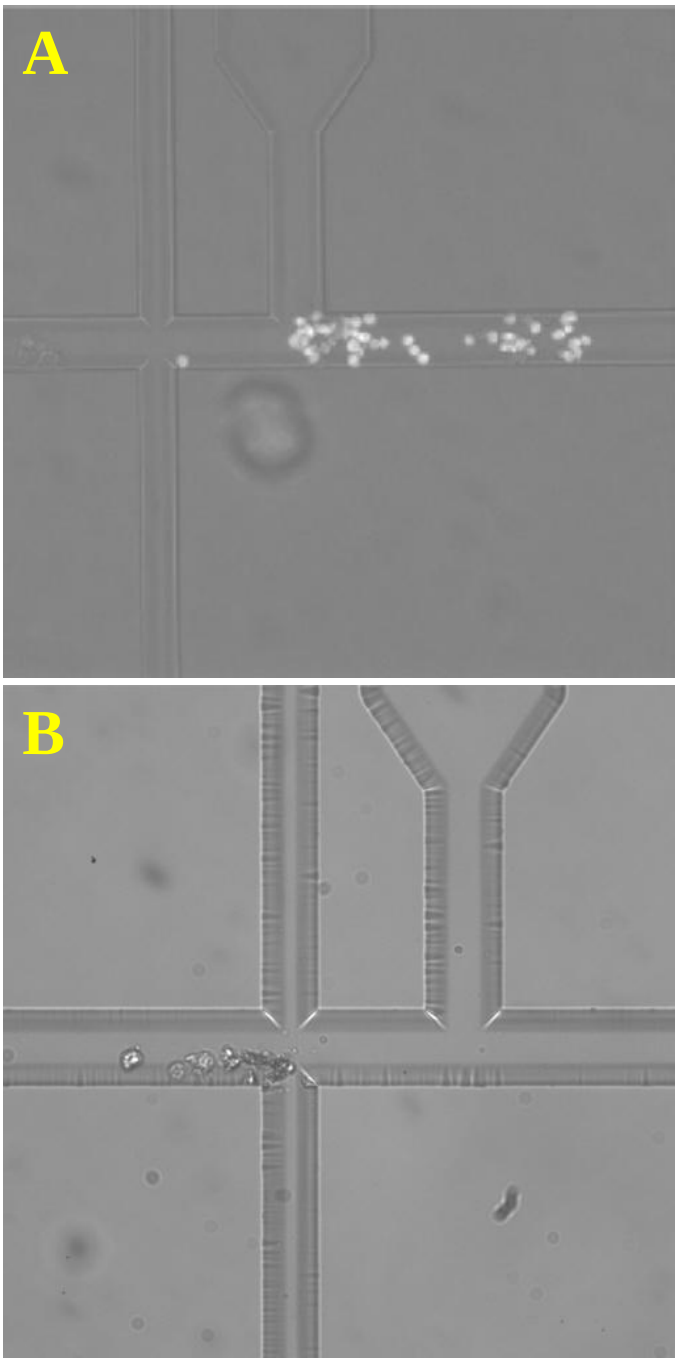

Figure 2.1 Images of a flow through device showing typical biofouling. In A), cellular adhesion that resulted in complete clogging of the cell flow channel is shown. In B), an example of post-lysis cellular debris collection at the lysis intersection is shown

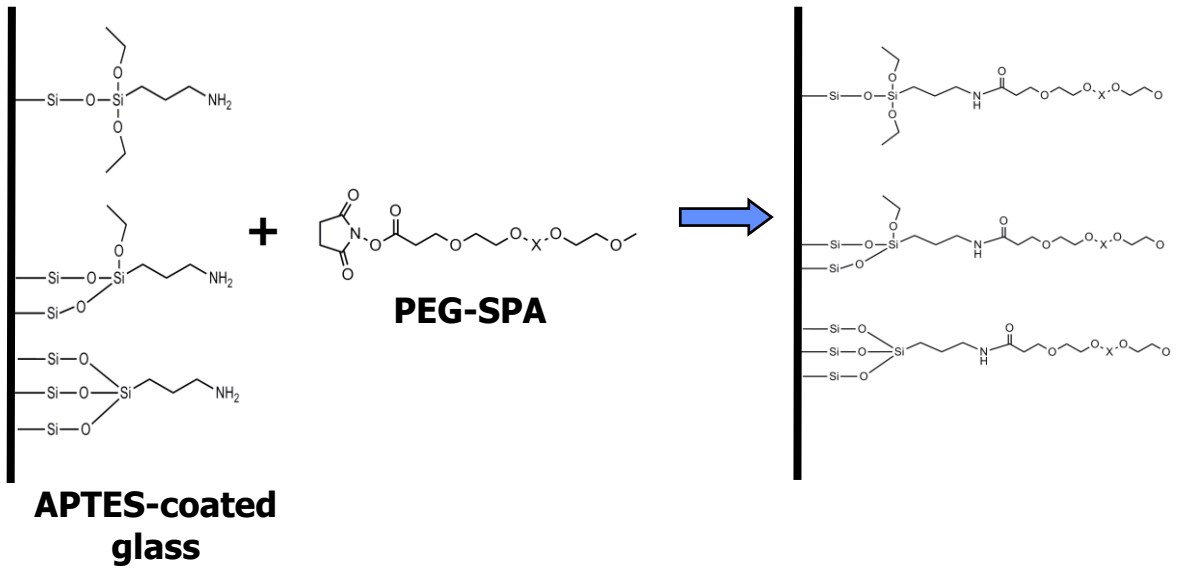

Figure 2.2 Reaction of PEG succinimidyl ester (PEG-SPA) with the amine groups of APTES

A

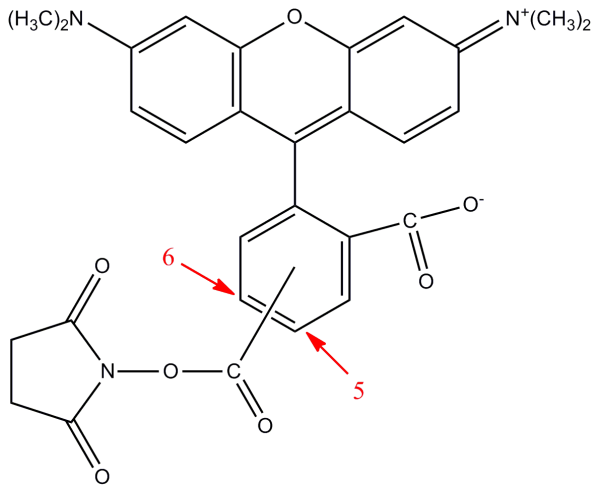

B

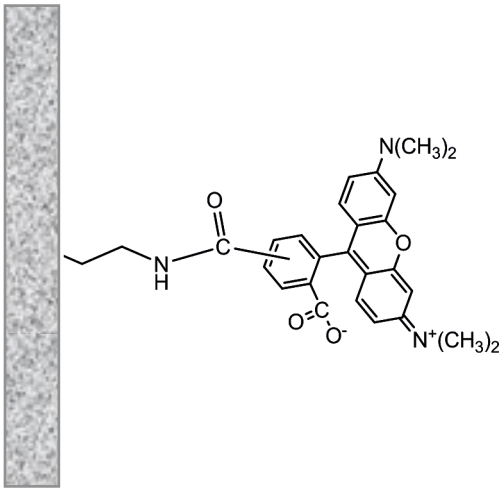

Figure 2.3 Structure for 5(and 6)-carboxytetramethylrhodamine, succinimidyl ester (5(6)-TAMRA) is shown in A). In B), an example of TAMRA covalently bound to APTES on a glass channel surface is shown.

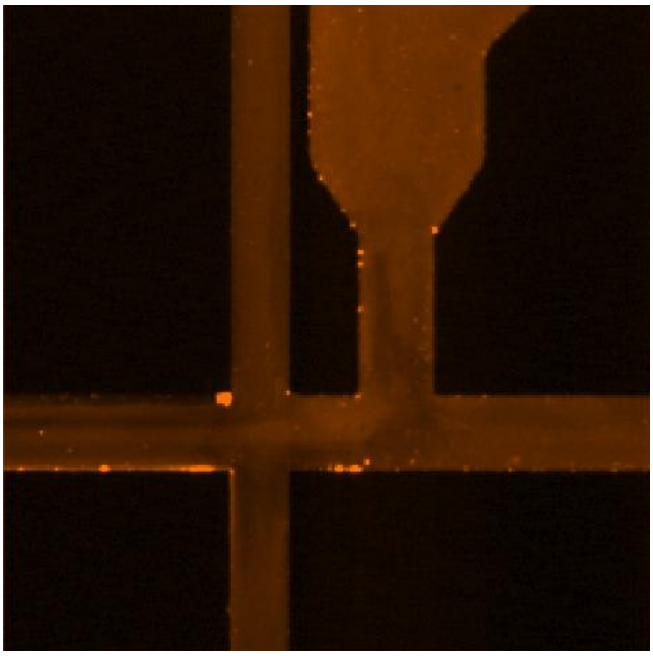

Figure 2.4 Image of flow through chip coated with APTES and TAMRA. This image demonstrates the channel fluorescence after the TAMRA has reacted with the amines of the APTES.

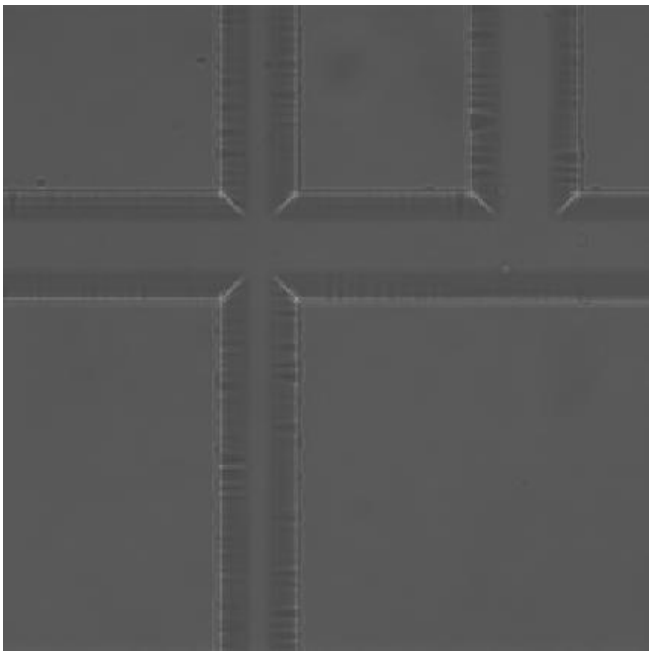

Figure 2.5 Image of a flow through chip coated with APTES/TAMRA demonstrating the lack of cell debris adhesion at the lysis intersection. Approximately 100 cells were lysed with no debris adhesion observed.

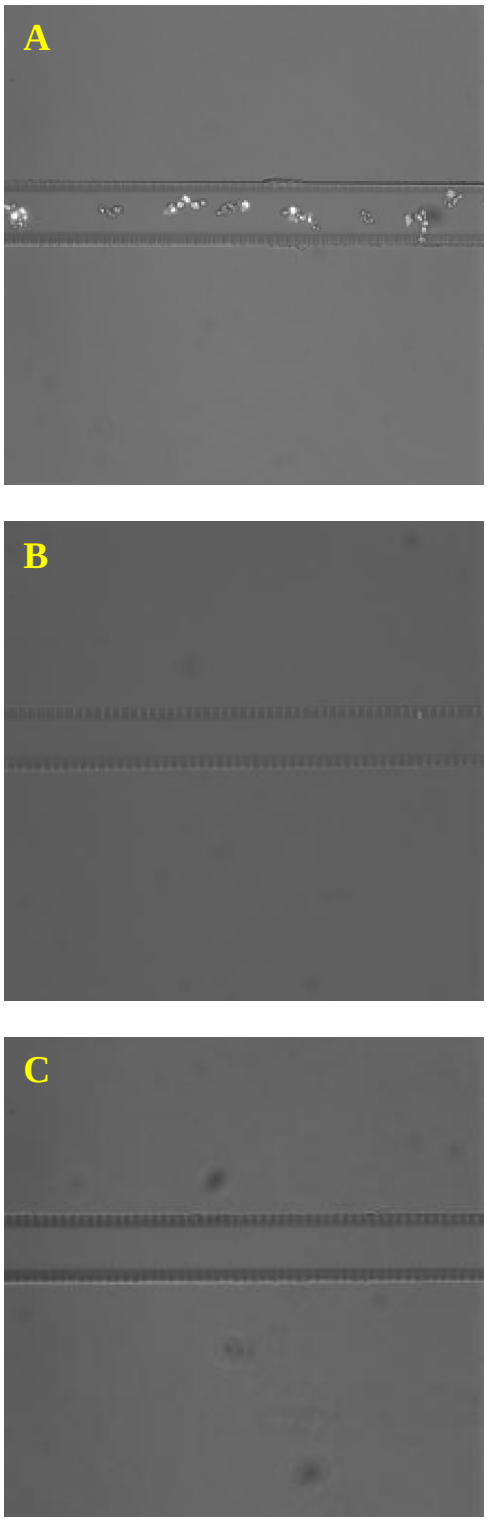

Figure 2.6 Images of an uncoated channel (A), APTES/TAMRA coated channel (B) and PEG-Urethane coated channel (C) to compare cell adhesion

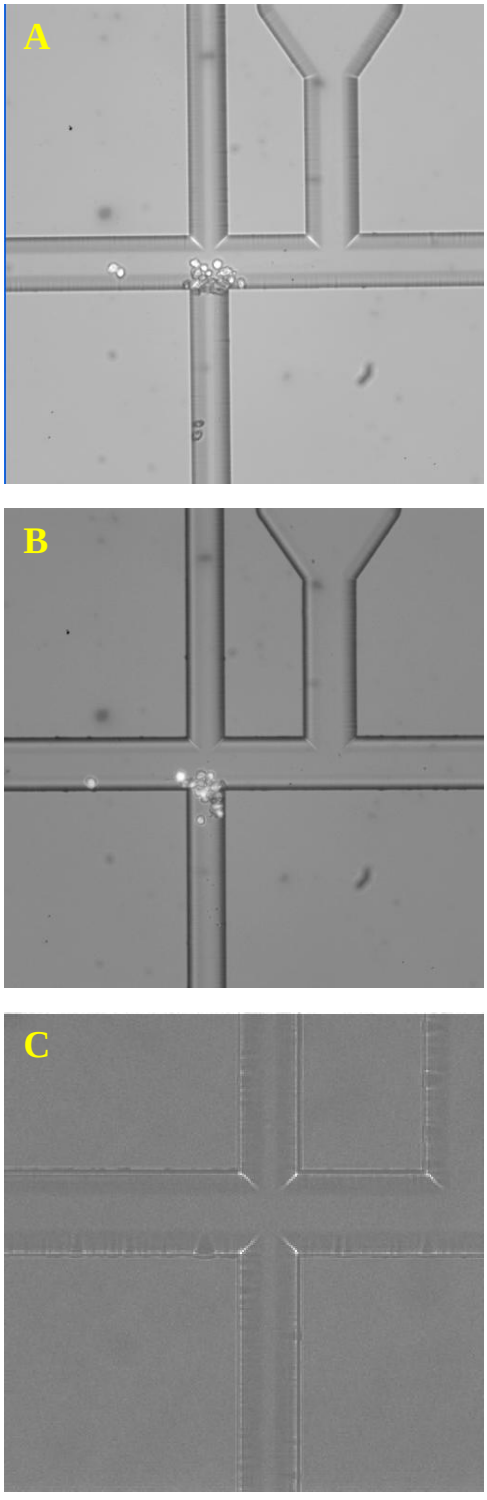

Figure 2.7 Pictures of the debris build-up on an uncoated (A), PEG-Urethane coated (B), and APTES/TAMRA coated (C) chip after on-chip cell lysis

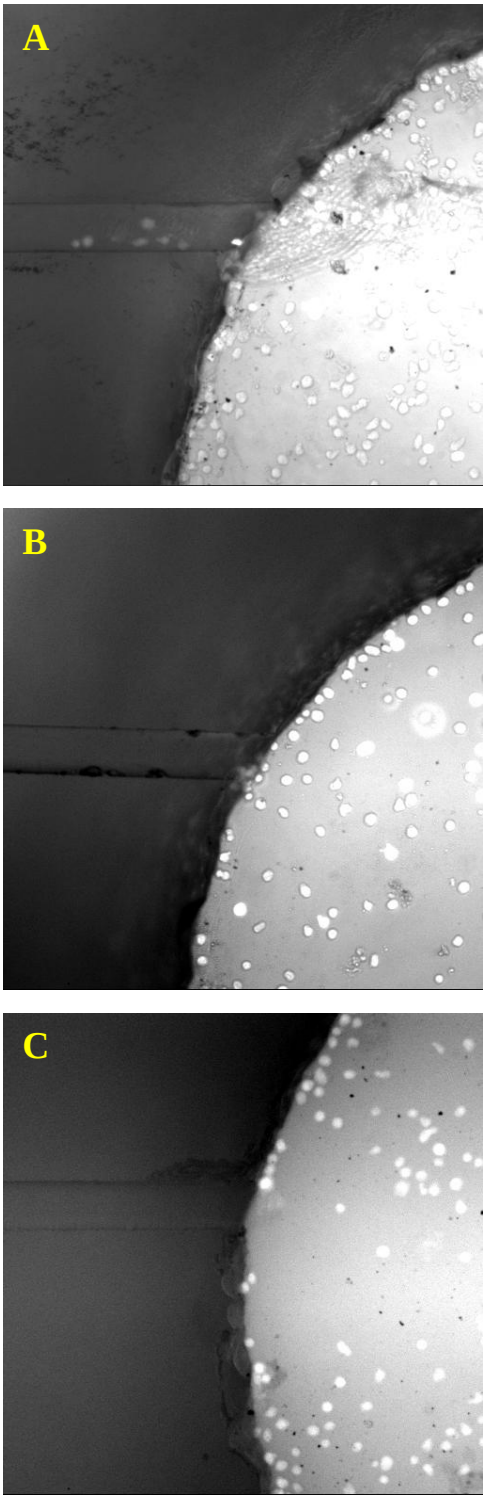

Figure 2.8 Images of cell adhesion at channel inlets for PEG-SPA (A), PEG-silane (B) and TAMRA (C) coated chips

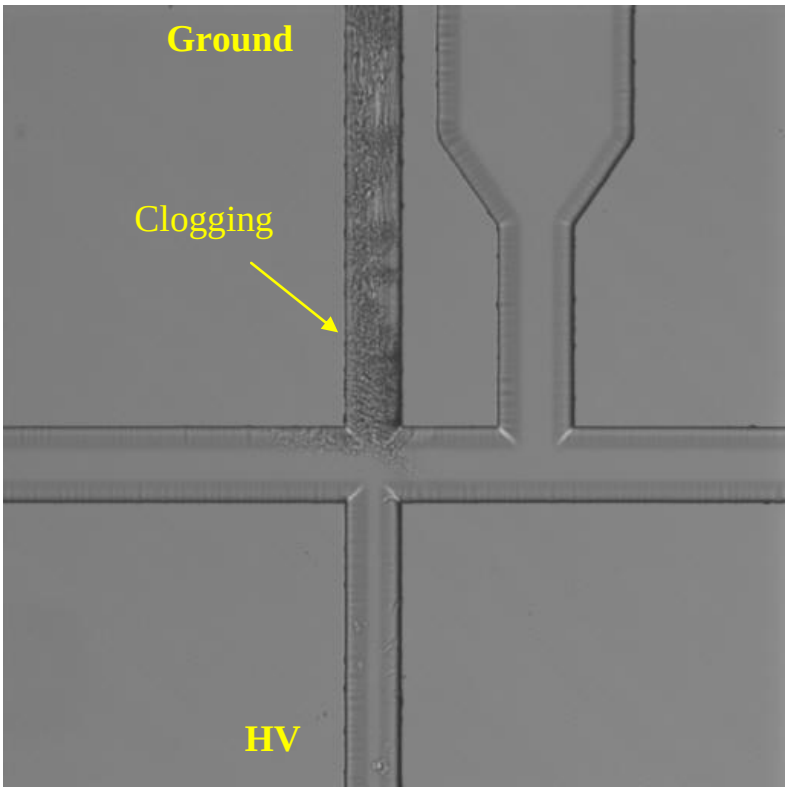

Figure 2.9 Image of a flow through chip channel showing the clogging that occurs when a high electric field is applied to a channel filled with FBS.

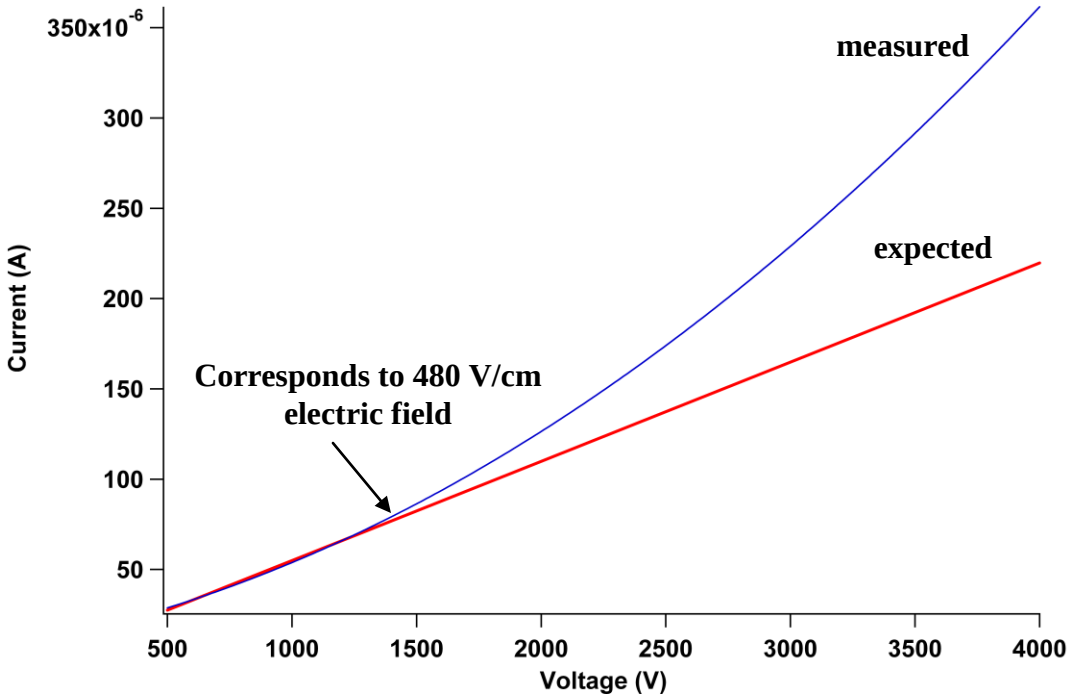

Figure 2.10 Current-voltage curve of the analysis channel filled with FBS. The red line indicates the expected current and the blue is the measured current. The deviation from linearity around 480 V/cm confirms Joule heating within the channels.

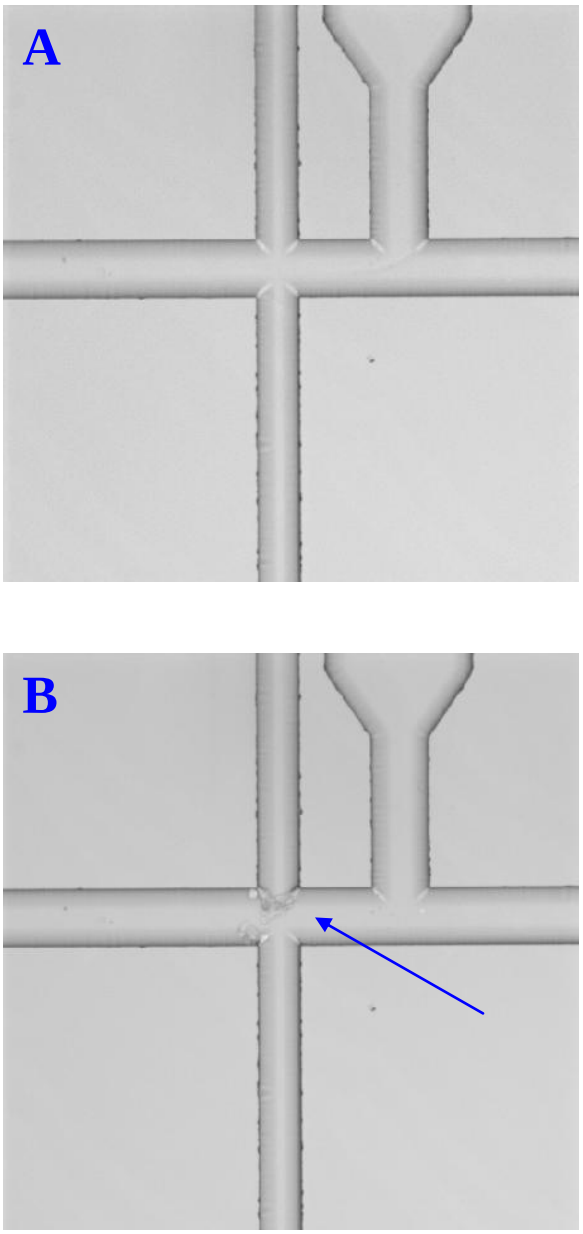

Figure 2.11 Images of a flow through chip, filled with 100% FBS, during operation. The start of chip operation is shown in A). The lysis intersection, after 413 cells were lysed, showing the accumulation of protein gelation at the upper corners of the intersection (indicated by the arrow) is shown in B).

2.6 References

(1) Yu, L. F.; Huang, H. Q.; Dong, X. L.; Wu, D. P.; Qin, J. H.; Lin, B. C. *Electrophoresis* **2008**, *29*, 5055.

(2) Gilman, S. D.; Ewing, A. G. *Analytical Chemistry* **1995**, *67*, 58.

(3) Sun, Y.; Yin, X. F. *Journal of Chromatography A* **2006**, *1117*, 228.

(4) Krylov, S. N.; Dovichi, N. J. *Electrophoresis* **2000**, *21*, 767.

(5) Yeung, E. S. *Journal of Chromatography A* **1999**, *830*, 243.

(6) Wu, H. K.; Wheeler, A.; Zare, R. N. *Proceedings of the National Academy of Sciences of the United States of America* **2004**, *101*, 12809.

(7) Bi, H.; Zhong, W.; Meng, S.; Kong, J.; Yang, P.; Liu, B. *Analytical Chemistry* **2006**, *78*, 3399.

(8) Groll, J.; Fiedler, J.; Engelhard, E.; Ameringer, T.; Tugulu, S.; Klok, H. A.; Brenner, R. E.; Moeller, M. *Journal of Biomedical Materials Research Part A* **2005**, *74A*, 607.

(9) Yang, M. S.; Li, C. W.; Yang, J. *Analytical Chemistry* **2002**, *74*, 3991.

(10) Dittrich, P. S.; Manz, A. *Nature Reviews Drug Discovery* **2006**, *5*, 210.

(11) Mehrishi, J. N.; Bauer, J. *Electrophoresis* **2002**, *23*, 1984.

(12) Chen, S. J.; Lillard, S. J. *Analytical Chemistry* **2001**, *73*, 111.

(13) Andersson, H.; van den Berg, A. *Current Opinion in Biotechnology* **2004**, *15*, 44.

(14) Sims, C. E.; Allbritton, N. L. *Lab on a Chip* **2007**, *7*, 423.

(15) Luk, V. N.; Mo, G. C. H.; Wheeler, A. R. *Langmuir* **2008**, *24*, 6382.

(16) Woods, L. A.; Roddy, T. P.; Ewing, A. G. *Electrophoresis* **2004**, *25*, 1181.

(17) Price, A. K.; Culbertson, C. T. *Analytical Chemistry* **2007**, *79*, 2614.

(18) Breslauer, D. N.; Lee, P. J.; Lee, L. P. *Molecular Biosystems* **2006**, *2*, 97.

(19) Sugiura, S.; Edahiro, J. I.; Sumaru, K.; Kanamori, T. *Colloids and Surfaces B-Biointerfaces* **2008**, *63*, 301.

(20) Kim, P.; Jeong, H. E.; Khademhosseini, A.; Suh, K. Y. *Lab on a Chip* **2006**, *6*, 1432.

(21) Li, H.; Wu, H. Y.; Wang, Y.; Sims, C. E.; Allbritton, N. L. *Journal of Chromatography B* **2001**, *757*, 79.

(22) Chang, Y.; Liao, S. C.; Higuchi, A.; Ruaan, R. C.; Chu, C. W.; Chen, W. Y. *Langmuir* **2008**, *24*, 5453.

(23) Huang, B.; Wu, H. K.; Bhaya, D.; Grossman, A.; Granier, S.; Kobilka, B. K.; Zare, R. N. *Science* **2007**, *315*, 81.

(24) Wheeler, A. R.; Throndset, W. R.; Whelan, R. J.; Leach, A. M.; Zare, R. N.; Liao, Y. H.; Farrell, K.; Manger, I. D.; Daridon, A. *Analytical Chemistry* **2003**, *75*, 3581.

(25) Li, P. C. H. *Microfluidic lab-on-a-chip for chemical and biological analysis and discovery*; Taylor & Francis/CRC Press: Boca Raton, 2006.

(26) Chang, H. T.; Yeung, E. S. *Analytical Chemistry* **1995**, *67*, 1079.

(27) Sun, X. F.; Liu, J. K.; Lee, M. L. *Electrophoresis* **2008**, *29*, 2760.

(28) Xue, Q. F.; Yeung, E. S. *Journal of Chromatography B-Biomedical Applications* **1996**, *677*, 233.

(29) Kennedy, R. T.; Oates, M. D.; Cooper, B. R.; Nickerson, B.; Jorgenson, J. W. *Science* **1989**, *246*, 57.

(30) Chao, T. C.; Ros, A. *Journal of the Royal Society Interface* **2008**, *5*, S139.

(31) Nevill, J. T.; Cooper, R.; Dueck, M.; Breslauer, D. N.; Lee, L. P. *Lab on a Chip* **2007**, *7*, 1689.

(32) Gao, N.; Wang, W. L.; Zhang, X. L.; Jin, W. R.; Yin, X. F.; Fang, Z. L. *Analytical Chemistry* **2006**, *78*, 3213.

(33) Wang, H. Y.; Bhunia, A. K.; Lu, C. *Biosensors & Bioelectronics* **2006**, *22*, 582.

(34) Phillips, K. S.; Cheng, Q. *Analytical Chemistry* **2005**, *77*, 327.

(35) McPherson, T.; Kidane, A.; Szleifer, I.; Park, K. *Langmuir* **1998**, *14*, 176.

(36) Revzin, A.; Sekine, K.; Sin, A.; Tompkins, R. G.; Toner, M. *Lab on a Chip* **2005**, *5*, 30.

(37) Kirby, B. J.; Wheeler, A. R.; Zare, R. N.; Fruetel, J. A.; Shepodd, T. J. *Lab on a Chip* **2003**, *3*, 5.

(38) Smetana, K.; Lukas, J.; Paleckova, V.; Bartunkova, J.; Liu, F. T.; Vacik, J.; Gabius, H. J. *Biomaterials* **1997**, *18*, 1009.

(39) Matsunaga, T.; Hosokawa, M.; Arakaki, A.; Taguchi, T.; Mori, T.; Tanaka, T.; Takeyama, H. *Analytical Chemistry* **2008**, *80*, 5139.

(40) Madou, M. J. *Fundamentals of microfabrication : the science of miniaturization*; 2nd ed.; CRC Press: Boca Raton, 2002.

(41) Jacobson, S. C.; Hergenroder, R.; Koutny, L. B.; Warmack, R. J.; Ramsey, J. M. *Analytical Chemistry* **1994**, *66*, 1107.

(42) Jacobson, S. C.; Koutny, L. B.; Hergenroder, R.; Moore, A. W.; Ramsey, J. M. *Analytical Chemistry* **1994**, *66*, 3472.

(43) Chuang, Y. J.; Huang, J. W.; Makamba, H.; Tsai, M. L.; Li, C. W.; Chen, S. H. *Electrophoresis* **2006**, *27*, 4158.

(44) McClain, M. A.; Culbertson, C. T.; Jacobson, S. C.; Allbritton, N. L.; Sims, C. E.; Ramsey, J. M. *Analytical Chemistry* **2003**, *75*, 5646.

(45) Ladd, J.; Zhang, Z.; Chen, S.; Hower, J. C.; Jiang, S. *Biomacromolecules* **2008**, *9*, 1357.

(46) Cunliffe, J. M.; Baryla, N. E.; Lucy, C. A. *Analytical Chemistry* **2002**, *74*, 776.

(47) Qiu, Y.-Z., Dou-Yong Min, Chi Ben, Jian Shen, Qiang Chen, Si-Cong Lin *Chinese Journal of Polymer Science* **2005**, *23*, 611.

(48) Fisher, L. *Journal of the Chemical Society-Faraday Transactions* **1993**, *89*, 2567.

(49) Kim, Y. L.; Im, Y. J.; Lee, Y. K.; Ha, N. C.; Bae, Y. S.; Lim, S. M.; Okajima, F.; Im, D. S. *Biochem Bioph Res Co* **2006**, *351*, 953.

Chapter 3: Characterization of Cell Lysis Events on a Microfluidic Device for High-Throughput Single Cell Analysis

3.1 Introduction

The flow through device, shown in Chapter 1, Figure 1.1, is capable of analyzing single cells at rates up to 7-12 cells per minute.[1] The device operates by hydrodynamically flowing cells through an electric field where subsequent electrical cell lysis occurs. The resulting cell lysate is electrokinetically injected into the analysis channel for electrophoretic separation and laser induced fluorescence (LIF) detection. A focusing channel just prior to the cell lysis intersection constricts the cell flow path and forces the cells into approximate single file for LIF detection. This cytometric signal marks the on-set of the lysate separation. Since its initial introduction, development has focused on characterizing the device and making it amenable to collection of biologically relevant data. The work discussed in this chapter aims to increase individual cell analyte detection capabilities and quantification accuracy.

For this microchip design, it is critical to maximize the amount of cell lysate injected into the analysis channel. During device characterization, it was observed that the cell flow path through the lysis intersection has an affect on the amount of cell lysate that injects into the analysis channel. Analyte loss can be problematic for detection of low concentration analytes; thus, improving the lysate injection efficiency will aid detection and provide improved quantification. We demonstrate that by controlling the surface charge on the analysis channel, we can eliminate variability in the cell flow path across the lysis

intersection. This improved control ensures that each cell experiences the same environment throughout the analysis and will eliminate potential device-imposed bias on the individual cell analyses.

3.2 Experimental

3.2.1 Chemicals

Unless otherwise stated, all chemicals were purchased from Sigma (St. Louis, MO, USA). B270 glass substrates, with chrome and positive photoresist (AZ1518) pre-applied, were purchased from Telic Company (Valencia, CA, USA).

3.2.2 Microchip fabrication

The microfluidic channel network layout is shown in Chapter 1, Figure 1.1. The microchip fabrication procedure is the same as that detailed in Chapter 2.

3.2.3 Pluronic channel coating

To reduce cell adhesion to the glass surfaces, the channels were coated with a 30% (w/w) solution of Pluronic F-127 (BASF, Mount Olive, NJ) in water. The coating procedure is described in Chapter 2.

3.2.4 Electroosmotic flow reversal

The chip was prepared with the Pluronic F-127 as stated above, however, only the cell flow channel was coated. This was accomplished by placing the 30% (w/w) Pluronic F-127 solution in the cell flow and focusing reservoirs only. Water was placed in the separation buffer and analysis reservoirs and vacuum pulled on the sample waste reservoir to coat. Throughout the Pluronic coating, the chip was placed on an ice block. After coating, the channels were rinsed with water to remove excess Pluronic solution. Immediately following the Pluronic coating procedure, the analysis channel was dynamically coated with

a polyamine compound, PolyE323 (synthesis and structure described elsewhere).[2-3] This coating was performed by placing a 6% (v/v) solution, pH 7.0, of PolyE323 in the separation buffer and analysis reservoirs. Water was placed in all other reservoirs. Vacuum was then applied to the cell waste channel for approximately 1 hour to pull the PolyE323 compound through the analysis channel to cell waste. The channels were then rinsed with water. All channels, except for the focusing channel, were filled with separation buffer for the experiments. The focusing channel was filled with a 50:50 mixture of separation buffer and 1% (v/v) Triton-X surfactant. The Triton-X was used to aid in removing cellular debris that often collects within the lysis intersection during chip operation.

3.2.5 Cell culture and preparation

Jurkat cells (TIB-152, ATCC) were prepared using the same procedure detailed in Chapter 2.

3.2.6 Device operation and data collection

The electrophoresis buffer consisted of 50 mM Tris, 10 mM Boric Acid, 1 mM Spermine, 1 mM TCEP-HCl and 30 mM PEG (MW 200 g/mol), pH 9.0. The loaded cells were transferred to the cell flow reservoir. The chip was positioned on a microscope (Nikon Eclipse TE2000-U, 10X objective) to observe the cell flow and lysis events. Cell fluorescence was observed by excitation with a mercury lamp. The emission light was filtered through a Semrock (Rochester, NY) Brightline GFP-3035B-NTE filter.

To operate the chip, cells were hydrodynamically pulled across the cell flow channel by applying negative pressure to the cell waste reservoir. Platinum electrodes, placed in the separation buffer and analysis reservoirs were used to apply a DC voltage for both electrical cell lysis and electrophoretic lysate separation. The electric field was applied only along the

separation buffer and analysis channels. The voltage was supplied by a Bertan power supply (Model 2866A, Bertan, Hicksville, NY). For all reported experiments, 8 kV was applied to the analysis channel electrode. This applied voltage gives electric field values in a range from 2400 to 2600 V/cm along the analysis channel between the 90º turn and the channel intersection where lysis occurs. The hydrodynamic flow was adjusted with the attached syringe until cell lysis was observed.

Cell lysis images were obtained using a Cascade II EMCCD camera (Photometrics, Tucson, AZ) controlled by the NIS-Elements Advanced Research software package (Nikon, Melville, NY). The camera was set to collect at the maximum frame rate possible and was operated at -80ºC. Both the NIS-Elements Basic and Advanced Research software packages were used to analyze the collected images and to determine the xy-coordinates for plotting the cell flow paths through the microfluidic device. A cell's xy-coordinates were measured at the approximate center of the observed cell.

For cell simulations, 10-μm fluorescently-labeled polystyrene beads (Polysciences, Inc., Warrington, PA) diluted in extracellular buffer were used. The bead solutions were placed in the cell flow reservoir and pulled through the chip in the same manner as the cells. The same electric fields used for the cell experiments were applied for the bead experiments, where applicable. For electroosmotic flow analysis, a concentrated solution of Rhodamine B, a neutral marker,[4] was placed in the sample cell reservoir and pulled through the chip in the same manner as the cells and beads.

3.3 Results and discussion

Rapid cell lysis is critical to accurately capture the state of intracellular analytes.[5-6] When the microchip operation was previously described,[1] complete cell lysis was reported to

occur in under 33 milliseconds (ms). Due to camera frame rate limitations (max 30 frames per second (fps)), an accurate cell lysis time measurement was difficult to determine. In the images taken of lysis events, the cells appear intact in one frame and completely lysed in the subsequent frame. However, it was apparent from the collected images that electrical cell lysis occurs faster than 33 ms. Using a Cascade II EMCCD camera and focusing on a region of interest, higher frame rate data acquisition of on-chip cell lysis events were collected. The region of interest used to capture the cell lysis event images is shown in Figure 3.1A. Typical frame rates for this set-up ranged from approximately 100 to 160 fps and the cell lysis events were observed at intervals of ~6-10 ms. This allowed for more precise determination of cell lysis event timing.

A sequence of frames from a cell lysis event recorded at 133 fps (8 ms/frame) is shown in Figure 3.1B. At high electric fields, irreversible damage to the cell membrane occurs. It can be inferred that once lysate is observed to be leaving the cell, the cell is lysed. In the images shown in Figure 3.1B, the cell enters the lysis intersection in frame 1 and lysate is observed to be exiting the cell in frame 2. Thus, the cell was lysed in approximately 8 ms. Another lysis event is shown in Figure 3.1C. In this instance, the cell enters the lysis intersection in frame 2 and lysate is observed to be exiting the cell in frame 4. This cell required approximately 16 ms to lyse. Thus, electrical cell lysis occurs faster than the maximum time originally reported and is a much faster lysis method compared to chemical or mechanical lysis methods. These lysis methods require >250 ms to lyse a cell.[1,7-10]

Using the higher time resolution made possible by the increased camera speed, two distinct events at the lysis intersection were observed. The lysate of some cells appeared to completely inject into the analysis channel as the cell passed through the lysis intersection, as

seen in Figure 3.1B. In these cases, the cell enters the lysis intersection and lyses (frames 1 and 2, respectively) and the cell remains in the lysis intersection long enough for the lysate to eject from the membrane and inject into the analysis channel (frames 3-5). The cell membrane debris then continues with the hydrodynamic flow (frames 6-8) down the cell waste channel. In other instances, the lysate did not fully inject into the analysis channel before the cell membrane continues to waste. An example of this is shown in the images of Figure 3.1C. Here the cell enters the lysis intersection and lyses (frames 1-4). However, the cell membrane flows to waste before all of the cell lysate is ejected (frames 5-8). This type of event results in significant loss of cell lysate to waste and potentially affects the ability to detect low concentration analytes. Because of the effect on analyte detection, it is important to maximize the amount of lysate that injects into the analysis channel for each cell.

Our goal was to determine the cause of the observed differences in lysate injection events and, if possible, maximize the amount of lysate injected for each cell analyzed. Because biofouling often occurred at the lysis intersection during chip operation, only a limited number of cells were analyzed in a single run of the device. In one run, a total of 72 cells were recorded and it was observed that four different types of events take place within the lysis intersection. These events were labeled as (1) ”type A” to describe instances where the majority of a cell’s lysate appeared to inject into the analysis channel and the membrane flowed to cell waste; (2) “type B” to describe events where the cell lysate is partially injected into the analysis channel and a significant portion is lost down the cell waste channel; (3) “whole cell injected” to describe events in which the cell is injected, intact, into the analysis channel; and (4) “no lysis” to denote an event in which the cell passes through the lysis intersection into the cell waste channel without lysing. Of the 72 cells recorded, 43 cells

were observed to undergo lysis type A and 24 cells were of lysis type B. Only one cell was whole cell injected and four cells fell into the no lysis category. In this particular study, we were concerned with understanding the variability of cell lysate injection into the analysis channel. Therefore, the "whole cell injected" and "no lysis" events were discarded and the study focused only on the cells that lysed within the channel intersection.

From the images, the cell flow paths through the microfluidic device were plotted by determining the cell's x- and y-coordinates in each frame. Representative cell flow paths were plotted for lysis type A and B events and are shown in Figure 3.2. Figure 3.2A displays the flow path of the cells of lysis type A. As can be seen, all cells in this lysis category take a similar flow path in which their trajectory involves a small deviation into the analysis channel during the lysing process. The cell membrane then flows back up into the cell waste channel and on to waste with the hydrodynamic flow. The flow paths for lysis type B show a different trajectory than type A. The type B flow paths all deviate within the lysis intersection toward the separation buffer channel as seen in Figure 3.2B. It is believed that, because these cells take an upwards flow path, the electrokinetic injection force is not strong enough to overcome the hydrodynamic force and, therefore, a significant portion of the lysate continues down the cell waste channel.

It is known that the linear velocity of a cell through the lysis intersection will have an affect on the lysis event. If a cell travels too quickly through the channel intersection, it will not experience the electric field long enough to lyse. On the other hand, if the hydrodynamic force is too weak to overcome the cell's electrophoretic migration toward the anode, then the whole cell will be injected into the analysis channel. To determine if the transit rate across the channel intersection is the cause of the event variability, the linear velocities of cells

displaying the four types of lysis events were measured. The linear velocity of each cell was determined by measuring the distance the cell travels, prior to lysis, over a certain number of frames. The lysis event type and resulting velocity are shown in Table 1. As can be seen from the results, the linear velocities and the corresponding lysis event types do not follow a particular trend. For instance, the three type A cells are all traveling at approximately 0.50 mm/s. The type B cell was traveling at a slower linear velocity than the type A cells. The cells for the two whole cell injected events had linear velocities both above and below that of the type A cells. The linear velocity affects the exposure time of a cell to the electric field, which determines the extent of lysis and, in turn, will affect how much lysate injects into the analysis channel. However, it can be concluded that the linear velocities are not the cause of the variable flow paths through the lysis intersection.

With cell velocity eliminated as a possible cause, additional theories to explain the differing flow paths focused on cell membrane heterogeneity and electroosmotic effects at the lysis intersection. It is well-established that genetically identical cells vary in terms of their size, intracellular chemical composition and exterior membrane composition. This heterogeneity could affect their behavior within the electric field used for lysis.[11-15] Additionally, the microchips are dynamically coated with Pluronic F-127 to prevent cell adhesion. This coating should suppress the EOF within the analysis channel. Incomplete surface coverage or the removal of the Pluronic over time could result in exposed surface silanols that would create a cathodic EOF at the pH of the separation buffer (pH = 9.0). The combination of heterogenic cells with a residual EOF could affect the cell path through the lysis intersection.

The effect of cell heterogeneity was tested using 10 μm fluorescent polystyrene beads to simulate the cells. The beads are similar in size to the Jurkat cells yet have uniform surface charge.[8] The previous experiments were repeated with a solution of beads placed in the sample reservoir. The resulting flow paths without an electric field applied (Figure 3.3A) and with an electric field applied across the analysis channel (Figure 3.3B) were plotted. With no electric field applied, the beads follow the expected path through the lysis intersection as flow from the focusing channel pushes them towards the entrance of the analysis channel. Upon application of an electric field, the beads take an upward flow path similar to that of the type B cells. This indicates that a residual EOF may be present within the separation buffer and analysis channels, which drives the cells toward the cathode.

The presence of a residual EOF in the Pluronic coated channels was investigated using Rhodamine B, a neutral fluorescent marker. A solution of Rhodamine B diluted with ECB was placed in the cell flow reservoir and pulled through the chip in the same manner as the cells. A fluorescence image of the Rhodamine B flow path was captured using the Cascade II EMCCD camera and is shown in Figure 3.4A. With the electric field applied, a small percentage of Rhodamine B flows up the separation buffer channel confirming the presence of a cathodic EOF. The majority of the sample, however, shows the same upward deflection seen for cells that follow the type B flow paths and continues on to the cell waste reservoir. In fact, when the flow paths for the type B cells are overlaid with the Rhodamine B flow path, the upward deflections seen for both flows align well. This indicates that the residual EOF is the cause for the type B flow path.

Because the homogeneously charged beads displayed a uniform flow path, the varying flow paths observed for the cells could be caused by their surface charge

heterogeneity. Although all eukaryotic cells have negative surface charges,[16-17] it is possible that some have a more negative surface charge than others. This would result in a higher electrophoretic mobility towards the anode. It is believed that these more negatively charged cells deviate into the analysis channel long enough to eject a large portion of their contents (type A). The lower electrophoretic mobility of other, less negatively charged, cells are pulled toward the cathode by the residual EOF as they pass through the lysis intersection. These cells follow the path indicated in Figure 3.4A and some of their lysate is lost to waste.

To achieve maximum lysate injection for each cell that passes through the lysis intersection, the flow path analysis indicates that they should deviate into the analysis channel during lysis (Figure 3.2A). Currently, a consistent flow path is not achieved with the Pluronic coating which leads to the various lysate injection events. A possible way to ensure that cells take the type A flow path would be to increase the flow toward the anode. This was tested by reversing the cathodic EOF within the separation buffer and analysis channels to an anodic EOF. The EOF reversal within these channels was achieved by coating with a polyamine compound, PolyE323.[2-3] This compound interacts electrostatically with the glass surface and results in a large number of amine groups exposed to the bulk solution. The cell flow and waste channels were still coated with Pluronic F-127 to retain their cell anti-adhesive properties. Figure 3.4B demonstrates the EOF reversal with Rhodamine B now flowing towards the anode upon application of the electric field. The experiment using 10-μm diameter fluorescently labeled beads was repeated and shows that, with the EOF reversed, the bead flow paths are now consistent with the type A cell flow paths (Figure 3.5A).

The extent of lysate injection was tested on a chip coated using the new procedure. Cells were loaded with Oregon Green diacetate cytosolic dye in order to visualize the lysis events. The chip was prepared as described above with Pluronic F-127 on the cell flow and waste channels and PolyE323 on the separation buffer and analysis channels. Cells were pulled hydrodynamically through the lysis intersection and the flow paths observed and plotted with several cell paths shown in Figure 3.5B. In one run of the device, 25 cell paths were recorded before cellular debris buildup was observed in the lysis intersection. All cells were observed to take the optimal trajectory for efficient lysate injection. Due to the combination of a cell's electrophoretic mobility towards the anode coupled with the strong anodic EOF, a greater hydrodynamic velocity was required to prevent whole cell injections. The higher cell velocity reduced the extent of deviation into the analysis channel compared to the original experiments and reduced the cell exposure time to the electric field. The results of these experiments were that all lysed cells fell into the type A flow path category, but only 56% of the cells lysed. It was decided that the gain in consistent injection efficiency was worth the loss in lysis efficiency.

It is noted for future experiments that the hydrodynamic force pulling the cells through the electric field needs to be carefully controlled. This is to ensure that the appropriate cell linear velocity is achieved for maximum lysate injection. Here, the change in the analysis channel coating procedure to reverse the EOF allows for greater control over the cell flow path through the lysis intersection. This device improvement forces each cell to experience similar flow paths through the lysis intersection and will reduce potential bias in the individual cell analyses.

3.4 Conclusion

One important aspect of the devices being developed for single cell analysis is that they provide reproducible conditions for each cell. This is to ensure that the data collected from each cell is as accurate as possible. Each cell is considered to be a different sample and therefore will display different results compared to the previous and subsequent cell analyzed. Since there is no blank available, it has to be inferred that the data collected from each cell is an accurate snapshot of the cellular state at the time of analysis. It is critical to ensure that the device used to collect the data is not biasing the analysis. This can best be achieved by ensuring that each cell is treated in exactly the same manner from the beginning to the end of the analysis. In the experiments shown here, we demonstrate that the fluid transport within the device must be appropriately controlled so that all cells pass through the lysis electric field with similar trajectories to achieve similar lysate injection characteristics. This will further improve the accuracy of single cell analysis by ensuring that varying results observed are due to cell heterogeneity, not to a bias imposed by the measurement device

3.5 Tables and figures

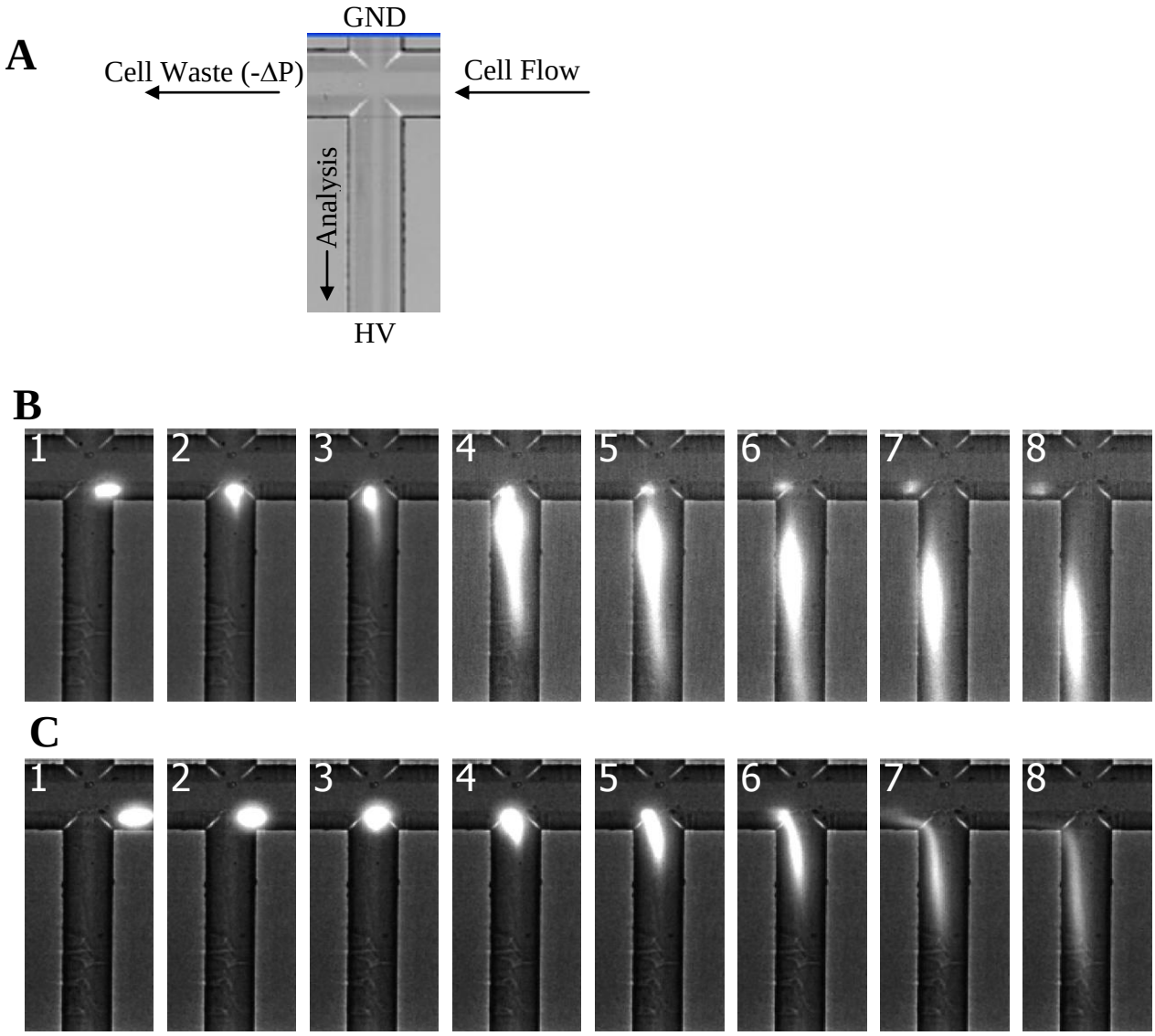

Figure 3.1 Images of cell lysis events collected at 132 fps. A) White light image of chip showing the region of interest (ROI) captured; B) Images of a cell lysis event in which the majority of the lysate is injected into the analysis channel. Images 1-2 display the cell lysing. Images 3-6 display the cell lysate ejecting from the cell membrane within the channel intersection. Images 7-8 show the flow of the cell membrane to waste and the migration of the cell lysate (Oregon Green) down the analysis channel to the detection point; C) Images of a cell lysis event in which a significant portion of the cell lysate is lost to waste. Images 6-8 demonstrate the flow of some cell lysate down the cell waste channel with the cell membrane post-lysis.

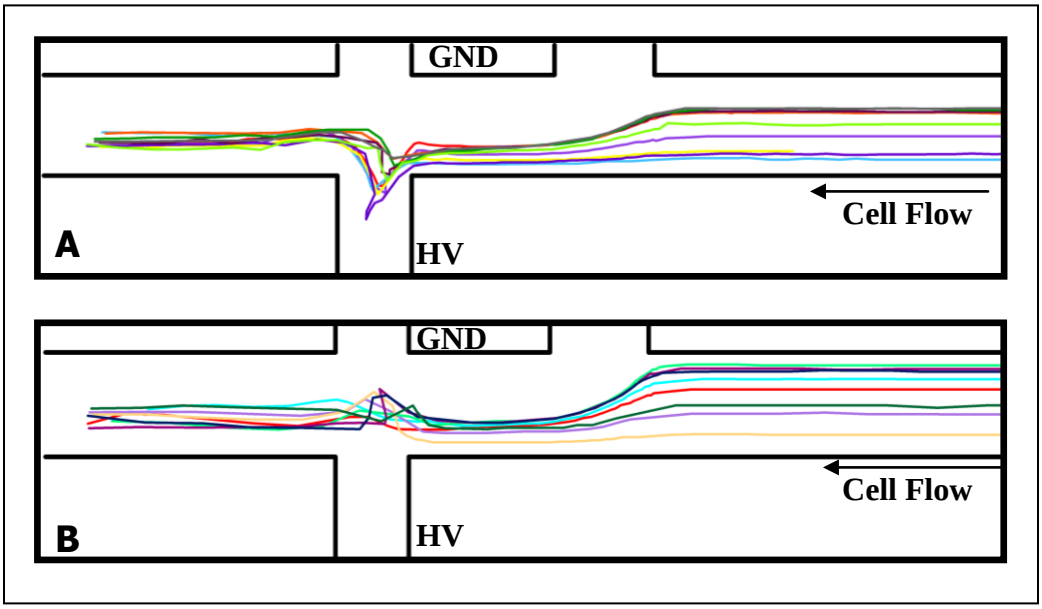

Figure 3.2 Cell flow paths plotted for A) lysis events in which the majority of lysate is injected into the separation channel (Type A events) and B) lysis events in which a significant amount of cell lysate is not injected and flows with the hydrodynamic flow to waste (Type B events).

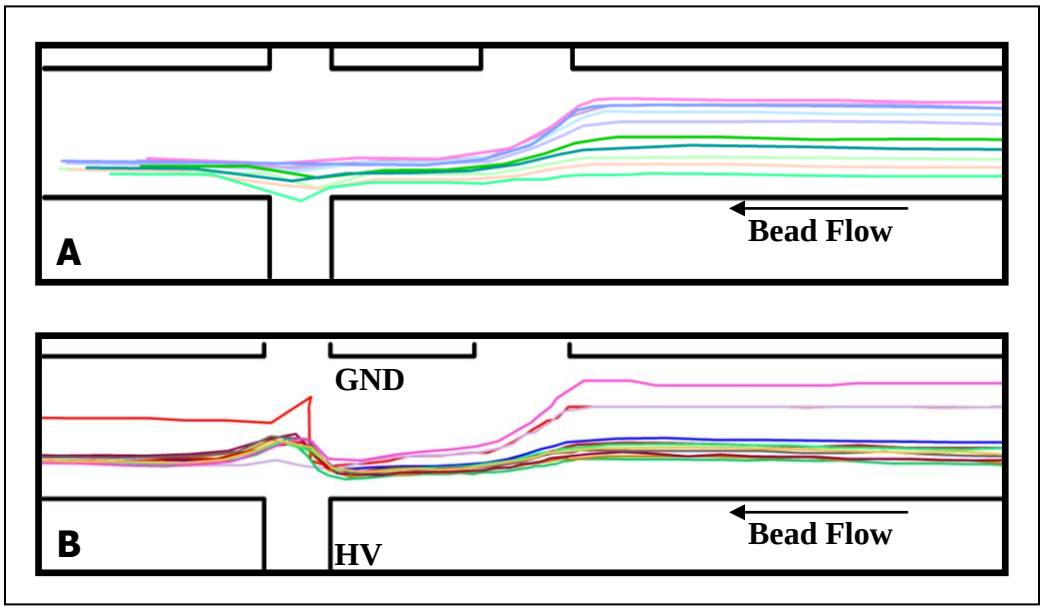

Figure 3.3 Plotted flow paths of 10 μm-diameter fluorescently labeled polystyrene beads with A) no electric field applied along the analysis channel and B) electric field applied along the analysis channel

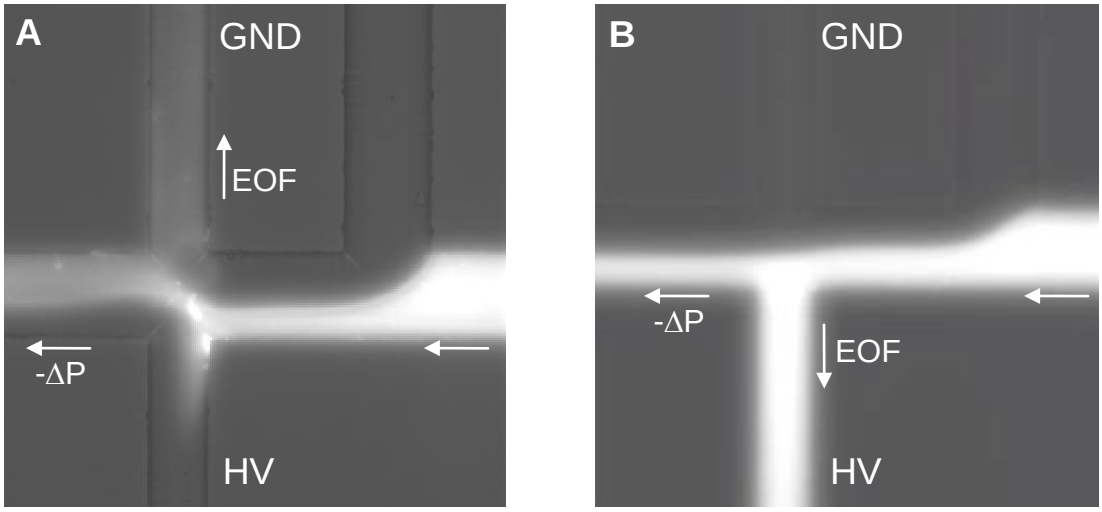

Figure 3.4 Images displaying the Rhodamine B flow path to visualize the direction of electroosmotic flow within the analysis channel. Rhodamine B was pulled from the sample reservoir to waste through application of negative pressure on the waste reservoir. A DC electric field was applied along the analysis channel. In A) the analysis channel was coated with Pluronic F-127 and the EOF was observed to be slightly cathodic. In B) the EOF was reversed by coating the analysis channel with a polyamine compound, PolyE323. The flow of Rhodamine B to the anode confirms the EOF reversal.

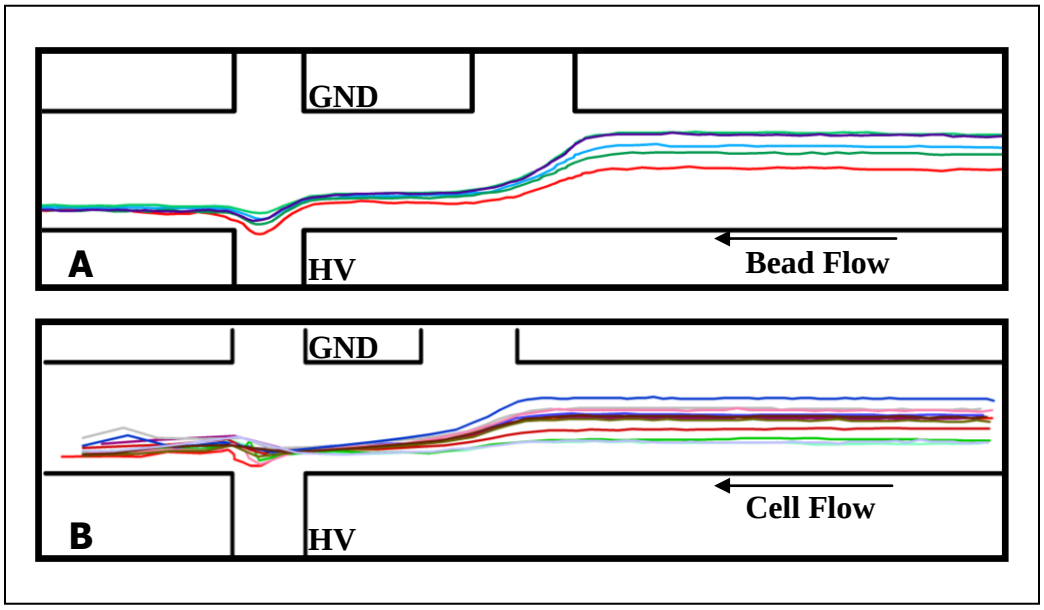

Figure 3.5 Plotted flow paths of A) beads and B) cells after electroosmotic flow reversal within the analysis channel. In A), 10-μm diameter fluorescently-labeled polystyrene beads all demonstrate a flow path in which they deviate into the analysis channel due to the pull of the anodic EOF. This flow path is similar to that of the type A cells. The flow path of Jurkat cells through the lysis intersection with the EOF reversed can be seen in B). All cells were observed to take similar flow paths.

Table 3.1 Event types and corresponding linear flow rates for cells that passed through the lysis intersection. During the data collection period, six cells passed through the lysis intersection and three event types were observed. For each cell, the linear flow rate was measured along the cell flow channel between the channel inlet and the intersection with the focusing channel.

Cell Number	Event Type Observed	Cell Linear Flow Rate (mm/s)
1	Type A	0.50
2	Whole Cell Injection	0.51
3	Type B	0.32
4	Type A	0.49
5	Type A	0.50
6	Whole Cell Injection	0.42

3.6 References

(1) McClain, M. A.; Culbertson, C. T.; Jacobson, S. C.; Allbritton, N. L.; Sims, C. E.; Ramsey, J. M. *Analytical Chemistry* **2003**, *75*, 5646.

(2) Hardenborg, E.; Zuberovic, A.; Ullsten, S.; Soderberg, L.; Heldin, E.; Markides, K. E. *Journal of Chromatography A* **2003**, *1003*, 217.

(3) Ullsten, S.; Zuberovic, A.; Wetterhall, M.; Hardenborg, E.; Markides, K. E.; Bergquist, J. *Electrophoresis* **2004**, *25*, 2090.

(4) Wang, W.; Zhou, F.; Zhao, L.; Zhang, J. R.; Zhu, J. J. *Journal of Chromatography A* **2007**, *1170*, 1.

(5) Sims, C. E.; Allbritton, N. L. *Lab on a Chip* **2007**, *7*, 423.

(6) Sims, C. E.; Meredith, G. D.; Krasieva, T. B.; Berns, M. W.; Tromberg, B. J.; Allbritton, N. L. *Analytical Chemistry* **1998**, *70*, 4570.

(7) Li, P. C. H.; Harrison, D. J. *Analytical Chemistry* **1997**, *69*, 1564.

(8) Price, A. K.; Culbertson, C. T. *Analytical Chemistry* **2007**, *79*, 2614.

(9) Munce, N. R.; Li, J. Z.; Herman, P. R.; Lilge, L. *Analytical Chemistry* **2004**, *76*, 4983.

(10) Han, F. T.; Lillard, S. J. *Analytical Chemistry* **2000**, *72*, 4073.

(11) Sweedler, J. V.; Arriaga, E. A. *Analytical and Bioanalytical Chemistry* **2007**, *387*, 1.

(12) Breslauer, D. N.; Lee, P. J.; Lee, L. P. *Molecular Biosystems* **2006**, *2*, 97.

(13) Sims, C. E.; Bachman, M.; Li, G. P.; Allbritton, N. L. *Analytical and Bioanalytical Chemistry* **2007**, *387*, 5.

(14) Danna, E. A.; Nolan, G. P. *Current Opinion in Chemical Biology* **2006**, *10*, 20.

(15) Huang, W. H.; Ai, F.; Wang, Z. L.; Cheng, J. K. *Journal of Chromatography B-Analytical Technologies in the Biomedical and Life Sciences* **2008**, *866*, 104.

(16) Chen, S. J.; Lillard, S. J. *Analytical Chemistry* **2001**, *73*, 111.

(17) Mehrishi, J. N.; Bauer, J. *Electrophoresis* **2002**, *23*, 1984.

Chapter 4: Improvements to the flow through single cell analysis device to provide rapid, high-throughput chemical cytometry of dye and enzyme reporter loaded cells

4.1 Introduction

In Chapters 1 and 2, the flow through microfluidic device for single cell analysis was described. The proof of concept showed that the device was capable of analyzing 7-12 cells per minute; however, this throughput rate was not sustained for long periods of time. The main obstacle to achieving the collection of large data sets in a single run of the device was the cellular debris buildup that oftentimes clogged the analysis channel. This obstacle was overcome by employing a channel pretreatment with fetal bovine serum (FBS) described in Chapter 2. Through a simple procedure of incubating the channels with 100% FBS prior to chip operation, cellular adhesion and cellular debris buildup were minimal. This reduction in biofouling allowed the flow through chips to be operated for extended periods of time. For chip operation, the channels were also filled with 100% FBS and, after loading with cytosolic dyes, cells were suspended in 100% FBS for analysis. It is believed that the cause for the reduction in biofouling is that the proteins and lipids in FBS adsorb to the glass surfaces and act as blocking agents to prevent cells and cellular debris from adhering. In this chapter, operation of the flow through device with FBS is described showing single cell analysis with separation of both cytosolic dyes and a reporter substrate and product pair for analyzing protein kinase C (PKC) activity. The limitations of using FBS are discussed and a new channel network that was designed to overcome these restrictions is demonstrated.

4.1.1 Analysis of kinase enzymes using fluorescent peptide reporters

In mammalian cells, signaling transduction pathways are responsible for controlling most cellular functions from cell proliferation to apoptosis.[1] These signaling pathways are complex and involve protein-protein interactions, post-translational modifications of proteins and protein cleavage events.[2] Protein kinases are a class of enzyme that play a pivotal role in signaling pathways by catalyzing the transfer of a phosphate group from adenosine triphosphate (ATP) onto hydroxyl groups of the substrate protein.[3-5] Phosphorylation of a protein results in a conformational change and alters the ability of that protein to function within its specific pathway. The phosphorylation of proteins by kinase enzymes works in conjunction with dephosphorylation by phosphatase enzymes to control signaling transduction pathways.[6-7] Because of their stochastic nature, kinases are considered on/off switching mechanisms for cellular functions.[8]

There are hundreds of identified kinase enzymes that are intricately involved in important cellular processes; therefore, when these enzymes are not functioning properly, whether due to environmental factors or genetic mutations, some serious consequences result.[9-10] For example, focal adhesion kinase enzymes have been shown to be over-expressed in head, neck, colon, breast, prostate and liver cancer.[11] In other findings, high PI-3 kinase activity was observed in tumor tissue and increased Src kinase activity was detected in colon, breast and epithelial carcinomas.[12-13] Besides cancer, other disease states including immunodeficiencies, diabetes and neurological disorders have been linked to kinase misregulation.[2,14-20] Because many diseases can be traced to kinase malfunction, these enzymes have become important therapeutic targets for diagnosis, treatment and prevention.[2,12,21-23]

In order to identify therapeutic targets, the cellular function of kinases must be studied and their roles in different signaling transduction pathways understood. The traditional method for analyzing kinase activity in cells and cell lysates monitors the transfer of a radioactive phosphate group from [γ-^{32}P]-labeled ATP onto the enzyme's substrate peptide or protein.[24] Other typical methods used to analyze mammalian cells for kinase enzyme activity include an in-gel assay and western blot analysis.[11,25] In-gel assays involve the incorporation of a kinase substrate into a sodium dodecyl sulfate gel. Cell lysate samples are then electrophoretically separated on the gel. After protein renaturation, [γ-^{32}P]-labeled ATP is incubated with the gel and autoradiography used to detect and measure any phosphorylation.[26-27] Although this method is commonly used, the assay requires special handling techniques, is not highly reproducible and is not suited for high-throughput applications.[28] Western blotting techniques are also not suitable for high-throughput analysis because the methods are cumbersome and expensive due to the requirement of specific antibodies for each kinase to be studied. Other methods used for kinase analysis include: microscopy[1], flow cytometry[29], phospho-flow cytometry[30-31], immunocytochemistry[32-33], TLC[12], HPLC with UV absorption or fluorescence detection[34-36] and in vitro assays.[3,37] For higher copy number proteins, mass spectrometry detection has also been used.[38]

Electrophoresis is one of the most useful techniques for studying kinase enzymes. The enzymatic addition of the negatively-charged phosphate group onto the product peptides and proteins allows them to be rapidly separated in an electric field from their respective substrates. Additionally, entire signaling pathways can be studied because multiple enzyme substrate-product pairs can be simultaneously separated.[28,39] In one instance, Yeung and coworkers analyzed protein kinase A (PKA) inhibition from crude cell extracts using a CE

separation with UV detection.[40] Krylov et al. also studied PKA activity in cell extracts by CE through the use of an endogenous kinase substrate that was tagged with green fluorescent protein for detection. Electrophoretic separation of kinase substrate and products from cell lysates and single cells has also been demonstrated by the Allbritton laboratory.[37,41-43]

Oftentimes, to study kinase enzymes, secondary messengers such as calcium, diacylglycerol and cyclic AMP have been used to monitor protein phosphorylation.[3] More accurate methods of analyzing specific enzymes utilize substrate peptides.[28,34,37,41,44] These peptides are recognized and phosphorylated by the kinase. The substrate and product are then separated and detected to provide a means for determining the enzyme activity level. Detection is often accomplished through UV absorbance, fluorescent labels or radiolabeling.

As discussed in Chapter 1, traditional kinase studies have been performed using population methods where cell lysates are pooled and tested. This can be problematic because the methods to purify the protein kinases and their signaling markers dilutes the lysate samples; thus, making detection problematic even with very sensitive techniques. It is believed that to truly study cellular signaling, it must be studied in vivo.[4] Another reason for studying kinases at the single cell level is that signaling pathways can be activated or deactivated very quickly.[41,45] The time required for cell lysis and pooling of cell lysate can result in alterations of the analyte concentrations. Additionally, kinase malfunction may occur in only a subset of a cell population. To detect this heterogeneity within a cell population, single cell analysis must be performed.

The goal of the microfluidic device being developed here is to perform high-throughput chemical cytometry. Ideally, the device would be capable of electrophoretically separating and detecting any intracellular analyte of interest. However, the initial

development work has targeted the separation and detection of fluorescently-labeled protein kinase substrates and products. The Allbritton laboratory has developed substrates that are specific for kinase enzymes of interest. The substrate peptide discussed in this chapter is specific for phosphorylation by PKC.

PKC, originally discovered by Nishizuka in rat brain tissues, consists of a superfamily of enzyme isoforms, each with unique characteristics.[46-47] These enzymes are serine/threonine kinases, meaning they phosphorylate serine and threonine amino acids on their substrate proteins, and are activated by calcium, diacylglycerol and phospholipids.[48-49] The "C" in the name comes from the requirement that calcium be present for its activation.[50] The PKC enzymes are known to regulate several different cellular processes including: cellular proliferation, tumor promotion, differentiation and apoptosis.[1,51] PKC is also involved in the cellular repair process and plays an important role in memory formation.[41,43] It is a critical therapeutic target because its mis-regulation is linked to many diseases including, but not limited to: diabetes, bipolar disorder, Alzheimer's, arteriosclerosis, and Human Immunodeficiency Virus (HIV).[52] The over-expression of PKC is also highly linked to breast cancer and both its over- and under-expression implicated in colon cancers.[53-56]

Because proteins within cells cannot be readily amplified, fluorescent reporters are commonly employed to provide an adequate method for their detection.[45] Fluorescence detection can easily provide subattomolar detection limits which are sufficient for the copy numbers of most intracellular analytes. The enzyme substrates used in these studies are labeled with a carboxyfluorescein tag (FAM) for detection using laser induced fluorescence (LIF).

The PKC substrate sequence is shown in Figure 4.1 and is referred to as Myr-ss-SPKC. Myr-ss-SPKC consists of a short peptide sequence with one phosphorylation site, on the Serine residue, that the PKC enzyme will recognize.[57] The N-terminus of the peptide is labeled with the FAM group for detection. At the C-terminus, a myristoyl group is attached via a disulfide linkage. The myristoyl group is a C-14 fatty acid chain, which gives the peptide enough lipophilic character to pass through the cell membrane. The purpose of the myristoyl tag is to provide a passive method for loading cells, which will eventually be important for on-chip cell loading for device automation. Cells can be loaded with the enzyme substrate through a simple incubation in a solution containing the myristoylated peptide and have been shown to remain viable in up to 100 μM solutions of the Myr-ss-SPKC.[57] Because a cell's cytosol is a reducing environment, once the Myr-ss-SPKC crosses the membrane into the cytosol of a cell, the disulfide bond is cleaved. The cleavage of the disulfide bond removes the fatty acid group and reduces the lipophilicity of the peptide. Thus, the peptide is "trapped" in the cell and cannot cross back out through passive means. Using this peptide, trials to collect biologically relevant information using the flow through device with FBS pretreatment are discussed.

4.2 Experimental

4.2.1 Chemicals

Unless otherwise stated, all chemicals were purchased from Sigma (St. Louis, MO, USA). B270 glass substrates, with chrome and positive photoresist (AZ1518) pre-applied, were purchased from Telic Company (Valencia, CA, USA).

4.2.2 Microchip fabrication

Flow through microchips were fabricated in the same manner described in Chapter 2. The Double-T microfluidic channel network layout is shown in Figure 4.2. These microchips were fabricated using the same materials and procedure for the flow through devices. Buffer and sample reservoirs were created by attaching cloning cylinders (Fisher Scientific, 4 mm i.d.) around the access holes using Norland 63 optical adhesive (Norland Products, Inc., Cranbury, NJ). Each reservoir holds a volume of approximately 200 μL. For application of vacuum, a syringe was connected to the waste reservoir of the chip, a 1/16″ barbed female Luer lock (Upchurch Scientific, Oak Harbor, WA) was altered by removing the barb and drilling an ~ 3 mm hole into the bottom using a Dremel tool. This Luer lock was then epoxied around the access hole of the cell waste channel. Tygon tubing (1/16" i.d.) was attached to the female Luer lock via a 1/16″ barbed male Luer lock (Upchurch Scientific).

Several different Double T microchips were used for this study. Channel depths and widths were determined using a stylus-based surface profiler (P-15; KLA-Tencor, Mountain View, CA). Widths are reported as the full channel width measured at the top of the channel. All channels were etched to a depth of approximately 25 μm. The cell flow (CF), cell waste (CW), analysis (A) and separation buffer (SB) channels were 62-64 μm wide. The total length of the channels (i.e., the A and SB channels) to which the electric field was applied was approximately 4.2 cm. The upper focusing (UF) channels were 221-226 μm wide at the widest part and ~16.5 mm long. The lower focusing (LF) channels were 82-83 μm wide and ~230 mm long. The CF channels were approximately 60 mm long.

4.2.3 Cell culture and preparation

Jurkat Cells (ATCC TIB-152, American Type Culture Collection, Rockville, MD; obtained from the University of North Carolina Tissue Culture Facility) were used for all experiments. Maintenance of the cell cultures was described in Chapter 2.

To load with dye, ~5 x 10^5 cells were pelleted (1000g for 3 minutes) and the supernatant discarded. The cells were re-suspended in an extracellular buffer (ECB: 135 mM NaCl, 15 mM KCl, 2 mM $MgCl_2$, 2 mM $CaCl_2$, 10 mM HEPES, pH 7.4) solution containing 18 μM Oregon Green 488 carboxylic acid diacetate 6-isomer and 17 μM carboxyfluorescein diacetate 6-isomer (Invitrogen, Carlsbad, CA). Oregon Green and carboxyfluorescein in diacetate form are membrane permeable and loading was achieved through simple incubation (~15 minutes) in a centrifuge vial while maintaining the cells at 37ºC. The cells were then washed three to four times by pelleting and re-suspension in ECB containing 10 mM glucose. Either ECB containing 10 mM glucose and 10% FBS or 100% FBS was used for the final re-suspension of cells.

To load cells with the Myr-ss-SPKC peptide, the cells were incubated in an approximately 5-10 μM solution of Myr-ss-SPKC for 15 to 30 minutes. The cells were then washed three to four times with ECB containing 10 mM glucose. The final suspension of the cells was in either ECB containing 10 mM glucose or 10% FBS or 100% FBS.

4.2.4 Microchip preparation

4.2.4.1 Flow through device preparation

The flow through devices were prepared with 100% FBS by pulling the FBS through the channels and allowing them to incubate for 15 to 30 minutes. The FBS was then flushed out and replaced with fresh FBS.

4.2.4.2 Double T chip preparation

The chip was first prepared by a brief rinse with 2X Nanostrip (Cyantek, Fremont, CA) followed by a thorough rinse with Nanopure H_2O. 1 N NaOH was pulled through the separation channel for approximately 15 minutes with DI water in the other channel reservoirs. The chip was flushed completely with DI water. 100% FBS was then pulled through only the CF channel by applying vacuum to the CW channel. During the FBS rinse, DI water was placed in the focusing (UF and LF) and separation channel (SB and A) reservoirs. While continuing to pull FBS through the CF channel, the focusing channels were filled with a buffer consisting of: 50 mM Tris, 10 mM boric acid, 1 mM spermine, 1 mM TCEP-HCl, 30 mM PEG (Tris/BA) that contained 0.1% Triton-X. The SB and A channels were filled with the Tris/BA buffer only. All solutions were pulled to waste for ~20 minutes prior to chip operation.

4.2.5 Chip operation and data collection

After the chips were prepared with FBS and the appropriate buffers, the loaded cells were transferred to the CF reservoir. The chip was positioned on a microscope stage (Nikon Eclipse TE2000-U, 10X objective) to observe the cell flow and lysis events. Cell fluorescence was observed through excitation with a Nikon Intensilight C-HGFIE (Nikon, Japan). The emission light was filtered through a Semrock (Rochester, NY) Brightline FITC-3540B-NTE filter.

To operate the chip, cells were hydrodynamically pulled through the CF channel to waste by applying negative pressure to the cell waste reservoir using a syringe. A wet/wet differential pressure transducer (0 to 1 psi, Omega Engineering, Inc, Stamford, CT) was used to monitor the applied negative pressure to the waste channel. The typical applied pressure

was between -0.2 and -0.4 psi (versus ambient pressure). A Sony ExwaveHAD color video camera was used to observe the on-chip cell flow and lysis. The cell flow rate was adjusted until cell lysis and lysate injection were observed. Platinum electrodes, placed in the SB and A reservoirs were used to apply a DC voltage for both electrical cell lysis and electrophoretic lysate separation. The electric field was applied only along the SB and A channels. The voltage was supplied by a Bertan power supply (Model 2866A, Bertan, Hicksville, NY). For the flow through device experiments, approximately 1.5 kV was applied between the SB and A channels to provide an electric field of 480 V/cm. For all reported experiments on the Double-T chip, voltages between 5 and 10 kV were applied between the SB and A channels. These applied voltages gave electric fields from 1190 to 2380 V/cm along the analysis channel. The flow path data was collected in the same manner described in Chapter 3.

For lysate data collection, an argon ion laser (Melles Griot, Carlsbad, CA) was used at the 488 nm line. The laser beam was passed through a dichroic filter and focused from the top of the chip onto the analysis channel, using a Mitutoyo M Plan Apo 20X long working distance (LWD) objective (Mitutoyo, Kanagawa, Japan). The laser was focused to a point on the analysis channel between 3 to 15 mm from the lysis intersection. A picture of the experimental setup and diagram of the laser optics is shown in Figure 4.3. The resulting fluorescence signal was passed back through the dichroic filter and then through a 530DF30 and 488 long pass filter (Semrock, Rochester, NY) The filtered fluorescence signal was collected using a Hamamatsu H7732-10 photosensor module (PMT) (Hamamatsu Photonics, Japan) and data was filtered using a Stanford Research Systems SR570 low noise current preamplifier (Stanford Research Systems, Sunnyvale, CA). Data was collected using a customized Labview program (National Instruments, Austin, TX).

4.2.6 Data Analysis

All data processing was performed using the Igor program (Wavemetrics, Inc, Lake Oswego, OR), version 6.0.0.0, or the Cutter 7.0 Labview program (University of Michigan).

4.3 Results and Discussion

4.3.1 Flow through chip for cytosolic dye separations

Once it was determined that a FBS channel pretreatment was highly effective in preventing biofouling of the channel surfaces, separation of cytosolic dyes was attempted. Using channels filled with 100% FBS provided the optimal reduction in biofouling; therefore, separations were attempted in 100% FBS. Cells were loaded with Oregon Green diacetate and carboxyfluorescein diacetate cytosolic dyes. The structures of these dyes are shown in Figure 4.4.

Prior to collecting lysate data, the electroosmotic flow within the separation channel was analyzed using Rhodamine B as a fluorescent neutral marker. It was believed that the EOF would be largely suppressed when using FBS as a channel pretreatment and separation solution. An image of the Rhodamine B flow path with an electric field applied along the SB and A channels is shown in Figure 4.5A, which clearly shows that the there is a cathodic EOF. Cells were also pulled through the chip with the electric field applied and the flow path of the cells at the lysis intersection determined. The flow path of two cells is shown in Figure 4.5B. The flow path of the cells in FBS takes a somewhat linear trajectory through the lysis intersection. According to the data discussed in Chapter 3, the trajectory is not optimal for maximum lysate injection. Yet, the injection of the negatively charged cytosolic dyes was sufficient for detection.

Next, the flow through microfluidic chip was operated to collect data from the dye-loaded cells. Cells, loaded with Oregon Green and carboxyfluorescein and suspended in

ECB containing 10% FBS and 10 mM glucose, were pulled through the chip at a linear flow rate of approximately 0.13 mm/s. An electric field of approximately 480 V/cm was applied along the analysis channel for collection of lysate data from the cells. It was found that the separation of Oregon Green and carboxyfluorescein is excellent (resolution >1.0) with good peak shape (i.e., no observed fronting or tailing). An example of the dye separation from a single cell is shown in Figure 4.6. Here, the laser was focused ~7 mm down the analysis channel from the lysis intersection. The dye resolution was calculated to be ~3.3. Because biofouling was not problematic when using FBS-filled channels, the chip could be operated for extended periods of time and large data sets collected. Data files were collected in five minute increments and in one operation of the device, hundreds of data points collected. From that data set, 129 useable data points were obtained, meaning that the cell lysate peaks did not co-migrate with the previous or subsequently lysed cells.

One issue that was noted during chip operation was that the resolution of the dyes decreased over time. It took only approximately 60 seconds of continuously applied electric field for the resolution between Oregon Green and carboxyfluorescein to become visibly degraded. An example of this resolution loss can be seen in Figure 4.7. It was hypothesized that this resolution loss was due to the high salt content of the ECB in which the cells are suspended. As the electric field was applied during chip operation, ECB flowed from the sample reservoir to waste with the hydrodynamic flow. Yet, some of the ECB components will also flow down the analysis channel because the ions present in the ECB electromigrate in the electric field (Figure 4.8). This flow of ions down the analysis channel changes the overall composition of the separation solution. It was found that the resolution loss was not as significant when cells were reconstituted in 100% FBS, rather than ECB, after loading, so

that all of the reservoirs contained the same solution composition. The resolution between Oregon Green and carboxyfluorescein from four cells suspended in 100% FBS during a one minute run of the chip is shown in Figure 4.9. A comparison of the resolution, over a five minute analysis run, between Oregon Green and carboxyfluorescein using ECB or 100% FBS to dilute the loaded cells is shown in Figure 4.10. When cells were constituted in ECB, the resolution between Oregon Green and carboxyfluorescein decreased from 3.2 at the beginning of the run to 1.4 at the end of a five minute analysis period. Using 100% FBS to suspend the cells, the resolution between the dye peaks was somewhat steady at 2.7 with a relative standard deviation of 5%. Some loss in resolution was still observed when cells were constituted in 100% FBS; however, the resolution loss was significantly less notable and is most likely due to depletion of the FBS salts within the electric field over time.

4.3.2 Analysis of cells loaded with Myr-ss-SPKC reporter peptide

After it was determined that cells should be suspended in 100% FBS to maintain resolution, cells were loaded with the PKC reporter peptide. These initial development runs were to determine if the peptide will inject into the analysis channel and could be detected in the FBS separation solution. It was found that the migration of the positively charged peptide to the detection region is slow. When the laser was focused ~11.5 mm from the lysis intersection, it took approximately 80 seconds for the peptide to reach the detection point. An example separation that was observed from a single cell loaded with the Myr-ss-SPKC peptide is shown in Figure 4.11. Because the separation was slow, only a few cells could be analyzed during a single five minute analysis run. In Figure 4.12, two five minute separations are shown displaying the analysis of 10 peptide-loaded cells. It is unknown which, if any, of the peaks observed is the phosphorylated product.

Because the separation was performed in FBS, which contains a great deal of lipids and proteins, it is unclear what type of electrophoretic separation is occurring (i.e., capillary zone electrophoresis (CZE), open tubular capillary electrochromatography (OTCEC) or micellar electrokinetic chromatography (MEKC)). Therefore, it is difficult to predict which peak will first migrate toward the detector. The SPKC and PSPKC peptides will be positively charged at physiological pHs (i.e., 7.4); therefore, the peptides should not electromigrate towards the anode. Yet, the fluorescently labeled peptide was observed to inject toward the anodic electrode. Filling the microchip channels with FBS results in a cathodic electroosmotic flow; therefore, it leads to the conclusion that a separation mode other than CZE is occurring. Additionally, FBS is known to contain protease enzymes. Proteases are enzymes that cleave proteins and peptides for cellular catabolism. It is possible that the peaks are due to protease cleavage of the peptide post-lysis. Because the separation time is long, there is time for the protease enzymes present to interact with the SPKC peptide while traveling down the analysis channel.

There are several major issues that arise when using 100% FBS not only for the channel pretreatment, but also for the lysate separation. The main problem, noted in Chapter 2, with using 100% FBS in the channels for the electrophoretic separation was that heat-induced gelation of the FBS proteins often occurred during application of an electric field higher than 480 V/cm. The limited electric field directly affects the separation efficiency and the ability to quickly separate the peptides. The content of the FBS also affects the separation and possibly breaks down the reporter peptide during the separation. FBS is, however, optimal for preventing debris build-up on the separation channels and allows chip operation for long periods of time. It was determined that a new chip design must be made

that separates the lysis region from the separation region so that the FBS can be used yet will not affect the electrophoretic separation. This alternative chip design would allow the use of FBS within the cell flow channel and at the lysis intersection while simultaneously allowing the application of much larger electric fields for the electrophoretic separation.

4.3.3 Development of a Double T chip

To overcome the electric field strength limitations and eliminate the affect of FBS on the separation of the peptide, yet still use FBS to prevent biofouling of the channels, a new chip design was employed. This new chip design is shown in Figure 4.2 and is similar to the flow through design with the exception that it incorporates an extra channel below the focusing channel. This lower focusing channel has a flow resistance that is approximately 36 times higher compared to the upper focusing channel, considering that resistance is directly proportional to the length of the channel and indirectly proportional to the area. In microfluidics, fluid flow is in the laminar flow regime and the low flow coming from the bottom focusing channel has a small effect on the cell flow path. It raises the cell flow path slightly upwards, away from the bottom corners of the lysis intersection. This flow path can be seen in Figure 4.13 where FBS, containing fluorescein for visualization, was pulled through the CF channel to waste. With the new design, FBS was used to suspend the cells and pull them through the cell flow channel to waste. The other channels were filled with separation buffer. Addition of a surfactant to the separation buffer in the focusing channels aided in cells lysis and prevented debris adhesion. As can be seen in Figure 4.13A, the fluorescein dye was significantly diluted by the time it reaches the lysis intersection. The dilution of the FBS allowed high electric fields (>2400 V/cm) to be applied for the cell lysis and analyte separation without causing heat-induced gelation of the FBS proteins. Using this

new design, hundreds of cells could be lysed in a single run of the device without resolution loss or need to stop the operation for cleaning.

Because the FBS was diluted at the lysis intersection, the anti-biofouling effect was diminished and post-lysis cellular debris could begin to collect over time. In order to help prevent and eliminate any biofouling, surfactant was added to the buffer in the focusing channels. A neutral surfactant, Triton-X, was used because of its compatibility with FBS. Triton-X was added to the Tris/Boric Acid buffer at 0.1% (v/v), which was above its critical micelle concentration (CMC = 0.033%). However, the dilution at the lysis intersection should reduce the Triton-X concentration to below the CMC level.

Addition of the surfactant to the focusing channels had a two-fold effect. It not only aided in preventing biofouling at the lysis intersection, it also helped to lyse the cells. Lysis of cells by chemical means is frequently used on microfluidic devices[4,58-60]; however, this lysis method is often too slow to get accurate time point analyses of cellular contents. Electrical lysis is one of the most effective cell lysis methods because it rapidly destroys the cell membrane and causes the cellular contents to disperse into the surrounding buffer, effectively terminating intracellular reactions. It was found, however, that using only electrical lysis becomes problematic when simultaneously using hydrodynamic flow to transport the cells. The membrane of each cell is different and irreversible electroporation of the cell membranes requires different exposure time to the electric field and/or different electric field strengths. In the flow through chip design, cells are pulled through the electric field to lyse and the resulting lysate simultaneously injected into the analysis channel. It was observed that the hydrodynamic force often pulled some of this lysate to waste. The lysate injection efficiency was improved through electroosmotic flow reversal within the separation

channel, as discussed in Chapter 3. On the Double T chip, using chemical lysis methods in conjunction with electrical lysis provided good lysate injection with minimal loss of the lysate to waste. This combination of chemical and electrical lysis was also used in the original proof of concept publication for the flow through device.[61] Still frame images of a cell being lysed on a Double T microchip can be seen in Figure 4.13B. Here, a dye-loaded cell can be seen entering the lysis intersection, lysing, the lysate injecting into the analysis channel and the remaining cellular material flowing on to waste.

The combination of FBS in the sample cell channel and surfactant additive to the buffer within the double focusing channels allowed, in one instance, for 328 cells to be analyzed in a single continuous run. An example of a 30 minute run showing 134 cells loaded with carboxyfluorescein and Oregon Green cytosolic dyes is shown in Figure 4.14. In a separate experiment, over 1000 dye-loaded cells were analyzed in a single run on the device.

4.4 Conclusion

In this chapter, the separation of lysate from individual cells loaded with a PKC reporter peptide substrate was demonstrated. Several peaks were observed which are believed to be the substrate and product of the kinase activity. Because of the limited electric field that could be applied when using FBS, the migration time of the peptides to the detector was slow and the analysis time for each individual cell was long. This limited the throughput rate for single cell kinase analysis. To be able to apply higher electric fields, and thus achieve more efficient and timely separations of the PKC substrate and product, an extra focusing channel was incorporated into the design. The two focusing channels were used to dilute the FBS at the lysis intersection. Addition of a surfactant to the focusing channels was also used to aid in cell lysis so that the entire lysis process does not take place simultaneously

with the electrokinetic injection of the lysate into the analysis channel. Using the new Double T microchip with the addition of surfactant to the buffer within the focusing channels, collection of large data sets (>100 cells) on a single run of the device was achieved in several instances. In one experiment, the chip was operated long enough to collect data from more than 1000 cells in a single run of the microchip with no biofouling.

4.5 Figures

A)

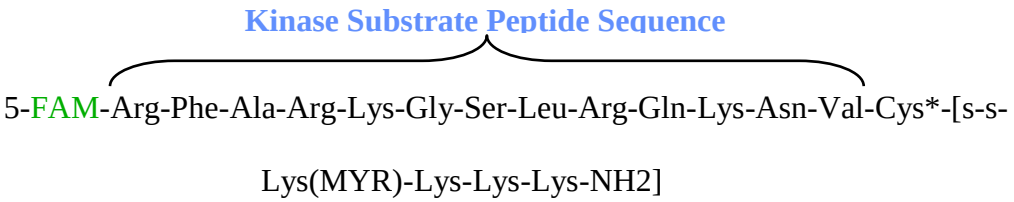

B)

SPKC:

5-FAM-Arg-Phe-Ala-Arg-Lys-Gly-Ser-Leu-Arg-Gln-Lys-Asn-Val-NH2

Phospho-SPKC (PSPKC):

5-FAM-Arg-Phe-Ala-Arg-Lys-Gly-Ser(phosphate)-Leu-Arg-Gln-Lys-Asn-Val-NH2

Figure 4.1 Protein kinase C substrate peptide sequence is shown in A). The substrate and phosphorylated substrate peptide standards without the myristoyl group attached are shown in B).

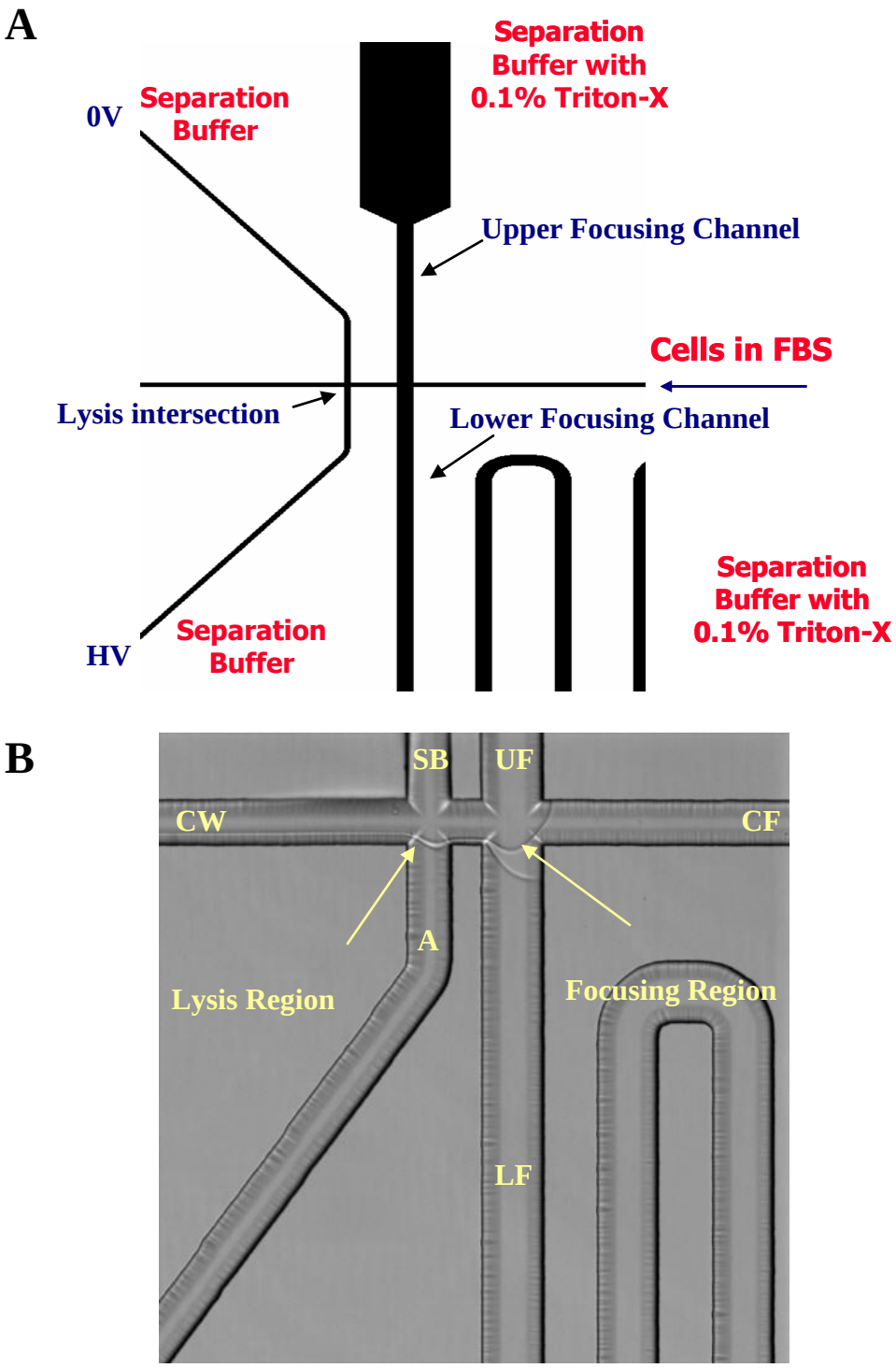

Figure 4.2 A schematic of the Double T microchip with channel descriptions is shown in A) and an image of the focusing and lysis regions is shown in B).

A

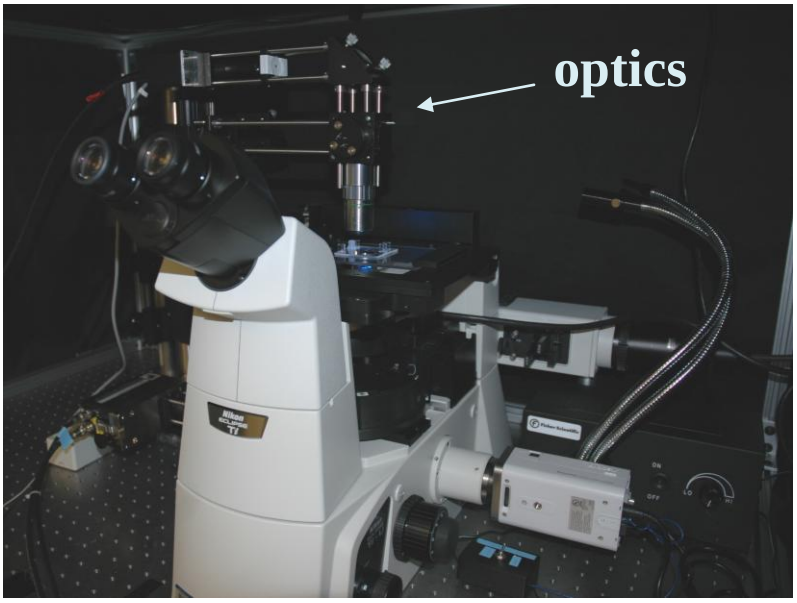

B

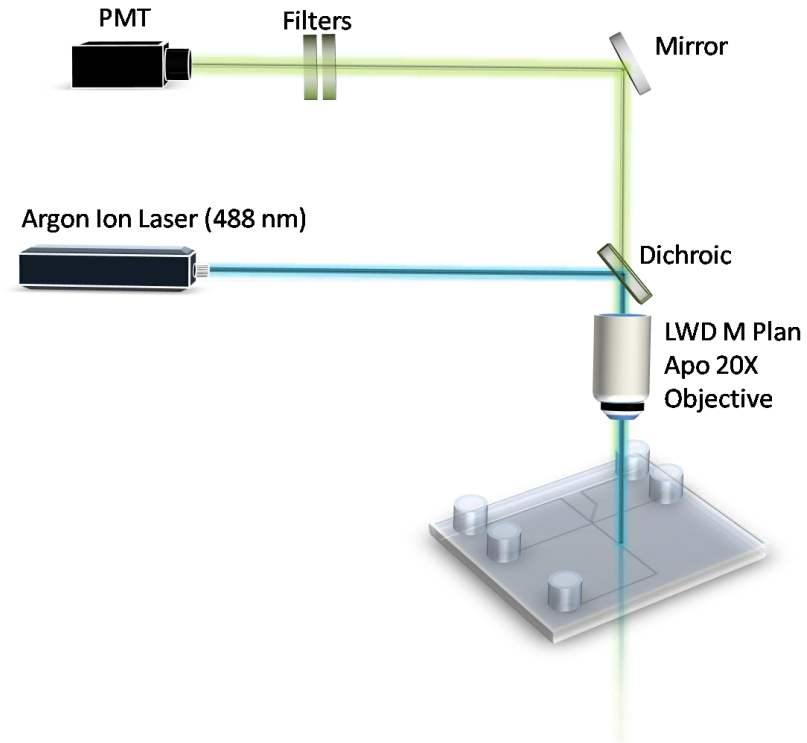

Figure 4.3 Experimental set-up for lysate data collection. Image A shows the microscope with the optical components for LIF detection. A microchip was placed on the microscope stage and the 488-nm line of an argon ion laser was focused onto the analysis channel for collection of lysate data. A schematic of the optical components used is shown in B. The laser was focused onto the chip channel using a LWD M Plan Apo 20X objective. The resulting fluorescence was passed through a dichroic filter, followed by a 530DF30 and a 488 long pass filter before detection using a photomultiplier tube.

A

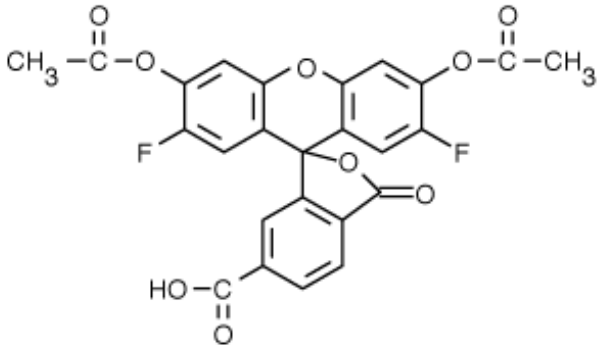

B

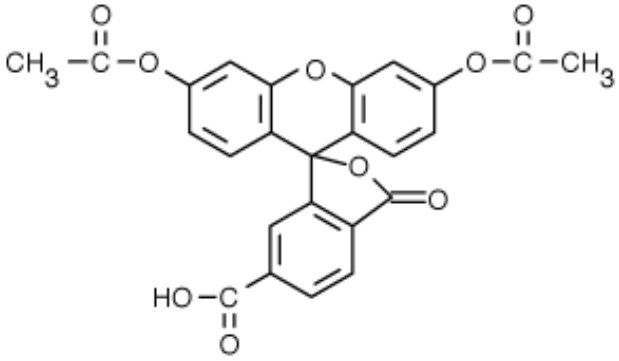

Figure 4.4 Chemical structure of A) Oregon Green® 488 carboxylic acid diacetate, CAS# 195136-74-4, and B) carboxyfluorescein diacetate, CAS# 3348-03-6, cytosolic dyes

A

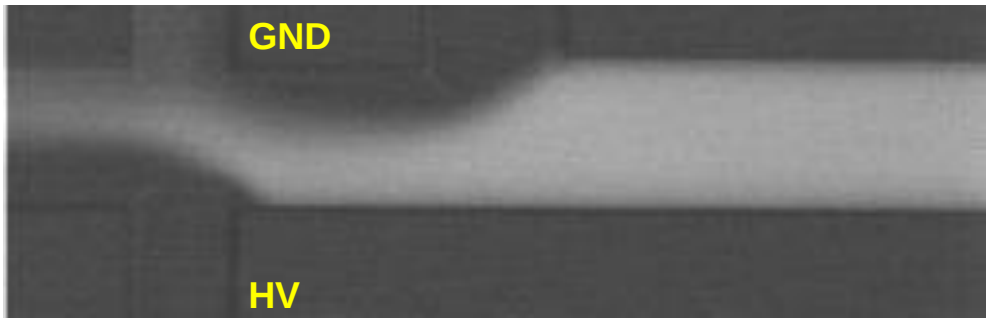

B

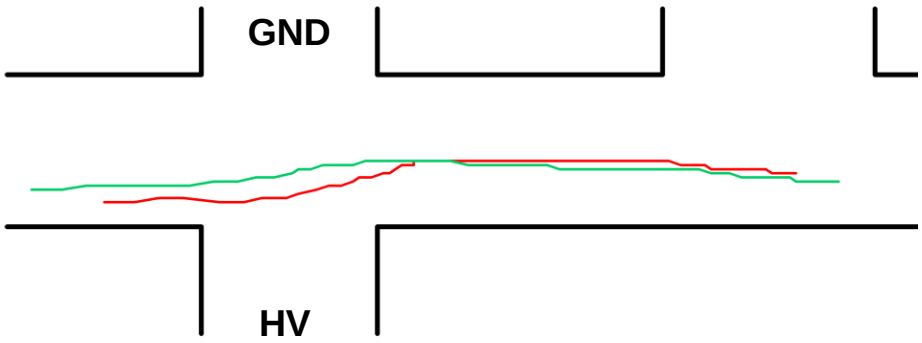

Figure 4.5 An image of the Rhodamine B flow path through the lysis intersection upon application of ~480 V/cm is shown in A). In B), the flow paths of two cells through the lysis intersection during application of the same electric field are shown.

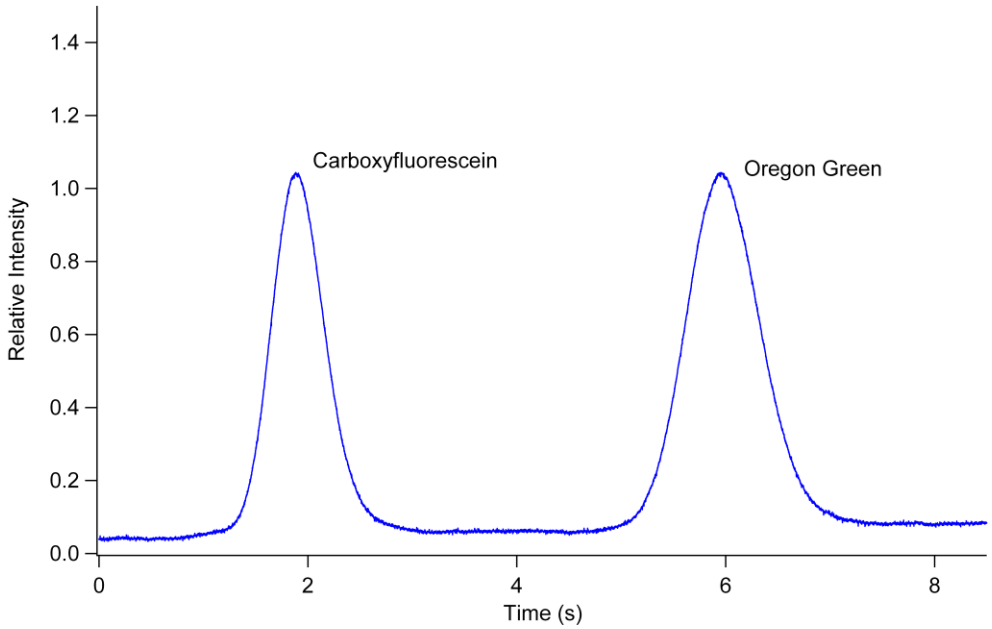

Figure 4.6 Separation of Oregon Green and carboxyfluorescein from the lysate of a single cell in 100% FBS-filled channels.

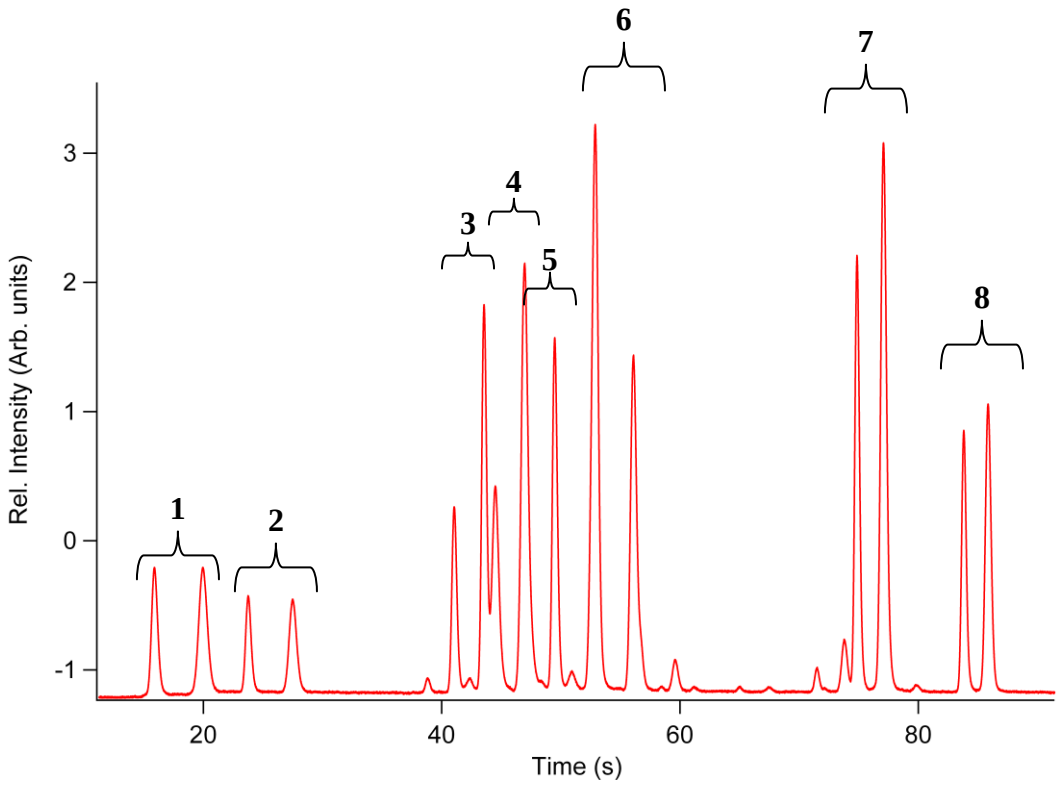

Figure 4.7 The separation of Oregon Green and carboxyfluorescein from eight individual cells analyzed in a single run. Some of the lysate peaks from different cells co-migrated (e.g., cells 3, 4 and 5) because the time between these lysis events was not sufficient to prevent lysate packet overlap. Loss of resolution was observed from the beginning to the end (i.e., from cell 1 to cell 8) of the ~1.3 minute period shown.

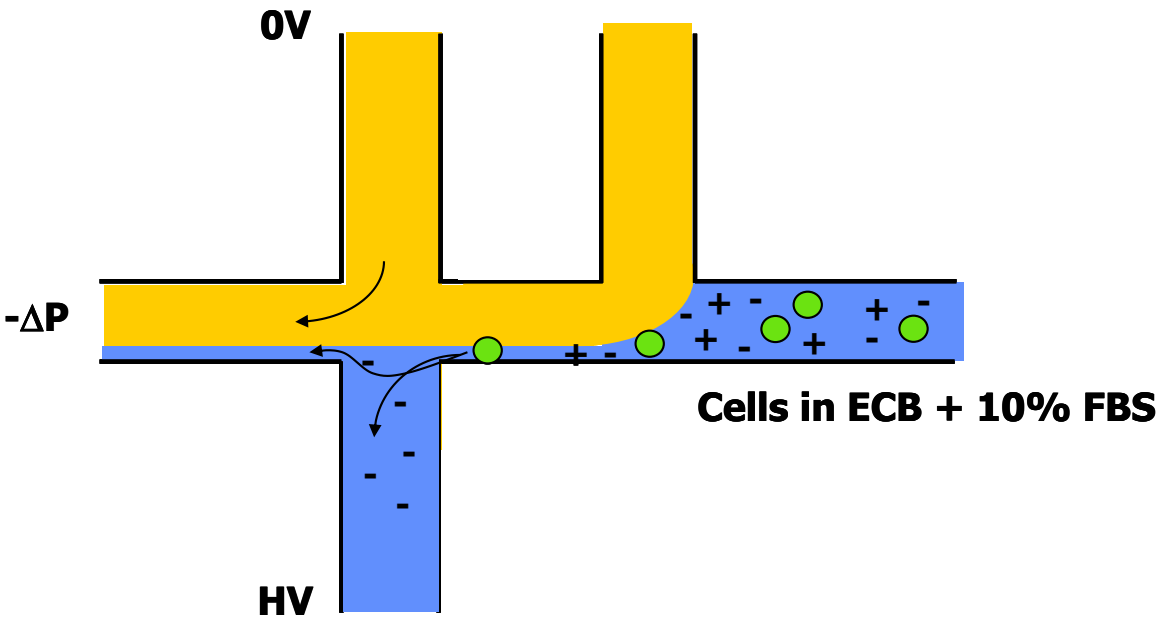

Figure 4.8 Schematic demonstrating the flow of ECB ions into the analysis channel of the flow through chip. This flow of ions changes the analysis channel buffer composition and affects the resolution of the cytosolic dyes from single cells

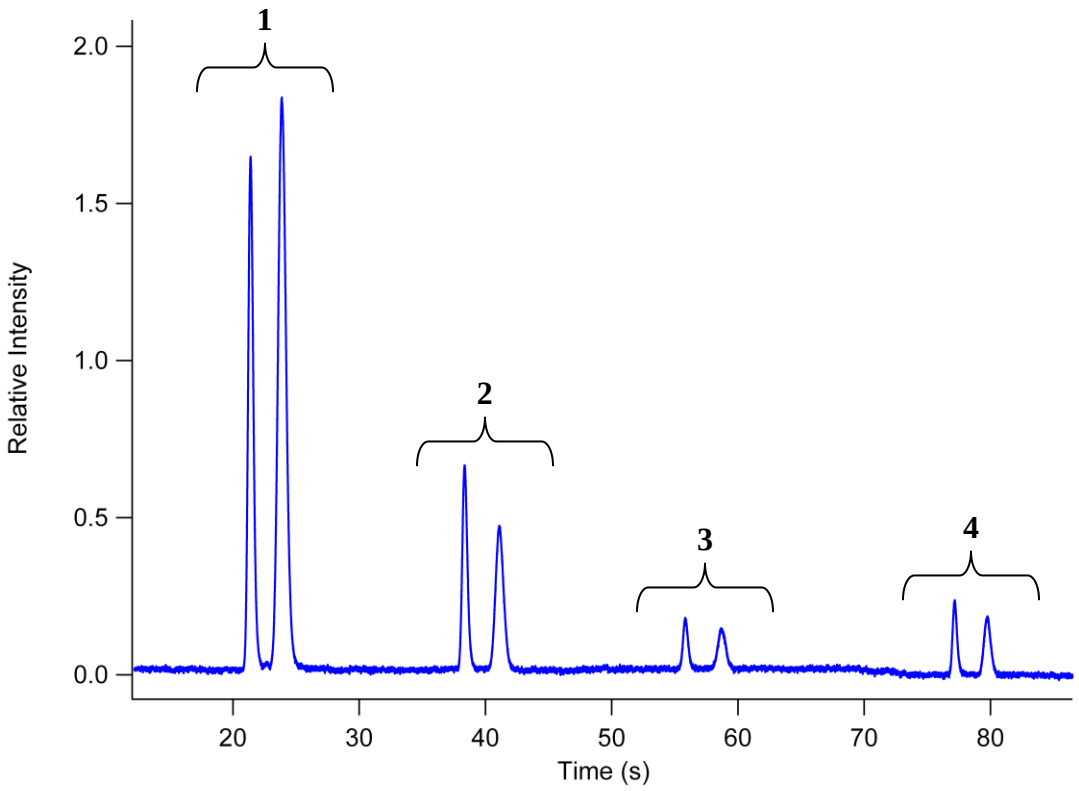

Figure 4.9 Electropherogram of Oregon Green and carboxyfluorescein separation from four individual cells. The cells were diluted in 100% FBS and the resolution loss from cell 1 to cell 4 was minimal.

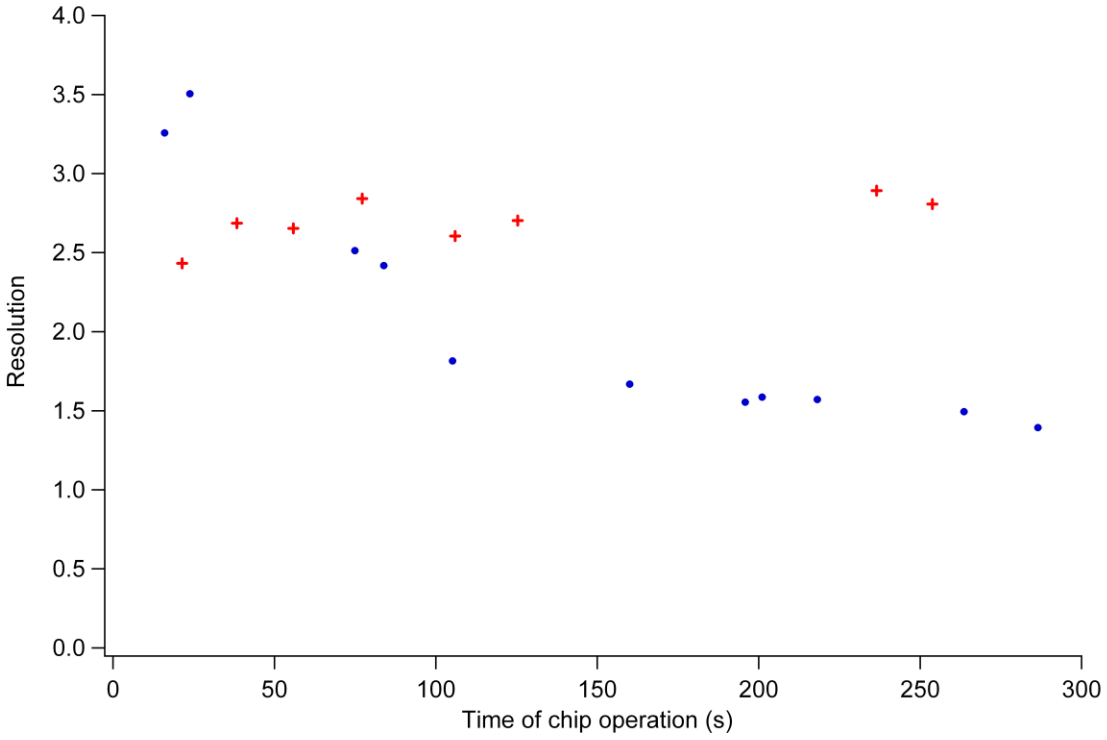

Figure 4.10 Graph showing the resolution between the carboxyfluorescein and Oregon Green peaks when cells were diluted in ECB with 10% FBS versus 100% FBS. The ECB + 10% FBS data are represented by the blue dots and the 100% FBS data are displayed as red crosses.

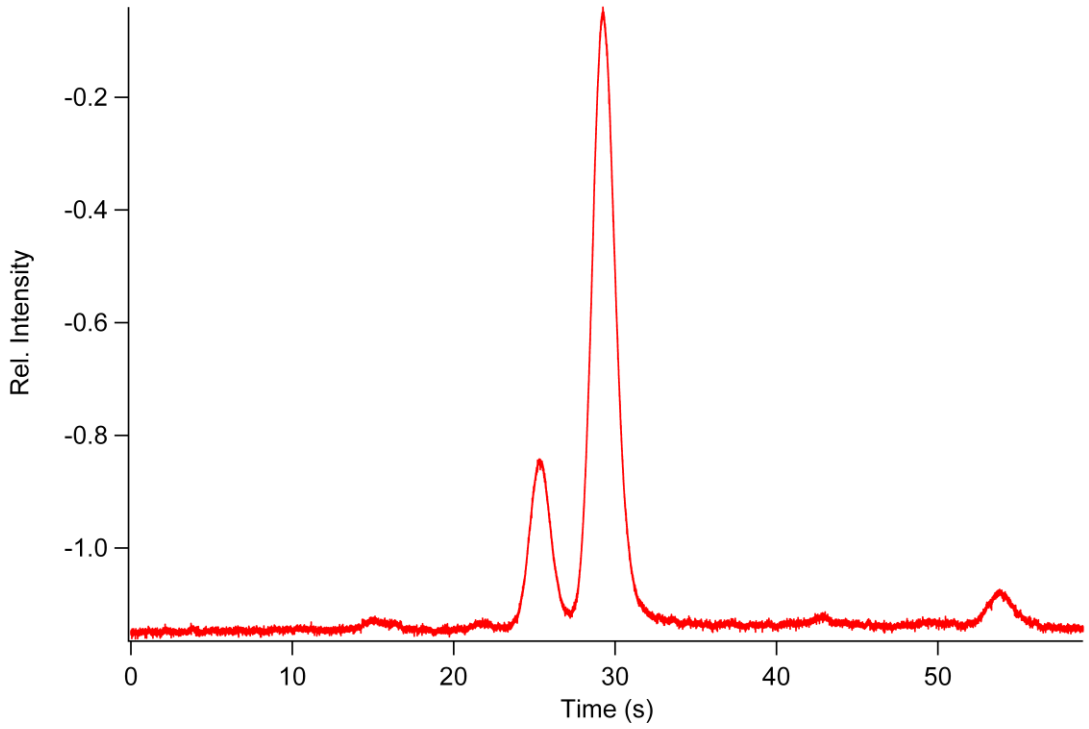

Figure 4.11 Separation observed from a single cell loaded with Myr-ss-SPKC reporter peptide.

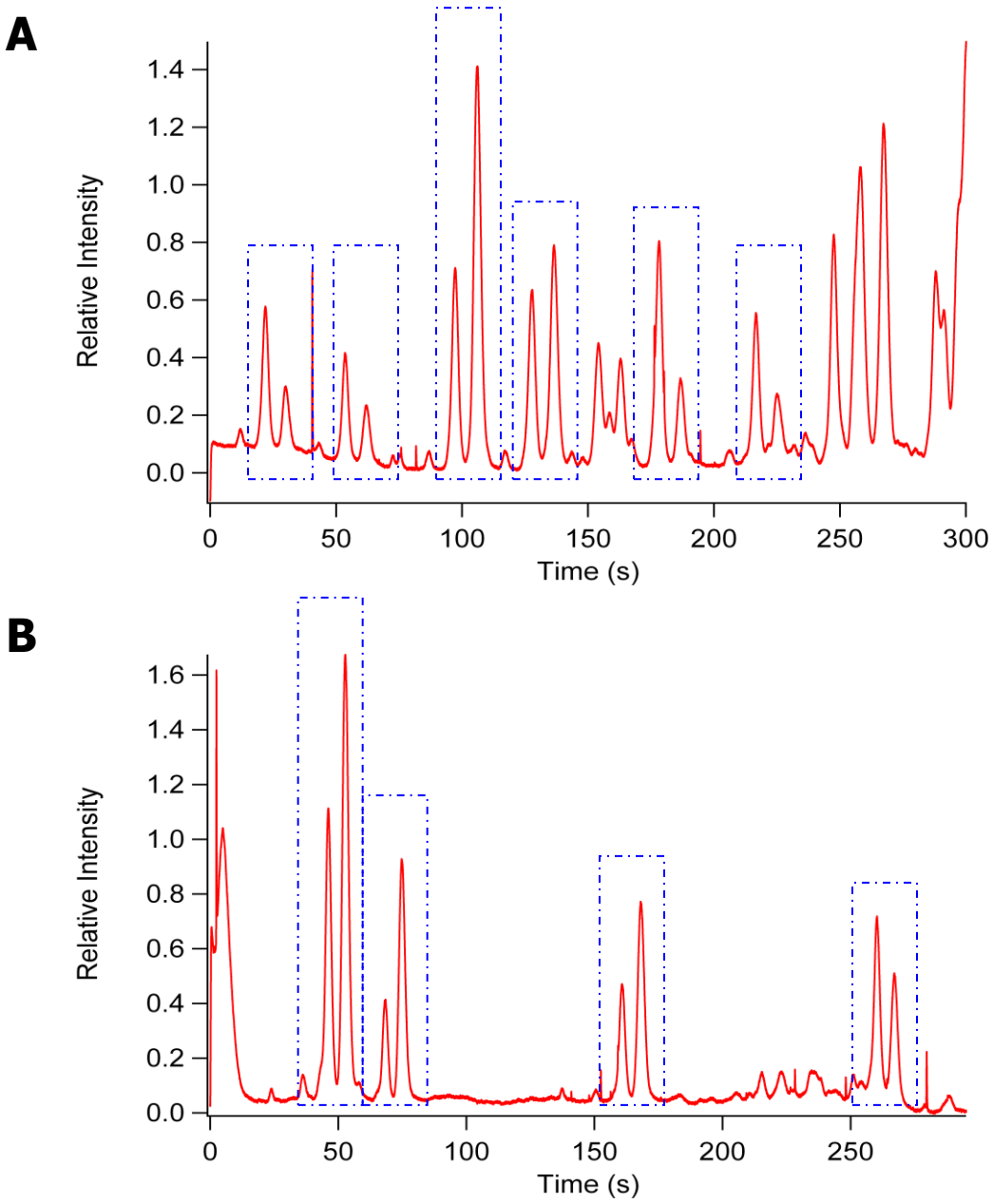

Figure 4.12 Five minute runs of the flow through chip analyzing Myr-ss-SPKC peptide-loaded Jurkat cells. Here, the analysis of ten lysed cells is shown. The peaks from individual cells are outlined with blue-dashed boxes. In A) the peaks from six individual cells are highlighted. These were lysate separations in which there were no interfering or overlapping peaks from previously or subsequently lysed cells. In B), the peaks from four lysed cells are highlighted.

A

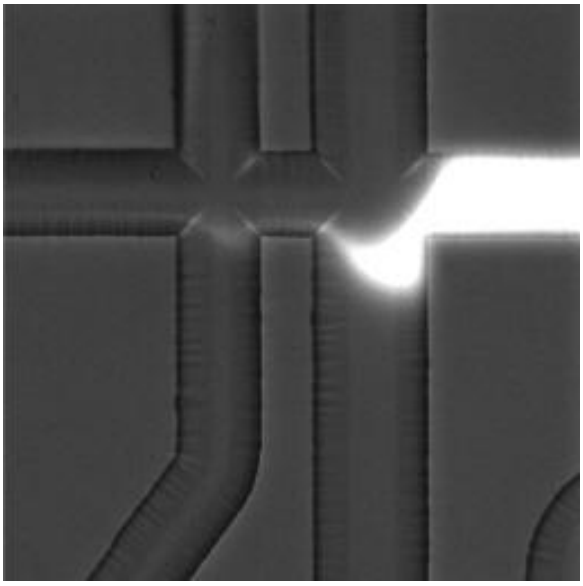

B

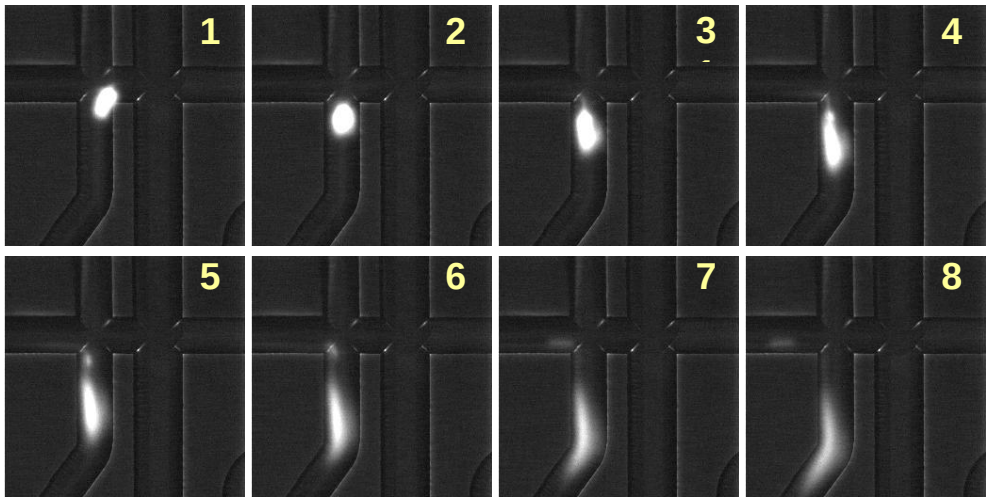

Figure 4.13 The flow path of fluorescein through the Double T chip is shown in A). Still frames from a video showing a cell passing through the lysis intersection, lysing and the cytosolic dye injecting into the analysis channel are shown in B).

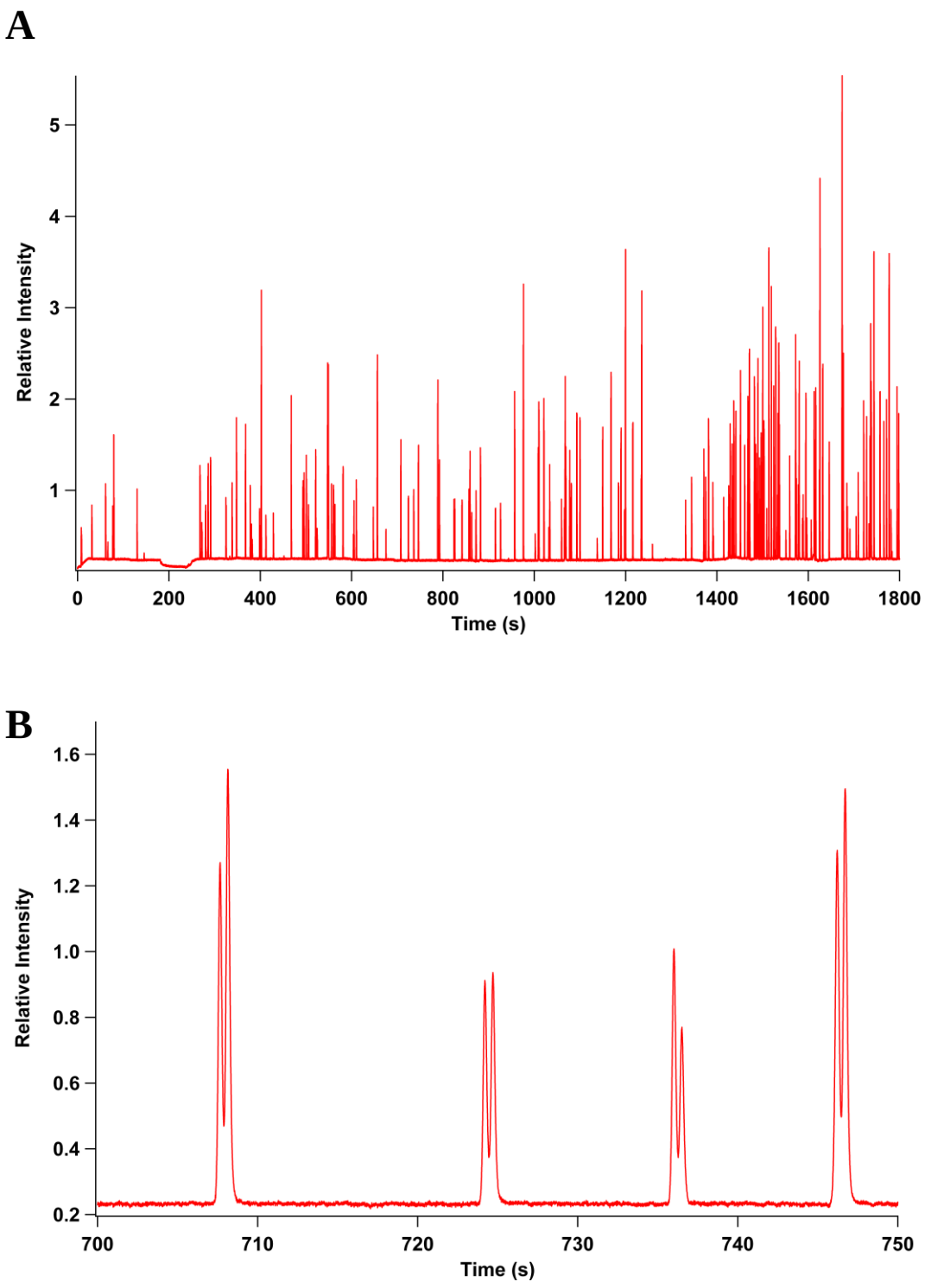

Figure 4.14 A 30-minute run on the Double T chip showing analysis of 134 cells that were loaded with carboxyfluorescein and Oregon Green cytosolic dyes. The entire run is shown in A) and a zoom in of four analyzed cells is shown in B).

4.6 References

(1) Gao, X. J.; Chen, T. S.; Xing, D.; Wang, F.; Pei, Y. H.; Wei, X. B. *Journal of Cellular Physiology* **2006**, *206*, 441.

(2) Danna, E. A.; Nolan, G. P. *Current Opinion in Chemical Biology* **2006**, *10*, 20.

(3) Sato, M.; Ozawa, T.; Inukai, K.; Asano, T.; Umezawa, Y. *Nature Biotechnology* **2002**, *20*, 287.

(4) Borland, L. M.; Kottegoda, S.; Phillips, K. S.; Allbritton, N. L. *Annual Review of Analytical Chemistry* **2008**, *1*, 191.

(5) Zarrine-Afsar, A.; Krylov, S. N. *Analytical Chemistry* **2003**, *75*, 3720.

(6) Posada, J.; Cooper, J. A. *Molecular Biology of the Cell* **1992**, *3*, 583.

(7) Hunter, T. *Cell* **1995**, *80*, 225.

(8) Ferrell, J. E.; Machleder, E. M. *Science* **1998**, *280*, 895.

(9) Gourley, P. L.; Hendricks, J. K.; McDonald, A. E.; Copeland, R. G.; Barrett, K. E.; Gourley, C. R.; Naviaux, R. K. *Biomedical Microdevices* **2005**, *7*, 331.

(10) Kolibaba, K. S.; Druker, B. J. *Biochimica Et Biophysica Acta-Reviews on Cancer* **1997**, *1333*, F217.

(11) Schneider, G. B.; Kurago, Z.; Zaharias, R.; Gruman, L. M.; Schaller, M. D.; Hendrix, M. J. C. *Cancer* **2002**, *95*, 2508.

(12) Phillips, W. A.; St Clair, F.; Munday, A. D.; Thomas, R. J. S.; Mitchell, C. A. *Cancer* **1998**, *83*, 41.

(13) Frame, M. C. *Biochimica Et Biophysica Acta-Reviews on Cancer* **2002**, *1602*, 114.

(14) Doshi, R.; Day, P. J. R. *Lab on a Chip* **2008**, *8*, 1774.

(15) Buckley, R. H. *New England Journal of Medicine* **2000**, *343*, 1313.

(16) Blume-Jensen, P.; Hunter, T. *Nature* **2001**, *411*, 355.

(17) Hartig, M. B.; Hortnagel, K.; Garavaglia, B.; Zorzi, G.; Kmiec, T.; Klopstock, T.; Rostasy, K.; Svetel, M.; Kostic, V. S.; Schuelke, M.; Botz, E.; Weindl, A.; Novakovic, I.; Nardocci, N.; Prokisch, H.; Meitinger, T. *Annals of Neurology* **2006**, *59*, 248.

(18) Yoshida, A. *Blood Cells Molecules and Diseases* **1996**, *22*, 265.

(19) Jones, D. R.; Varela-Nieto, I. *Molecular Medicine* **1999**, *5*, 505.

(20) O'Shea, J. J.; Husa, M.; Li, D.; Hofmann, S. R.; Watford, W.; Roberts, J. L.; Buckley, R. H.; Changelian, P.; Candotti, F. *Molecular Immunology* **2004**, *41*, 727.

(21) Fan, A. C., Deb-Basu, D., Orban, M.W., Gotlib, J.R., Natkunam, Y., O'Neill, R., Padua, R., Xu, L., Taketa, D., Shirer, A.E., Beer, S., Yee, A.X., Voehringer, D.W., Felsher, D.W *Nature Medicine* **2009**, *Advanced online publication - search for actual reference later*.

(22) Cohen, P. *Nature Reviews Drug Discovery* **2002**, *1*, 309.

(23) Boutin, J. A. *International Journal of Biochemistry* **1994**, *26*, 1203.

(24) Burnett, G.; Kennedy, E. P. *JBC*.

(25) Nair, V. D.; Yuen, T.; Olanow, C. W.; Sealfon, S. C. *Journal of Biological Chemistry* **2004**, *279*, 27494.

(26) Burridge, K.; Nelson, A. *Analytical Biochemistry* **1995**, *232*, 56.

(27) Wooten, M. W. *Sci. STKE* **2002**, *153*, pl15.

(28) Babu, C. V. S.; Cho, S. G.; Yoo, Y. S. *Electrophoresis* **2005**, *26*, 3765.

(29) Butts, C. L.; Shukair, S. A.; Duncan, K. M.; Harris, C. W.; Belyavskaya, E.; Sternberg, E. M. *Nuclear Receptor Signaling* **2007**, *5*, e007.

(30) Krutzik, P. O.; Nolan, G. P. *Nature Methods* **2006**, *3*, 361.

(31) Krutzik, P. O.; Crane, J. M.; Clutter, M. R.; Nolan, G. P. *Nature Chemical Biology* **2008**, *4*, 132.

(32) Chen, H. X.; Kovar, J.; Sissons, S.; Cox, K.; Matter, W.; Chadwell, F.; Luan, P.; Vlahos, C. J.; Schutz-Geschwender, A.; Olive, D. M. *Analytical Biochemistry* **2005**, *338*, 136.

(33) Niswender, K. D.; Gallis, B.; Blevins, J. E.; Corson, M. A.; Schwartz, M. W.; Baskin, D. G. *J Histochem Cytochem* **2003**, *51*, 275.

(34) Higashi, H.; Sato, K.; Omori, A.; Sekiguchi, M.; Ohtake, A.; Kudo, Y. *Neuroreport* **1996**, *7*, 2695.

(35) Nakanishi, S.; Kase, H.; Matsuda, Y. *Analytical Biochemistry* **1991**, *195*, 313.

(36) Cann, A. D.; Wolf, I.; Kohanski, R. A. *Analytical Biochemistry* **1997**, *247*, 327.

(37) Li, H.; Sims, C. E.; Kaluzova, M.; Stanbridge, E. J.; Allbritton, N. L. *Biochemistry* **2004**, *43*, 1599.

(38) Greif, D.; Galla, L.; Ros, A.; Anselmetti, D. *Journal of Chromatography A* **2008**, *1206*, 83.

(39) Gamble, T. N.; Ramachandran, C.; Bateman, K. P. *Analytical Chemistry* **1999**, *71*, 3469.

(40) He, Y.; Yeung, E. S. *Electrophoresis* **2003**, *24*, 101.

(41) Meredith, G. D.; Sims, C. E.; Soughayer, J. S.; Allbritton, N. L. *Nature Biotechnology* **2000**, *18*, 309.

(42) Li, H.; Wu, H. Y.; Wang, Y.; Sims, C. E.; Allbritton, N. L. *Journal of Chromatography B* **2001**, *757*, 79.

(43) Li, H. N.; Sims, C. E.; Wu, H. Y.; Allbritton, N. L. *Analytical Chemistry* **2001**, *73*, 4625.

(44) Han, A. S.; Hosokawa, K.; Maeda, M. *Electrophoresis* **2009**, *30*, 3507.

(45) Sims, C. E.; Allbritton, N. L. *Lab on a Chip* **2007**, *7*, 423.

(46) Nishizuka, Y. *Faseb Journal* **1995**, *9*, 484.

(47) Ogawa, Y.; Takai, Y.; Kawahara, Y.; Kimura, S.; Nishizuka, Y. *Journal of Immunology* **1981**, *127*, 1369.

(48) de Thonel, A.; Ferraris, S. E.; Pallari, H. M.; Imanishi, S. Y.; Kochin, V.; Hosokawa, T.; Hisanaga, S.; Sahlgren, C.; Eriksson, J. E. *Molecular Biology of the Cell* **2010**, *21*, 1423.

(49) Dekker, L. V.; Parker, P. J. *Trends in Biochemical Sciences* **1994**, *19*, 73.

(50) Nishizuka, Y. *Journal of Biochemistry* **2003**, *133*, 155.

(51) Chen, S. J.; Klann, E.; Gower, M. C.; Powell, C. M.; Sessoms, J. S.; Sweatt, J. D. *Biochemistry* **1993**, *32*, 1032.

(52) Fields, A. P.; Gustafson, W. C. *Protein Kinase C Protocols*; Humana Press, 2003; Vol. 233.

(53) Carey, I.; Williams, C. L.; Ways, D. K.; Noti, J. D. *International Journal of Oncology* **1999**, *15*, 127.

(54) Choi, P. M.; Tchouwong, K. M.; Weinstein, I. B. *Molecular and Cellular Biology* **1990**, *10*, 4650.

(55) Kuranami, M.; Cohen, A. M.; Guillem, J. G. *American Journal of Surgery* **1995**, *169*, 57.

(56) Scaglione-Sewell, B.; Abraham, C.; Bissonnette, M.; Skarosi, S. F.; Hart, J.; Davidson, N. O.; Wall, R. K.; Davis, B. H.; Sitrin, M.; Brasitus, T. A. *Cancer Research* **1998**, *58*, 1074.

(57) Nelson, A. R.; Borland, L.; Allbritton, N. L.; Sims, C. E. *Biochemistry* **2007**, *46*, 14771.

(58) Wang, H. Y.; Bhunia, A. K.; Lu, C. *Biosensors & Bioelectronics* **2006**, *22*, 582.

(59) Dittrich, P. S.; Tachikawa, K.; Manz, A. *Analytical Chemistry* **2006**, *78*, 3887.

(60) Hellmich, W.; Pelargus, C.; Leffhalm, K.; Ros, A.; Anselmetti, D. *Electrophoresis* **2005**, *26*, 3689.

(61) McClain, M. A.; Culbertson, C. T.; Jacobson, S. C.; Allbritton, N. L.; Sims, C. E.; Ramsey, J. M. *Analytical Chemistry* **2003**, *75*, 5646.

Chapter 5: Separation development for kinase enzyme reporter substrates and products

5.1 Introduction

In this chapter, method development for electrophoretic separation conditions of several enzyme reporter substrates and products is reported. This development included investigation of various buffers and surface coatings to control the electroosmotic flow and increase the separation efficiency. It was necessary to determine the detection limits of the enzyme reporters to ensure that the levels found in an individual cell could be detected. Finally, the effect of the hydrodynamic flow on the lysate separation and injection into the analysis channel was studied.

The majority of this work was performed using the protein kinase C (PKC) enzyme substrate peptide, referred to as Myr-ss-SPKC. This peptide was discussed in Chapter 4 and the sequence of this peptide is shown in Chapter 4, Figure 4.1. The substrate standard peptide, SPKC, and phosphorylated product standard peptide, PSPKC, were used for method development. In addition to PKC activity, another fluorescently-labeled reporter substrate for the analysis of sphingosine kinase enzyme activity was tested.

Like most kinases, sphingosine kinase is involved in several cellular functions. It helps to control such processes as angiogenesis, proliferation and movement of immune cells.[1] It operates through the phosphorylation of sphingosine (S-1) to sphingosine-1-phosphate (S-1-P). One of the important effects of sphingosine kinase activity is that it initiates a cell's pro-survival mechanism through suppression of apoptosis.[2] In cancerous cells, there is a major up-regulation of sphingosine kinase, which prevents normal apoptosis

from occurring. In this way, cancerous cells essentially live indefinitely. The structures of S-1 and S-1-P are shown in Figure 5.1. Because of the natural lipophilic character of S-1, this substrate will cross the cell membrane passively. Incubation of cells in a solution of S-1 will result in transport into the cell membrane or across the cell membrane into the cytosol. Once in the cell, S-1 and S-1-P are commonly compartmentalized and will not transport back out of the cell.[1]

5.1.1 Separation development for single cell kinase analysis

One of the main difficulties in performing chemical cytometry is that the buffers necessary for maintaining cell viability are not optimal for electrophoretic separations. This is because cell-friendly buffers generally have high salt content in order to maintain isotonic conditions. Upon application of an electric field for separation, the high conductivity of cell buffers will result in high current through the channels. This current causes Joule heating, which can affect channel surface coatings and can cause solution boiling within the channels resulting in bubble formation. To prevent these issues, the electric field must be controlled at a low value. Another method that has been used to prevent Joule heating is to use alternating current with a base direct current (DC) offset.[3] The ideal solution would be to place the cells in a buffer that is appropriate for the electrophoretic separation. However, this is not plausible because non-physiological buffers can cause stress on the cells, which invokes survival signaling transduction pathways. The activation of signaling pathways can alter the activity of the enzyme that is to be measured.

Another difficulty occurs when performing separation of positively charged enzyme reporter peptides on uncoated channel surfaces using biological buffers. Some enzyme reporter peptides carry a positive charge at physiological pH, where the magnitude of the

charge depends on the amino acid sequence. The interaction of the positively-charged peptide with the negatively charged glass channel walls results in peak broadening and asymmetric peaks.[4] In addition to affecting the efficiency of the separation, the non-specific adsorption of the peptide onto the channel wall will lead to analyte loss and affect the migration time reproducibility. As mentioned, detection of the analyte concentration within a single cell is challenging; therefore, adsorptive loss of the analyte must be minimized.[5] To prevent the channel wall interaction, a number of methods have been employed including buffer pH adjustment, buffer additives and surface coatings.[4,6] Buffer additives, such as betaine[4], spermine[7] and PEG[8], have been shown to decrease the peptide-wall interaction to improve the peak shape and precision of the migration times. Channel coatings to reduce the interaction have included PEG silanization or other derivatizations with neutral polymers, such as polydimethylacrylamide[4], to reduce analyte adsorption. Positively charged compounds, such as polyethyleneimine[9], polybrene[10], polyarginine[11], spermine[12] and triethylamine[13] have also been effectively utilized to reduce the electrostatic interaction between positively charged peptides and the channel surface.

5.1.2 Detection of analytes from a single cell

Cells contain complex mixtures of a large variety of different molecule types, all with varying concentrations. The concentration of many compounds that are of biological interest (e.g., amino acids, proteins, DNA and RNA) are often present at such low concentrations that their detection is difficult.[14-15] Within a single cell, proteins make up about 15% of the cell content and individual proteins are generally present around an attomole (10^{-18}).[16] Given the picoliter volumes of most mammalian cells, this gives micromolar concentrations for detection; however many individual enzyme substrates and products are present in the

nanomolar range.[17] For detection of low abundant proteins, the detection limit must be around 100 nM for accurate measurement.[18-20] Many other cellular analytes are present between femtomole (10^{-15}) and zeptomole (10^{-21}) levels.[21] To effectively analyze these low-concentration analytes on a microfluidic device, very sensitive detection techniques must be used.[22]

For measuring single cell analytes on microfluidic devices, optical methods such as absorbance, fluorescence, chemiluminescence and bioluminescence have been used.[23] Fluorescence detection provides some of the best detection limits compared to other detection techniques. Although the native fluorescence of proteins has been successfully used for detection[19], a more common strategy is to label the cellular analytes with a fluorescent tag.[15] The analytes can either be labeled prior to introduction into the cells or can be derivatized post-lysis.[21,24-27] Electrochemical detection, including amperometry, potentiometry and conductometry, has also been incorporated on microchips to achieve low detection limits for single cell analyte concentrations. Other methods used include mass spectrometry detection and NMR; however, laser induced fluorescence and electrochemical detection methods have proven to provide the optimal detection limits, with detection commonly around the sub-attomolar level.[15,28]

5.1.3 Method characterization for high-throughput single cell analysis

Besides achieving specificity and the appropriate detection limits for separating and detecting single cell analytes, it is necessary that the methods developed possess other characteristics for successful high-throughput data collection. One of these characteristics is that the method be highly efficient with rapid separation of the substrate and product reporter peptides. In this research, a goal of 10 cells per minute is desired; therefore, it is necessary

that the slowest migrating, detectable peak from the lysate of each cell pass through the detector before the fastest migrating peak of the next lysed cell. The throughput rate of the microfluidic device will therefore be dependent on the time required for analyte separation from each cell.

High precision from injection to injection is also necessary. This reproducibility is critical in order to positively identify peaks from each cell in high throughput analysis. Typical biomolecule migration time relative standard deviations (RSD) on capillary electrophoresis (CE) systems are on the order of 0.2-3%.[11,28-29] In one example of single cell lysate analysis on a microfluidic device, the RSD of a single marker from each cell was around 6%.[28] To improve the peak migration time RSDs, several strategies have been implemented, but the most effective method found in the literature includes the use of polyethylene glycol (PEG) additives to the separation buffers.[8]

The use of the Double-T design with FBS to prevent biofouling, described in Chapter 4, allows the separation channel to be coated with a number of surfaces to allow for efficient separation of the peptide enzyme substrates. Additionally, a wide variety of separation buffers can be employed without affecting the anti-adhesion properties when using FBS in the cell flow channel. In this chapter, the method development for rapid separation of the substrate and product pairs is reported. The various surface coatings and buffers used to develop separation conditions for the peptide reporter substrates and their phosphorylated products are demonstrated. Additionally, studies performed to determine the affect of the hydrodynamic flow on the separation are discussed. For certain neutrally charged species, the hydrodynamic flow was found to greatly affect the injection.

5.2 Experimental

5.2.1 Reagent information

Unless otherwise stated, all chemicals were purchased from Sigma (St. Louis, MO, USA). B270 glass substrates, with chrome and positive photoresist (AZ1518) pre-applied, were purchased from Telic Company (Valencia, CA, USA).

5.2.2 Microchip fabrication

The separation development was performed on either simple cross chips or on the flow through microchips. These chips were fabricated in the same manner described in Chapter 2. The flow through devices had the same dimensions as those previously described. The cross chip channels were 21 μm deep and 50 μm wide.

5.2.3 Channel preparations and coatings

The majority of the channel coating procedures were described in Chapter 2. For separation development on uncoated channels, the microchannels were rinsed with 1 N NaOH for 30 to 60 minutes. The channels were then flushed with deionized (DI) water and filled with the appropriate separation solution. The polyamine silane, 3-[2-(2-aminoethylamino)ethylamino]propyl-trimethoxysilane (AEPTMS), coating was performed in the same manner as the aminopropyltriethoxysilane procedure described in Chapter 2.

5.2.4 Device operation for separation development

SPKC and PSPKC (structures shown in Chapter 4) stock solutions were prepared in DI water. The concentration of some stock solutions was determined by peptide analysis at the University of California at Davis. Some stock solutions were not analyzed in this manner and their concentrations are assumed to be similar to that of the analyzed stock solutions. The unanalyzed standards were used for specificity, reproducibility and peak shape analysis.

The analyzed standards were used for limit of detection (LOD) determinations. The sphingosine kinase substrate and product standards (1-5 μM) were prepared in the appropriate buffers from 10 or 100 μM stock solutions. The S-1 and S-1-P stock solutions, along with their stock concentrations were provided by the Allbritton Laboratory (University of North Carolina at Chapel Hill).

The injections on both the cross chip and flow through devices were performed as either gate or pinch injections. The voltages were supplied by a Bertan power supply (Model 2866A, Bertan, Hicksville, NY). For the cross chips, platinum electrodes were placed in one of each of the four reservoirs to apply the DC voltages for the sample loading and injection. When performing injections on the flow through microchips, a platinum electrode was placed in the separation buffer (SB), analysis (A), waste (W) and cell flow (CF) reservoirs. The focusing channel was left floating for all separations. The applied voltages for the injections and separations were varied for each buffer and channel coating type; therefore, only the electric field along the analysis channel is reported. The electric field along the analysis channel was calculated using a combination of Kirchoff's and Ohm's laws. For channel resistance measurements, the chip channels were prepared, filled with the appropriate separation buffer and the resistances between each channel measured using a Keithley 6487 picoammeter (Keithley Instruments, Inc., Cleveland, OH) set to 10 V and 25 mA current limit.

For data collection, the chips were place on a stage and the laser aligned at a position down the analysis channel from the injection point. In some instances, the chip was placed on the stage of a Nikon Eclipse (Nikon, Japan) microscope and the channel intersection was observed using a Sony ExwaveHAD color video camera that was mounted onto the side of

the microscope. Fluorescence excitation at the channel intersection, to observe the injection, was accomplished with a Nikon Intensilight C-HGFIE (Nikon, Japan). The emission light was filtered through a Semrock (Rochester, NY) Brightline FITC-3540B-NTE filter.

To collect the LIF data, an argon ion laser (Melles Griot, Carlsbad, CA) was used at the 488 nm line. The laser beam was focused with the appropriate optics from the top of the chip onto the analysis channel between 3 to 15 mm from the injection point. The experimental set-up is shown in Chapter 4, Figure 4.3. The fluorescence signal was collected using either a Hamamatsu R928 or a Hamamatsu H7732-10 photosensor module (PMT) (Hamamatsu Photonics, Japan). The emission was filtered using a 530DF30 filter and a 488 notch filter or a 488 long pass filter (Semrock, Rochester, NY). The signal was processed using a Stanford Research Systems SR570 Preamplifier (Stanford Research Systems, Sunnyvale, CA) and data collected using a customized Labview program (National Instruments, Austin, TX). The general settings for the preamplifier, used throughout development, are shown in Table 5.1. Any changes or individual settings are listed and discussed in the Results and Discussion or Figures and Tables sections.

5.2.5 Device operation for assessment of hydrodynamic flow on the injection and separation of reporter substrates and products

Negative pressure was applied to the flow through device at the waste channels through attachment of a syringe as described in previous chapters. The amount (psi) of vacuum applied was monitored with a 0-1 psi differential pressure transducer (Omega, Stamford, CT). The pressure transducer was operated at 10 V and was calibrated using an Omega digital pressure gauge (Model DPG1200).

5.2.6 Data analysis

All data processing was performed using the Igor program (Wavemetrics, Inc, Lake Oswego, OR), version 6.0.0.0, or the Cutter 7.0 Labview program (University of Michigan).

5.3 Results and discussion

The device being developed in this work is to provide single cell analysis throughput rates of 10 cells per minute. This means that it is necessary to achieve rapid separation of the enzyme reporter substrates and products. To avoid overlapping peaks from subsequently analyzed cells, the maximum separation time should be around six seconds. It is also a goal to collect large data sets (>100 cells per sample). To collect data from that many cells in a single run will require that the separation method provide high reproducibility so that the peak identities can be confirmed through their migration times. Method development to achieve these goals is detailed in the following sections. As the adjustments to reduce on-chip biofouling were performed (described in Chapter 2) it was necessary to assess the ability to separate the reporter substrates and products on these channel coatings. Additionally, several different buffers and buffer additives were studied to determine the optimal separations. There were several conditions that provided no separation and/or poor peak shape. Both the successful and unsuccessful separation conditions are described.

5.3.1 Development of separation conditions for the positively charged SPKC and PSPKC reporter peptides

Achieving highly efficient separation of the PKC standard substrate reporter peptide, SPKC, from the standard phosphorylated product, PSPKC, is a challenging task. This is because the peptides carry a net positive charge and will interact with the surface silanols of the glass microchannels. To separate positively charged peptides, it is a typical strategy to lower the pH in order to keep the silanols hydroxylated and eliminate the electrostatic

interaction between the peptide and the channel wall.[30-31] In the development performed here, lowering the pH is not an option because the reporters are tagged with a fluorescein label for detection. As shown in Figure 5.2, the quantum yield of fluorescein is highly dependent on pH. The absorption and emission both peak at pH 9.0 and drop off rapidly as the pH decreases. Therefore, to achieve optimal detection limits, the pH should be maintained near pH 9.0.

5.3.1.1 Separation development on uncoated microfluidic channels

The initial separation development was performed using uncoated glass channels. This work was performed initially to establish standard separation conditions in which to compare separations performed on coated chips. CE buffer separation conditions for SPKC and PSPKC were developed utilizing a Tris/Boric Acid buffer containing spermine. Spermine is a polyamine compound that interacts with the surface silanols such that the peptide interaction with the walls is minimized.[12] Using a 50 mM Tris/10 mM boric acid buffer containing 1 mM spermine and 30 mM polyethylene glycol (PEG) additives, separation of the SPKC and PSPKC was observed. In Figure 5.3A, the electropherograms of ten separate injections of a mixture of the substrate and product peptides are shown where the laser was focused on the analysis channel, 10 mm from the injection point. The PEG additive was found to be necessary in order to provide migration time reproducibility. The poorer precision of the PSPKC peak was emphasized when the laser was moved closer to the injection point. In Figure 5.3B, ten separations of the same SPKC/PSPKC mixture are shown, where the laser was focused on the analysis channel, 3 mm from the injection point. The separation conditions are detailed in Table 5.2. The RSDs of the migration times for both the substrate and product peaks are shown in Table 5.3. The migration time relative

standard deviations (RSD) of the PSPKC and SPKC were found to be 3.2% and 2.0%, respectively. These migration RSDs are in the same range as typically reported in the literature for peptide separations in glass channels.[4,9,11,28]

The conditions, shown in Figure 5.3, were optimal for separation of the SPKC and PSPKC peptides on an uncoated channel. There is a peak that co-migrates with the PSPKC peak, as shown by the shoulder on the PSPKC peak in the electropherograms. It is known that the reporter peptides are not highly stable in solution and this degraded product peak was observed only after the standards had been used for some time at room temperature.

The LOD, determined as 3 times the signal-to-noise (S/N) level, of the SPKC and PSPKC peptides were determined using the conditions listed in Figure 5.3A. To determine the amount of sample injected using a gate injection, the following calculations were performed. First, the apparent mobility of each peptide, μ_{app}, was calculated using Equation 5.1,

Equation 5.1 $$\mu_{app} = (L_d/t_r)/(E)$$

where, Ld is the channel length from the injection to the detection point, t_r is the migration time of the peptide to the detection point and E is the electric field within the analysis channel. Using the calculated μ_{app} value, the injection plug length, I_l, was calculated using Equation 5.2,

Equation 5.2 $$I_l = (t_i)(\mu_{app})(E_i)$$

where, t_i is the injection time in seconds and E_i is the electric field used to inject the sample. From the injection plug length, the amount of sample (in attomole) injected, M_d, was determined using Equation 5.3,

Equation 5.3 $$M_d = (I_l)(w)(d)(C)$$

where, w is the width of the separation channel, d is the depth of the separation channel and C is the concentration of the sample placed in the sample reservoir.

An electropherogram of an injection of a mixture containing 2 nM each of the SPKC and PSPKC standards, where each peptide was detected near the LOD, is shown in Figure 5.5. The values used for calculating the mass amount injected are shown in Table 5.5. At a S/N level of ~3, the LOD for the SPKC and PSPKC peptide was found to be 1.3 and 0.9 attomole, respectively. These LOD levels should be sufficient for detection of the peptides from individual cells. For instance, if the cells are loaded with 10 μM Myr-ss-SPKC, the amount of reporter peptide in a Jurkat cell with an average volume of 1 pL will be approximately 10 attomole.

To improve the LOD, several adjustments to the detection equipment were attempted. First, the preamplifier sensitivity was adjusted, from its initial value of 500 nA/V, to increased sensitivities. A comparison of injections of the same peptide standard mix with different preamplifier sensitivities is shown in Figure 5.6. The S/N ratios are listed in Table 5.1. Because the noise is amplified along with the peak signals, the sensitivity adjustment did not improve the S/N ratios. Next, the laser power was increased in an attempt to improve the signal. The laser power was varied between 5 mW to 20 mW. The electropherograms for these injections are shown in Figure 5.7 with the S/N ratios listed in Table 5.7. Again, the laser power increase does not improve the detection limits. Other options to potentially

improve the LOD include adjustments of the optical filters to reduce the noise, post-collection processing of the data and/or improved separation efficiency to decrease band broadening. Various channel coatings and separation solutions were investigated to determine if improved efficiency could be achieved.

5.3.2 Separation of SPKC and PSPKC with channel coatings

In parallel to the coating development described in Chapter 2 and Chapter 3, the separation of the SPKC and PSPKC peptides on these channel coatings was investigated. The first change from the original PDMS/Pluronic surface was a simple 30% (w/w) Pluronic F-127 coating. The SPKC/PSPKC separation on this channel surface can be seen in Figure 5.4 and the separation conditions listed in Table 5.4. Here, baseline separation was again achieved with migration times for the SPKC and PSPKC peptides similar to the conditions shown in Figure 5.3B.

After it was determined that the electroosmotic flow (EOF) in the separation channel should be reversed to control the cell flow path and improve the lysate injection efficiency (Chapter 3), the separation of SPKC and PSPKC on channels coated with PolyE323 was investigated. The structure of PolyE323 can be seen in Figure 5.8.[32] Using a flow through device, the entire chip was coated and a pinch injection of the peptides standards was performed. The injection was switched from a gate to a pinch injection to better simulate the flow of the chip when being operated with hydrodynamic flow to pull the cells through the electric field. The separation of the peptides on a chip coated with PolyE323 was rapid with a total separation time of approximately five seconds. Examples of the separation are shown in Figure 5.9 and the separation conditions are listed in Table 5.8. Using the PolyE323 coating, the anodic EOF was calculated to be -2.3×10^{-4} $cm^2/V*s$. Because the EOF reversal

is so strong, the electric field had to be reversed for the peptides to migrate to the detector. Here, the anode was placed in the analysis channel reservoir and the separation buffer reservoir was grounded. The reversed electric field also reverses the migration order of the peptides. Additionally, because the channel surface is positively charged, coulombic repulsion of the positively charged peptides occurs and improves the efficiency of the separation.

One issue that was noted when using the PolyE323 coated channels was that, over time, the EOF reversal was not maintained. It is believed that this is due to the high pH of the Tris/boric acid buffer. The pH of the Tris/BA buffer is 9.0, which according to the literature, it close to the upper limit for maintaining a positive charge on the PolyE323 amines.[32] Several other separation solutions with lower pH were tested to observe the separation characteristics. First, a 0.1% acetic acid solution containing 30 mM PEG, pH 3.0, was used to maintain the positive charge on the PolyE323 amines. An example separation of a mixture of the SPKC and PSPKC peptides is shown in Figure 5.10 and the separation conditions are listed in Table 5.9.

The low pH of the acetic acid separation solution provided rapid separation of the peptides; however, as mentioned in the introduction, the low pH severely affected the detection. The peak response shown is for a mixture of approximately 1 μM SPKC and PSPKC. In order to maintain the EOF reversal, yet increase the fluorescent signal, the pH must be increased. A 10 mM HEPES (4-(2-hydroxyethyl)-1-piperazineethanesulfonic acid) buffer containing 30 mM PEG and 1 mM TCEP-HCl (tris(2-carboxyethyl) phosphine hydrochloride) was prepared and pH adjusted to 6.5. TCEP-HCl is a reducing agent and was added to the buffer to determine if it affected the peptide separation. TCEP-HCl is

sometimes added to the ECB after cell loading to reduce any Myr-ss-SPKC that attaches to the outside of the cell through a hydrophobic interaction between the membrane proteins and the C14 myristoyl group. An example separation of the SPKC/PSPKC mixture using the HEPES buffer is shown in Figure 5.11 with separation conditions in Table 5.10. The separation is still adequate with a total separation time of < 3 seconds. The total separation time will allow for the rapid analysis of individual cells. To show the increase in signal from pH 3.0 to pH 6.5, an overlay of the separation in 0.1% Acetic Acid and 10 mM HEPES Buffer is shown in Figure 5.12. The HEPES buffer was used for some single cell data collection, despite the signal loss that occurs by lowering the pH from the optimal pH of 9.0 to the buffer pH of 6.5.

In an attempt to have more stable EOF reversal within the analysis channel, a polyamine silane was used to covalently bind amine groups to the glass surfaces. The structure of the polyamine silane, AEPTMS, is shown in Figure 5.13. This silane should provide EOF reversal and create electrostatic repulsion of the positively charged peptides. However, the results indicated that the polyamine silane does not provide good surface coverage to block the surface silanols. This can be inferred from the poor peak shape that was observed. In one instance, a 10 mM acetate buffer containing 30 mM PEG and 3 mM β-cyclodextrin, pH 4.5, was used. This buffer was used to maintain a steady pH in a range that maintains the EOF reversal. The addition of the β-cyclodextrin was to provide a complexing agent to reduce the effects of the positive charges on the peptide with the channel walls. Cyclodextrins are known to complex with amines and are frequently used to affect the electromobility of various analytes. Example injections of a mixture of SPKC and PSPKC

are shown in Figure 5.14. No resolution of the peptides was observed. The broad peak shape indicates a large amount of interaction between the peptides and the channel walls.

A 0.1% acetic acid, pH 3.0, containing 30 mM PEG separation solution was also used in conjunction with a chip whose channels were coated with the AEPTMS polyamine silane. This separation solution was used to compare the results to the peptide separation on a PolyE323 coated chip (seen in Figure 5.10). The results of the SPKC/PSPKC mix injections are shown in Figure 5.15. Again, broad peak shape was observed, especially for the SPKC peptide, and no resolution was achieved. It was concluded that the polyamine silane did not provide the necessary surface coverage to prevent peptide-wall interactions.

To date, the PolyE323 coating provides the optimal separation of the SPKC and PSPKC peptide. Separation conditions on an uncoated chip with 50 mM Tris/10 mM boric acid, containing 30 mM PEG and 1 mM spermine also provide adequate separation, peak shape and detection for the analysis of single cells. The separation was also performed in a standard TBE (89 mM Tris, 89 mM boric acid, 2 mM EDTA) buffer containing 30 mM PEG and 1 mM spermine, pH 9.0. The separation appeared unaffected by the change in Tris and boric acid concentration. Prior to the development of the Double T chip, it was necessary to coat the separation channel separately from the cell flow channel. This was because the cell flow channel required a coating that prevented biofouling while the analysis channel required a coating that was optimal for reporter peptide separation. With the development of the Double T chip, virtually any separation channel coating and buffer composition for separation of the cell analytes, providing they are compatible with the fetal bovine serum (FBS) pretreatment, can be used.

5.3.3 Development of separation conditions for a negatively charged sphingosine kinase substrate and product reporter

Some intracellular analytes carry a net negative charge. These compounds are somewhat easier to separate within a glass microchannel because the interaction with the negatively charged surfaces is minimal. Therefore, specialized coatings are not imperative to achieve optimal separation. As an example, a sphingosine kinase substrate and its phosphorylated product are separated on a flow through device. The structures of the kinase substrate and product are shown in Figure 5.1. The separation of this substrate and product have previously been established in the literature.[31] The buffer used in the literature reference included an ionic detergent, sodium deoxycholate (SDC), and an EOF reversal agent, EOtrol LR (Target Discovery, Palo Alto, CA). It was found that the ionic detergent was not compatible with the FBS that is needed to prevent biofouling (Chapter 2). However, nonionic detergents such as Triton-X and Tween-20 were compatible with the FBS. Therefore, a buffer consisting of TBE with 5% EOtrol LR and 1% Tween-20 was used for the separation development. It was found that on an uncoated glass microchannel, the sphingosine kinase substrate and product separated easily. An example separation is shown in Figure 5.16 and the separation conditions listed in Table 5.11. The double peaks observed for both the substrate and product are a result of the fluorescein isomers that are used to label the substrate and product.

5.3.4 Effect of hydrodynamic flow on separation conditions

The last parameter studied, prior to analyzing cells loaded with the Myr-ss-SPKC and sphingosine kinase reporters, was the effect that the hydrodynamic flow on the separation. A negative pressure is applied to the waste channel on both the flow through device and the

Double T device to pull the cells through the lysis intersection. It is possible that this hydrodynamic flow can affect the injection and/or the separation of the substrate and product.

The affect of the hydrodynamic flow on the separation was assessed using a modified gated injection (shown in Figure 5.17). Using a flow through device, the sample was place in the SB channel reservoir and pulled to waste using a syringe attached to the waste reservoir. Simultaneously, high voltage was applied between the CF reservoir and the A reservoir. This created an electric field down the analysis channel while, at the same time, varying hydrodynamic forces could be applied to the waste channel to simulate operation of the device. To inject a plug of sample into the analysis channel, the high voltage was briefly switched to the SB channel reservoir and the CF reservoir was floated (Inject Mode). After a plug of sample was injected, the voltages were switched back to the run conditions and the SB channel was again floated (Run Mode). The high voltage switching was accomplished using a high voltage (HV) switching relay circuit assembled in house using a Kilovac (CII Technologies, Santa Barbara, CA) 10 kV HV switching relay. This circuit is described in detail in Chapter 6. A diagram of the run conditions and the inject conditions are shown in Figure 5.17 with the exception that the HV and ground are switched for each mode when analyzing the SPKC/PSPKC separation.

The effect of the hydrodynamic flow on the SPKC/PSPKC injection and separation can be seen in Figure 5.18. Here, the negative pressure applied to the waste channel was varied between -0.06 to -0.46 psi (as compared to ambient pressure). The separation conditions were similar to those shown in Figure 5.3A; however, the buffer was prepared with TBE buffer containing 1% spermine and 30 mM PEG. The electric field applied along the analysis channel during the separation was calculated to be ~900 V/cm. As the

hydrodynamic flow increased, the overall amount injected decreased for both the substrate and product peptides. This result was expected; however, there also appeared to be an injection bias such that the injection amount of the PSPKC peptide decreased faster than that of the SPKC. As the hydrodynamic flow (negative pressure) increases, the ratio between the SPKC and PSPKC changes significantly. The average SPKC/PSPKC height ratios of three subsequent injections for each applied pressure are shown in Table 5.12. This injection bias is important to note because it may be difficult to detect the product peptide if it does not inject into the analysis channel as the cells pass through the lysis intersection. For SPKC and PSPKC, the application of vacuum to the waste channel does not appear to affect the separation.

The same experiment was performed using the sphingosine kinase substrate and product. Here the same modified gate injection was used but, because the EOF was reversed with the EOtrol LR additive and the analytes carry a slight negative charge (due to the fluorescein tag on both substrate and product, and the phosphate group on the product), the high voltage was applied to the analysis channel and the ground was switched between the CF and SB channels to inject a plug of sample (as shown in Figure 5.17). The results of increasing the hydrodynamic flow on the separation are shown in Figure 5.19. Here, the hydrodynamic flow does not appear to affect the migration time or isomer separation of the phosphorylated product. However, the substrate is more neutrally charged. Because of this, as the hydrodynamic flow increases, the electrokinetic force in not strong enough to overcome the hydrodynamic flow to waste. The sphingosine substrate therefore injects to a lesser amount as the hydrodynamic force increases. Additionally, the migration time is affected and the resolution between the isomers is severely degraded. The broadening of the

substrate peak will affect the ability to detect it at low concentrations. It is thought that an increase in the EOF or electric field might improve the substrate separation; however, any increase in total mobility toward the anode will require a proportional increase in the vacuum applied on the waste channel to maintain flow to waste.

5.4 Conclusion

Method development for separation of the SPKC and PSPKC reporter peptides included an assessment of several different channel coatings and separation solutions. Several separation conditions for the positively charged reporter peptides were established and the LOD confirmed to be in the attomole range. This detection limit should be sufficient for detecting the reporter peptides from individual cells. Additionally, the hydrodynamic flow required to pull the cells through the electric field for lysis does not appear to affect the separation of the substrate and product on an uncoated chip. The application of hydrodynamic flow does, however, create an injection bias for the PSPKC peptide. This injection bias could potentially affect the ability to detect the PSPKC and will most likely affect the accuracy of any quantification that is to occur from individual cells.

Separation conditions were also established for the negatively charged sphingosine kinase substrate and product. The separation is rapid and baseline resolution of the fluorescein-labeled isomers for both the substrate and product was achieved. The effect of the hydrodynamic flow on the injection and separation was demonstrated. Due to its near neutral charge, there is a severe degradation of the injection and peak shape for the sphingosine substrate. It is unclear at this time how to combine the hydrodynamic flow required of the flow through and Double T devices and still maintain adequate injection of the sphingosine kinase substrate.

The effect of the hydrodynamic flow on the injection of the reporters further emphasizes the need to remove the cells from the hydrodynamic flow during the lysis process. The flow paths described in Chapter 3 show that, when lysing, cells can briefly enter the analysis channel, out of the hydrodynamic flow. These flow paths will potentially allow for injection of the cell lysate analytes without injection bias due to the vacuum applied at the waste reservoir.

5.5 Tables and figures

Table 5.1 Preamplifier settings used for reporter peptide separation development

Filter Frequency:	3 Hz
Invert:	On
Filter:	12 dB
Gain Mode:	Low Noise

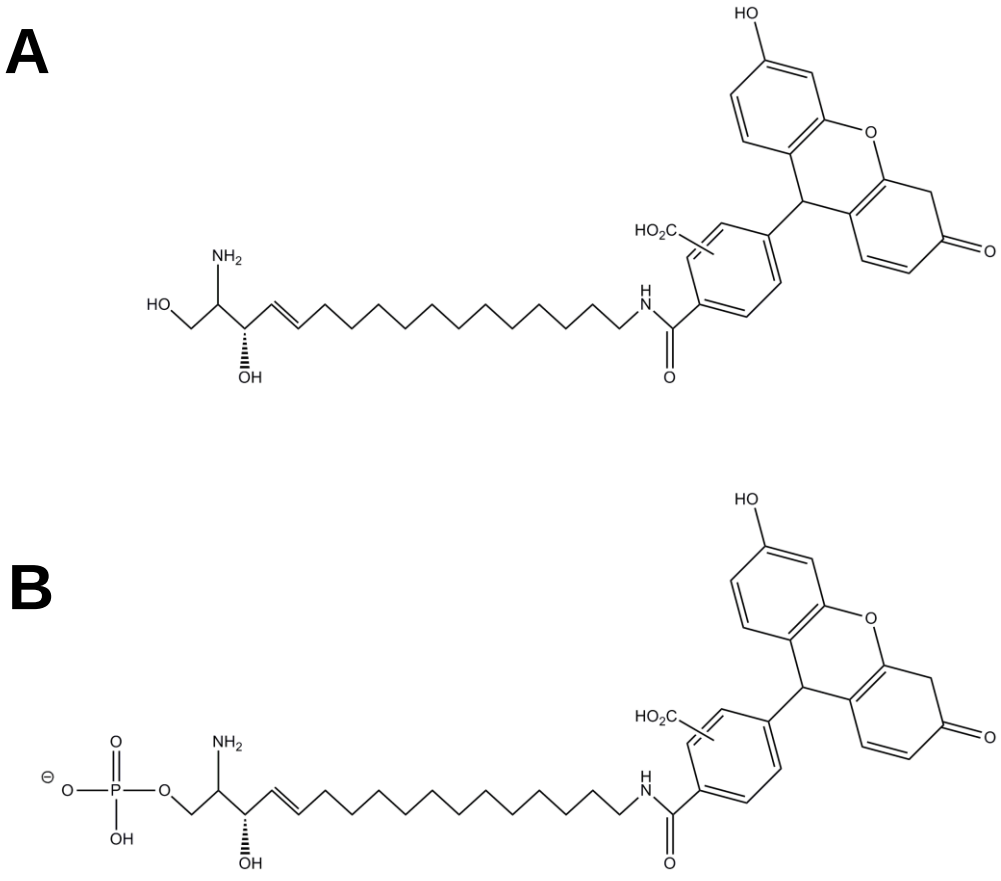

Figure 5.1 Structure of A) sphingosine kinase substrate (S-1) and B) phosphorylated product (S-1-P)

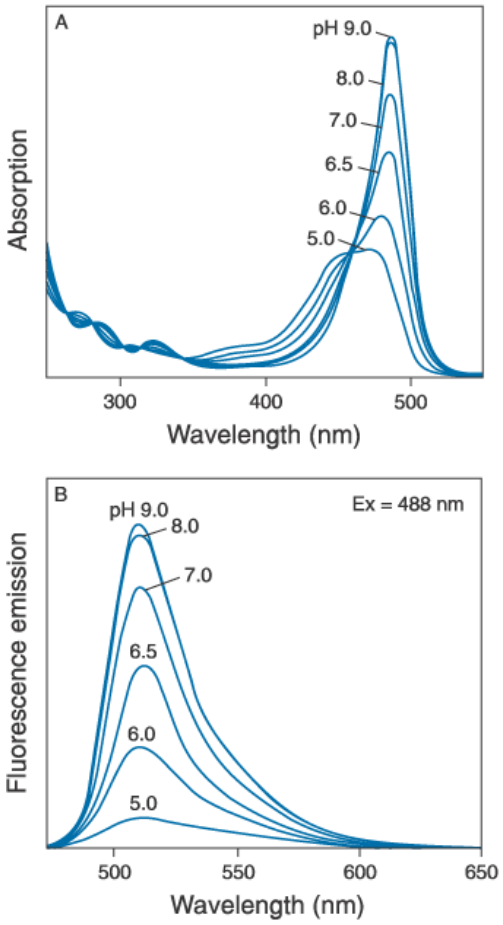

Figure 5.2 Absorption and emission of fluorescein shown as a function of pH. (Source: www.invitrogen.com)

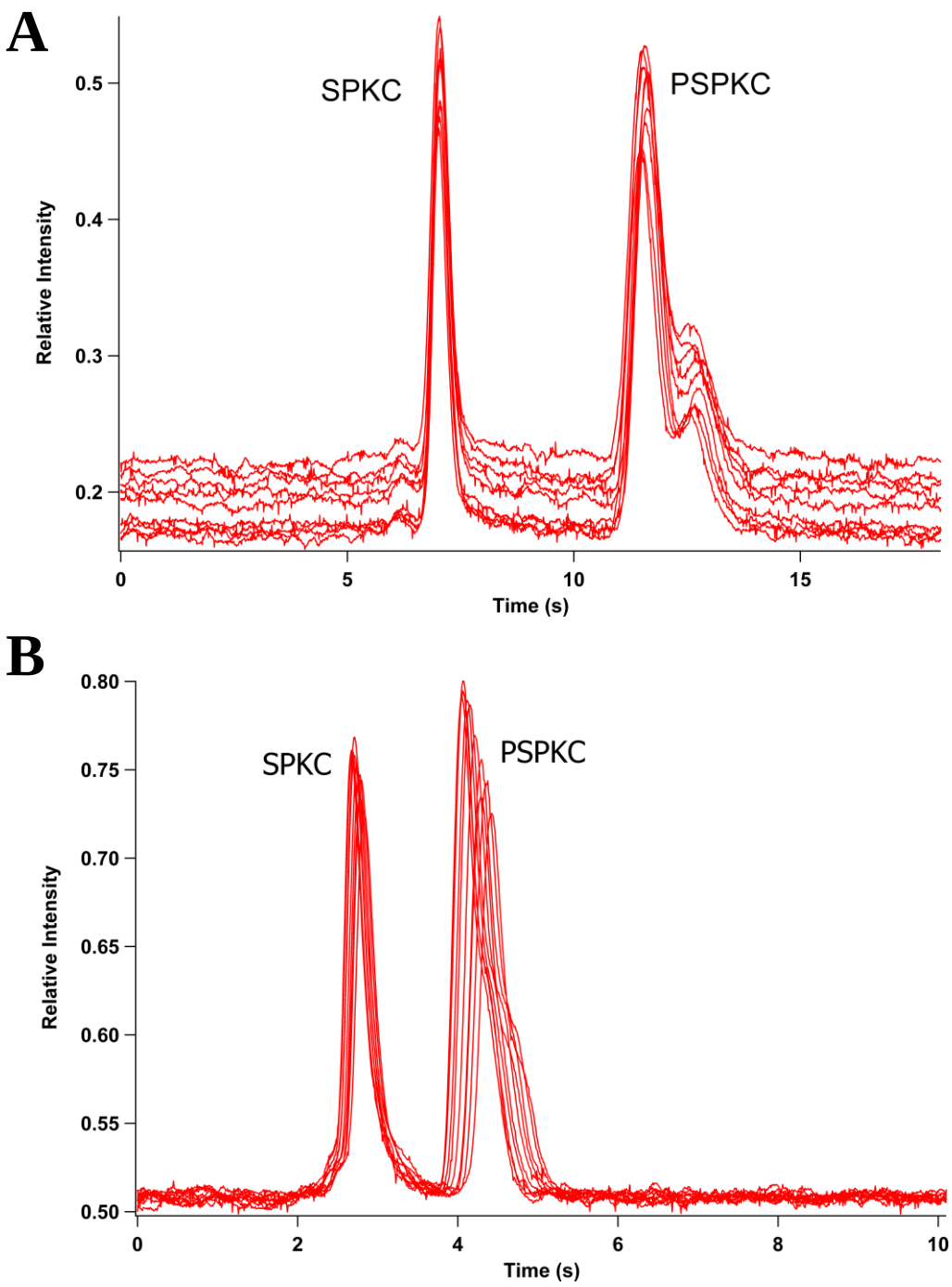

Figure 5.3 Electropherograms showing the separation of SPKC and PSPKC peptides on an uncoated cross chip using Tris/boric acid buffer. The separation with the laser focused on the analysis channel 10 mm from the injection point is shown in A). The separation with the laser focused on the analysis channel 3 mm from the injection point is shown in B).

Table 5.2 Separation conditions for the electropherograms shown in Figure 5.3A and Figure 5.3B

Separation Conditions	**Figure 5.3A**	**Figure 5.3B**
Channel Coating	Uncoated	Uncoated
Buffer	50 mM Tris, 10 mM boric acid, 1 mM spermine, 30 mM PEG	50 mM Tris, 10 mM boric acid, 1 mM spermine, 30 mM PEG
Buffer pH	9.0	9.0
Injection Type	Gate	Gate
Electric Field (V/cm)	1050	1050
Laser Power (mW)	6	6
Laser focal distance from the injection point (mm)	10	3

Table 5.3 Relative standard deviations of the migration times for the SPKC and PSPKC peaks shown in Figure 5.3B

	SPKC	**PSPKC**
Migration times (s)	2.827	4.423
	2.778	4.291
	2.710	4.120
	2.673	4.048
	2.683	4.066
	2.676	4.069
	2.709	4.150
	2.741	4.212
	2.768	4.294
	2.792	4.367
Average	**2.736**	**4.204**
Standard Deviation	**0.054**	**0.134**
RSD (%)	**1.9**	**3.2**

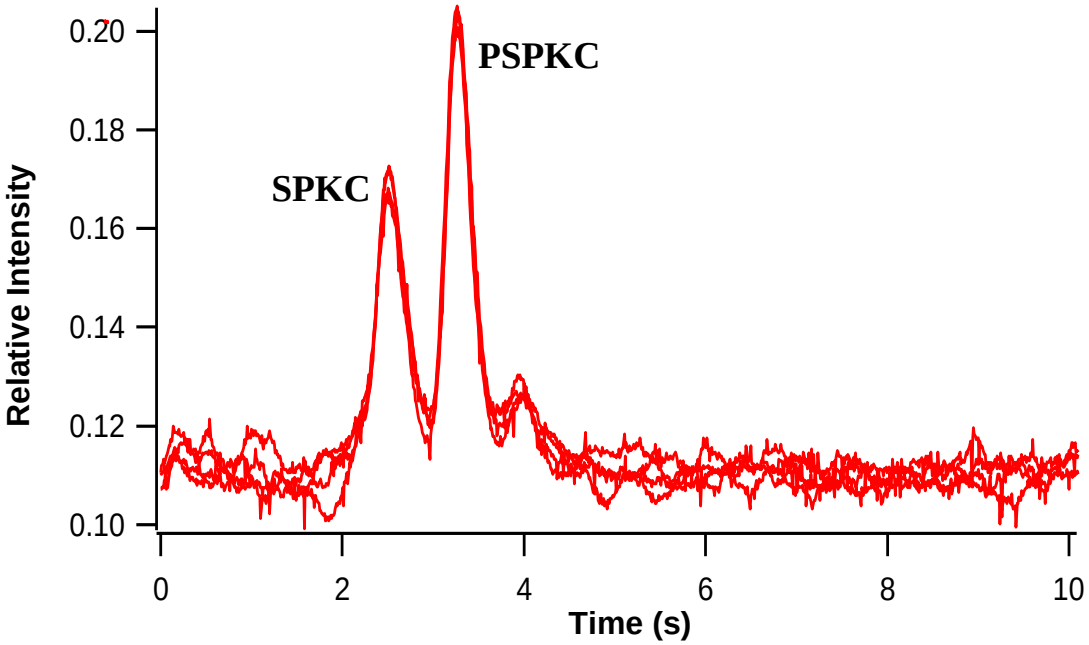

Figure 5.4 Separation of SPKC and PSPKC on a cross chip coated with 30% (v/v) Pluronic F-127

Table 5.4 Separation conditions for the electropherogram shown in Figure 5.4

Separation Conditions	**Figure 5.4**
Channel Coating	30% (v/v) Pluronic F-127
Buffer	50 mM Tris, 10 mM boric acid, 1 mM spermine, 30 mM PEG
Buffer pH	9.0
Injection Type	Gate
Electric Field (V/cm)	840
Laser Power (mW)	6
Laser focal distance from the injection point (mm)	3

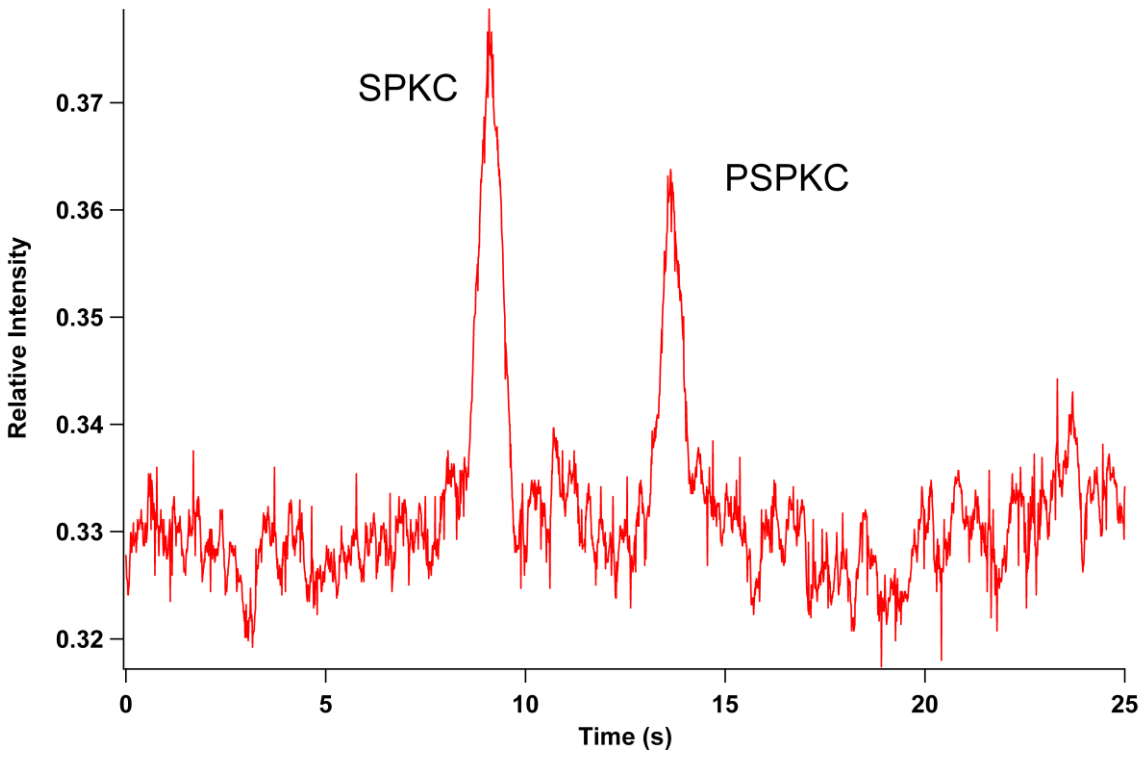

Figure 5.5 Electropherogram showing the LOD for the SPKC and PSPKC peptide. Here, 1.3 and 0.9 attomole of SPKC and PSPKC, respectively, was injected and the S/N for each peak was between 3 and 4.

Table 5.5 Calculation of the amount of SPKC and PSPKC injected using a gate injection.

Parameter	**SPKC**	**PSPKC**
E-Field, E, (V/cm)	776	776
Length to detector, Ld, (mm)	10	10
Migration time, tr, (s)	8.97	13.44
μ_{app} (cm^2/V*s)	**1.44E-04**	**9.59E-05**
Injection time, t_i, (s)	0.5	0.5
E-Field at time of injection, E_i, (V/cm)	1129	1129
Length of sample plug (cm)	**8.11E-02**	**5.41E-02**
Depth of Channel, d, (cm)	0.0021	0.0021
Width of Channel, w, (cm)	0.0039	0.0039
Volume Injected (μL)	**6.64E-04**	**4.43E-03**
Concentration of Sample, C, (μM)	0.002	0.002
Moles Detected, M_d, (attomole)	**1.3**	**0.9**

Note: The bold values are calculated.

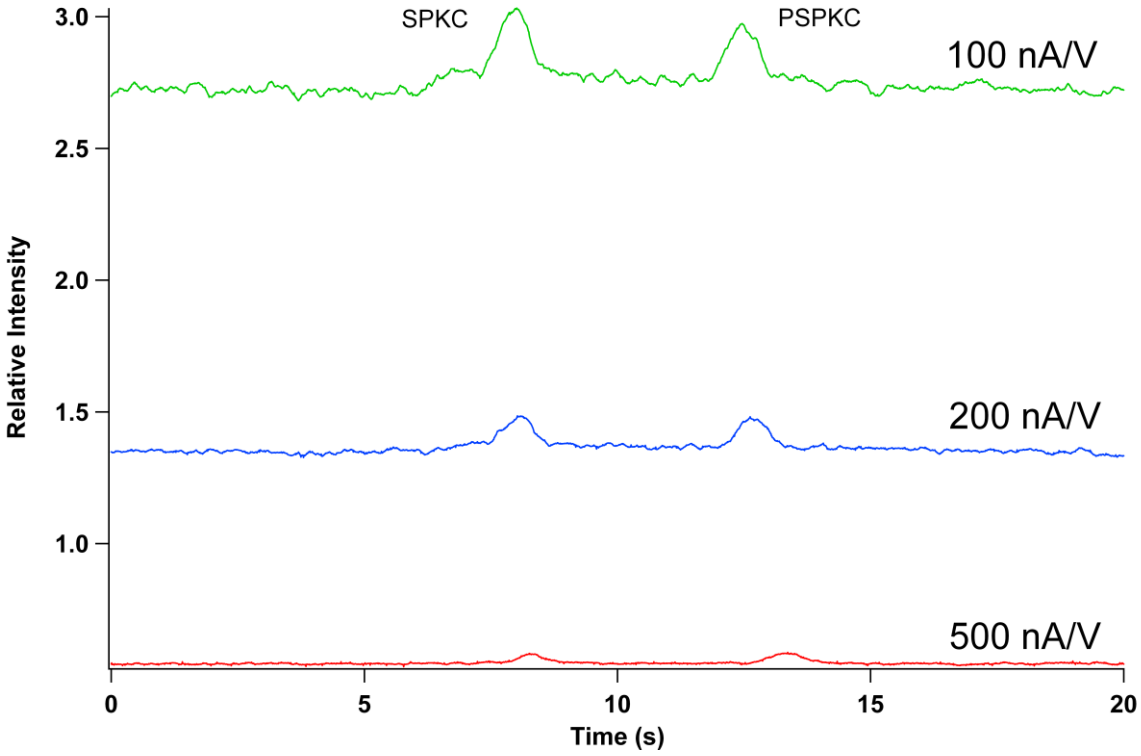

Figure 5.6 Electropherograms of the injection of ~1.3 attomole SPKC and ~0.9 attomole PSPKC peptide, using a gated injection, with varying preamplifier sensitivities. The preamplifier was set at 500, 200 and 100 nA/V.

Table 5.6 Comparison of SPKC and PSPKC S/N ratios at varying preamplifier sensitivities

Preamplifier Sensitivity (nA/V)	**SPKC (S/N)**	**PSPKC (S/N)**
100	5.6	4.5
200	6.4	7.4
500	3.4	4.0

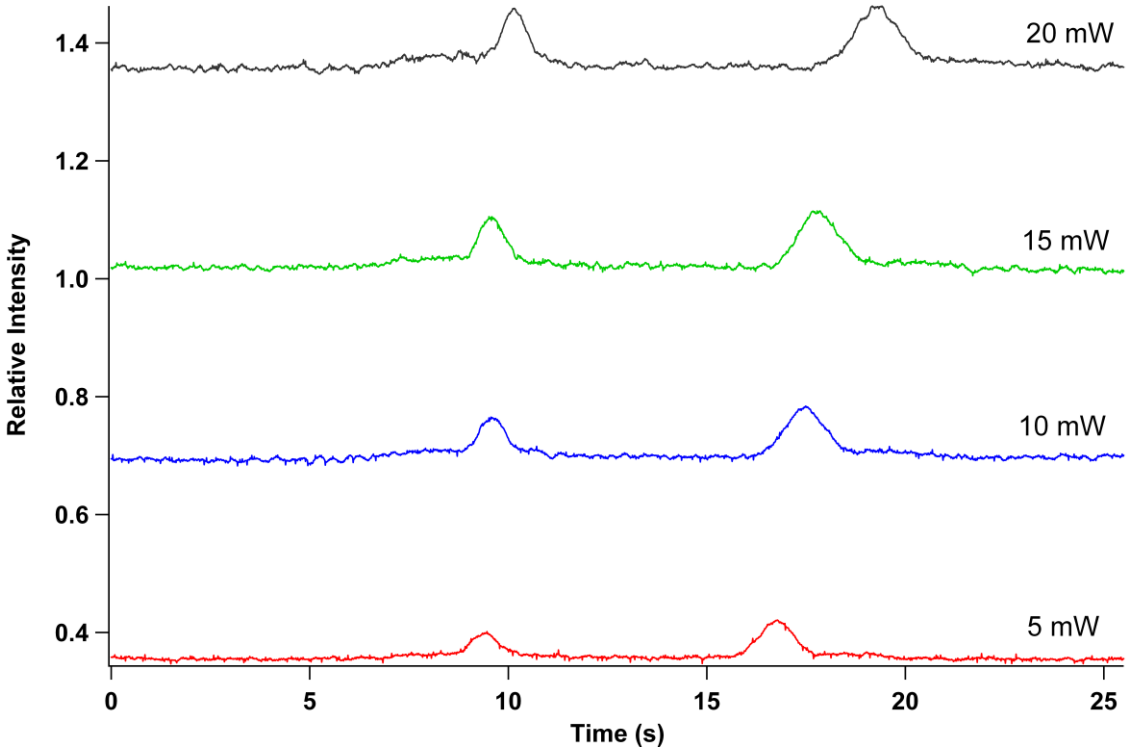

Figure 5.7 Electropherograms of the injection of ~1.3 attomole SPKC and ~0.9 attomole PSPKC peptide, using a gated injection, with varying laser power. The laser power was varied between 5 and 20 mW.

Table 5.7 Comparison of SPKC and PSPKC S/N ratios at varying laser powers

Laser Power (mW)	**SPKC (S/N)**	**PSPKC (S/N)**
5	3.8	7.2
10	3.7	7.6
15	4.0	8.9
20	4.6	8.9

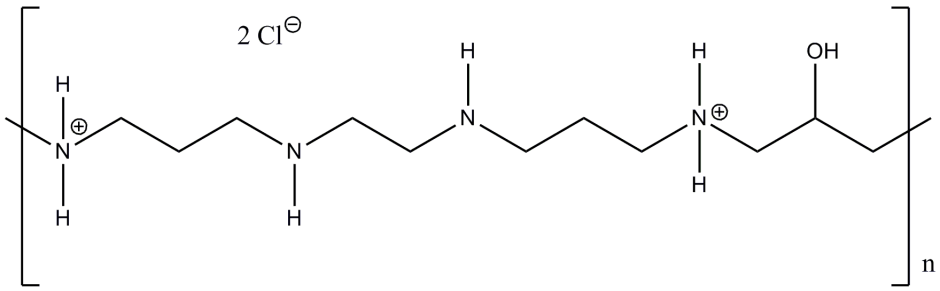

Figure 5.8 Structure of PolyE323

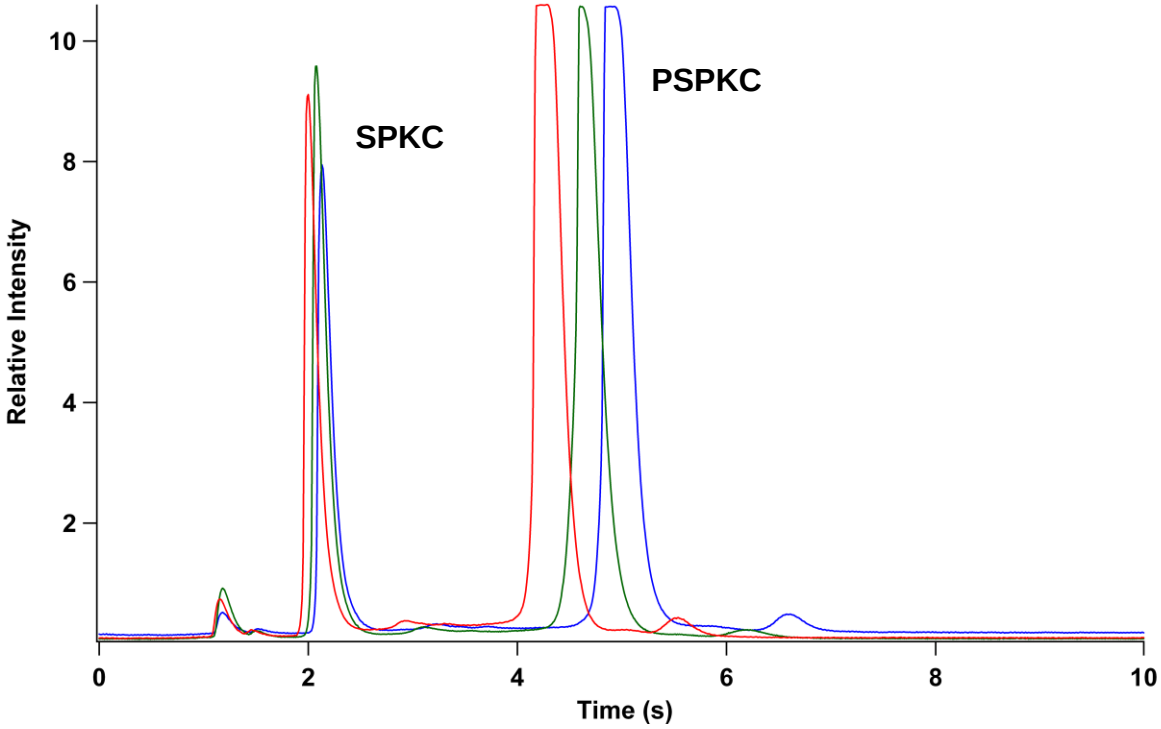

Figure 5.9 Separation of SPKC and PSPKC on three separate flow through chips coated with PolyE323 using a pinch injection

Table 5.8 Separation conditions for the electropherogram shown in Figure 5.9.

Separation Conditions	**Figure 5.9**
Channel Coating	PolyE323
Buffer	50 mM Tris, 10 mM boric acid, 1 mM spermine, 30 mM PEG
Buffer pH	9.0
Injection Type	Pinch
Electric Field (V/cm)	2300
Laser Power (mW)	6
Laser focal distance from the injection point (mm)	6

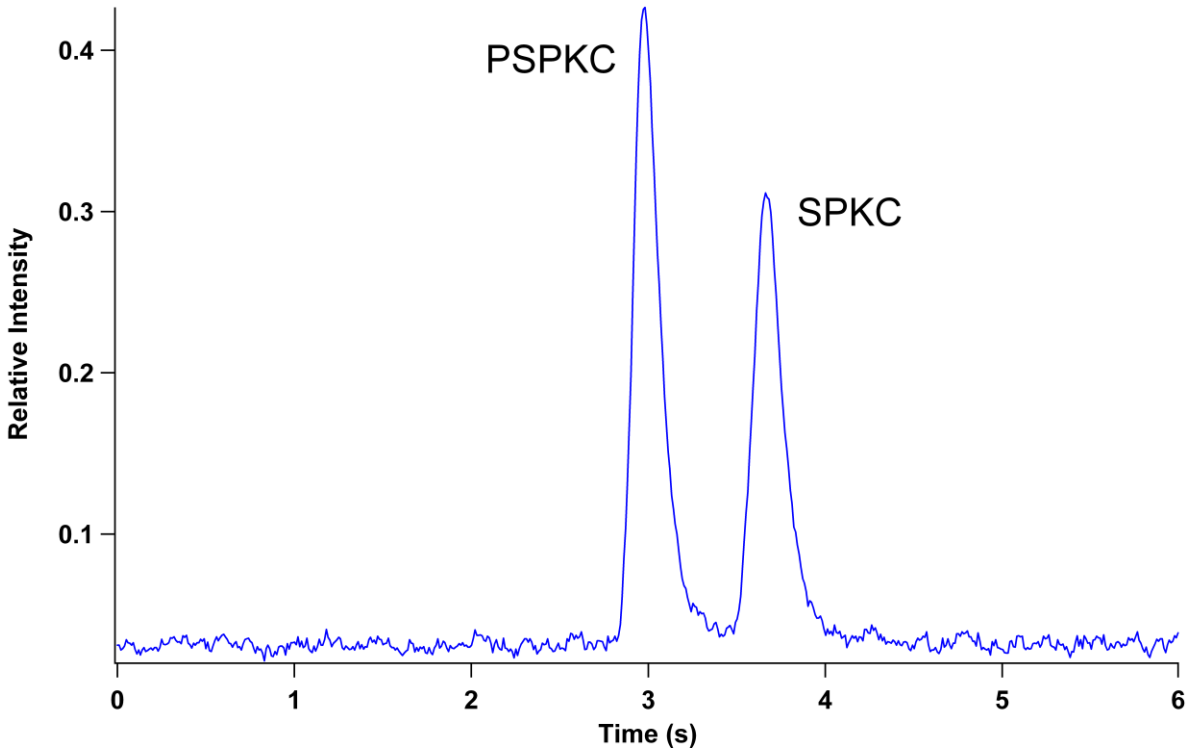

Figure 5.10 Separation of SPKC and PSPKC on a PolyE323 coated flow through device with 0.1% Acetic Acid, pH 3.0, separation solution

Table 5.9 Separation conditions for the electropherogram shown in Figure 5.10.

Separation Conditions	**Figure 5.10**
Channel Coating	PolyE323
Buffer	0.1% acetic acid + 30 mM PEG
Buffer pH	3.0
Injection Type	Pinch
Electric Field (V/cm)	1013 V/cm
Laser Power (mW)	6
Laser focal distance from the injection point (mm)	6

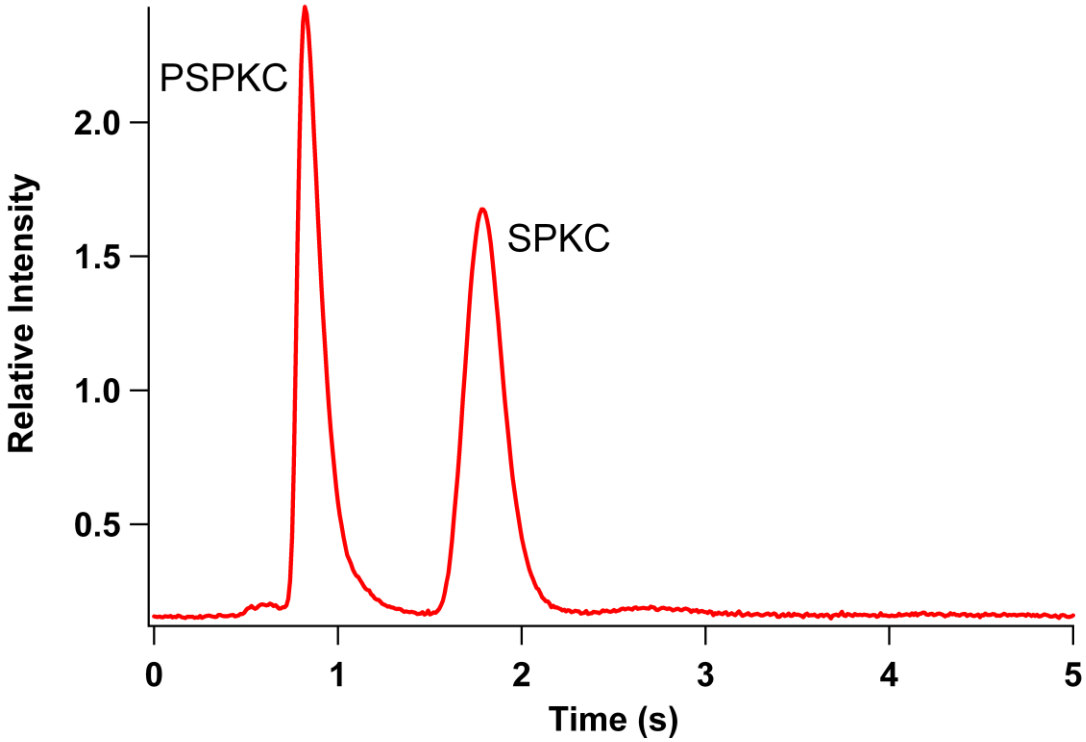

Figure 5.11 Separation of PSPKC and SPKC on a PolyE323 coated chip with 10 mM HEPES containing 30 mM PEG and 1 mM TCEP-HCl, pH 6.6

Table 5.10 Separation conditions for electropherogram shown in Figure 5.11.

Separation Conditions	**Figure 5.11**
Channel Coating	PolyE323
Buffer	10 mM HEPES, 30 mM PEG, 1 mM TCEP HCl
Buffer pH	6.6
Injection Type	Pinch
Electric Field (V/cm)	1820 V/cm
Laser Power (mW)	6
Laser focal distance from the injection point (mm)	3

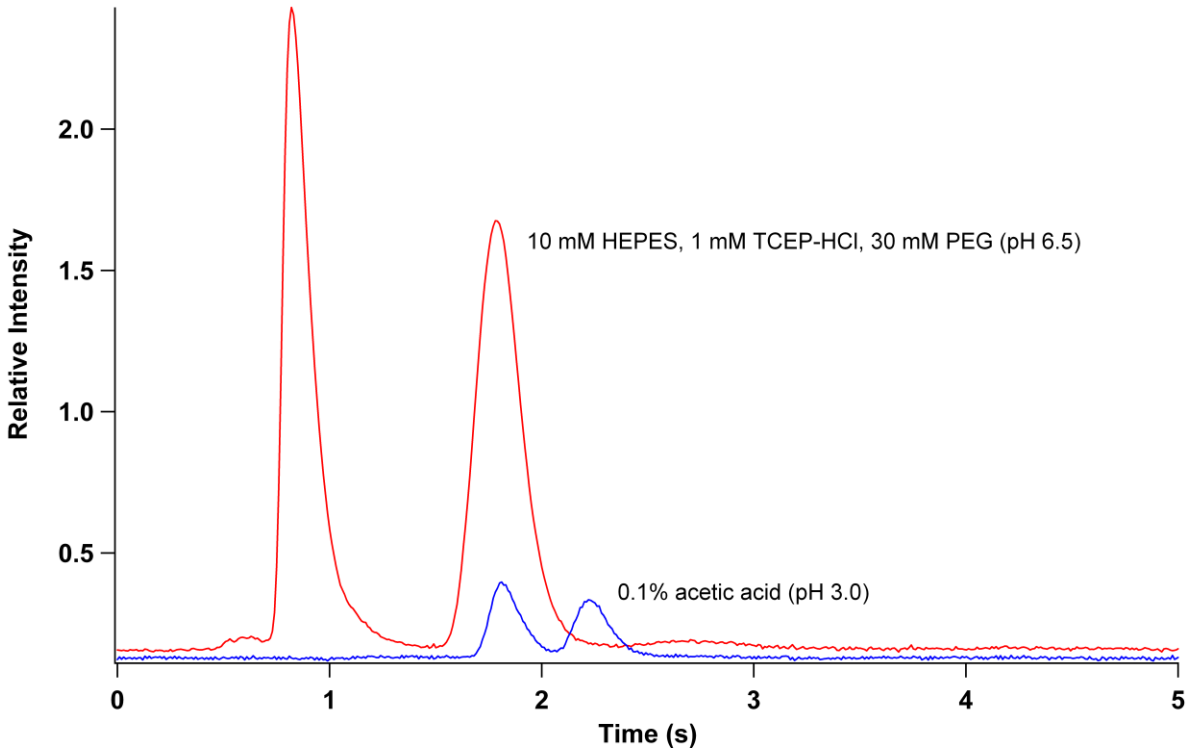

Figure 5.12 Overlay of separations with similar concentration mixtures of SPKC and PSPKC to show the signal increase with pH.

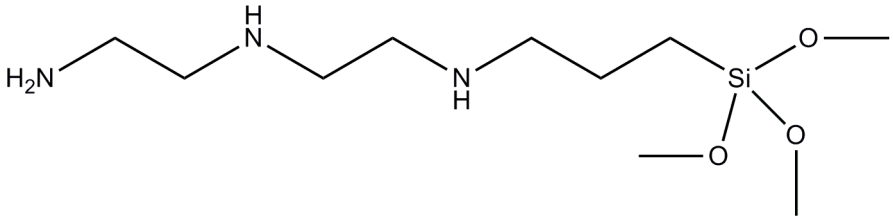

Figure 5.13 Structure of AEPTMS polyamine silane

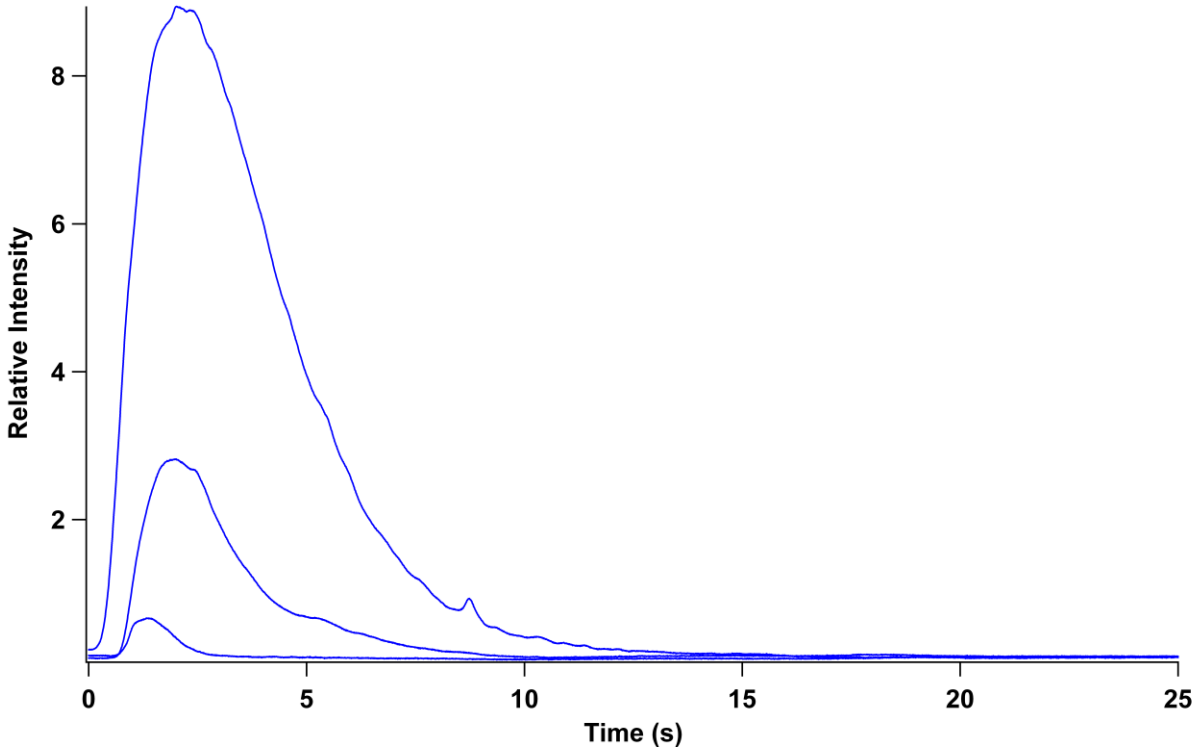

Figure 5.14 Electropherograms showing three injections of a SPKC and PSPKC peptide mixture on a polyamine coated chip using a 10 mM acetate buffer, 30 mM PEG, 3 mM B-cyclodextrin, pH 4.5.

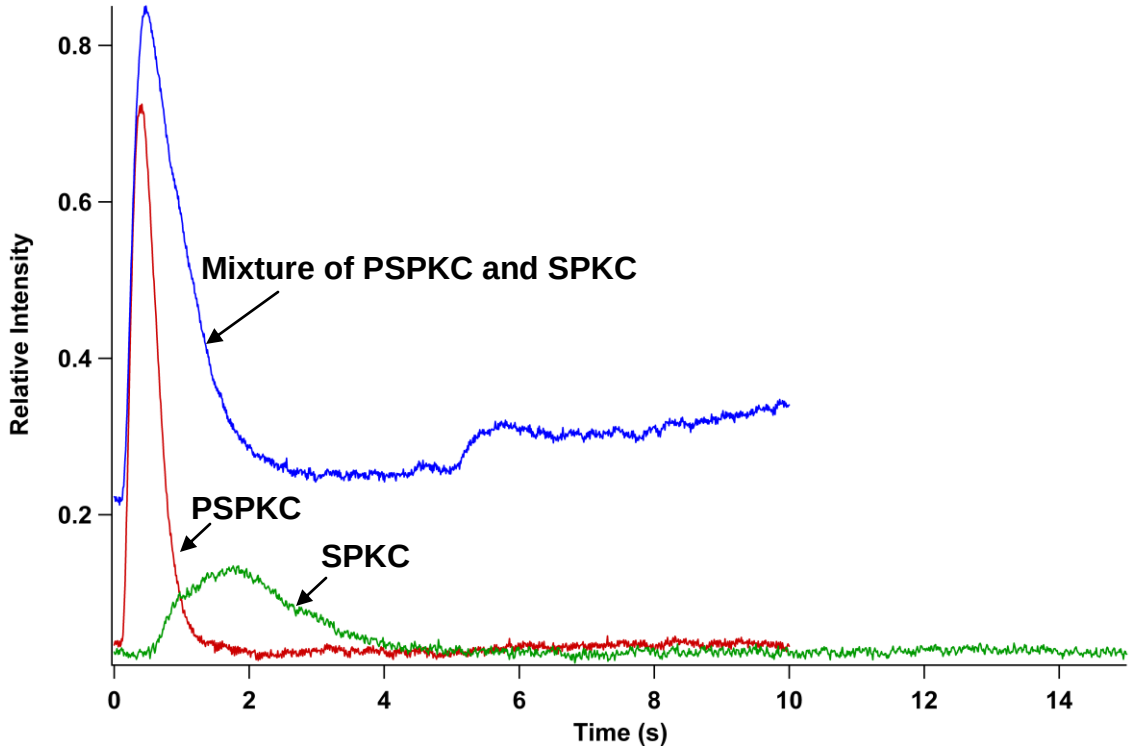

Figure 5.15 Separation of SPKC and PSPKC on a polyamine silane coated chip with 0.1% Acetic Acid, pH 3.0

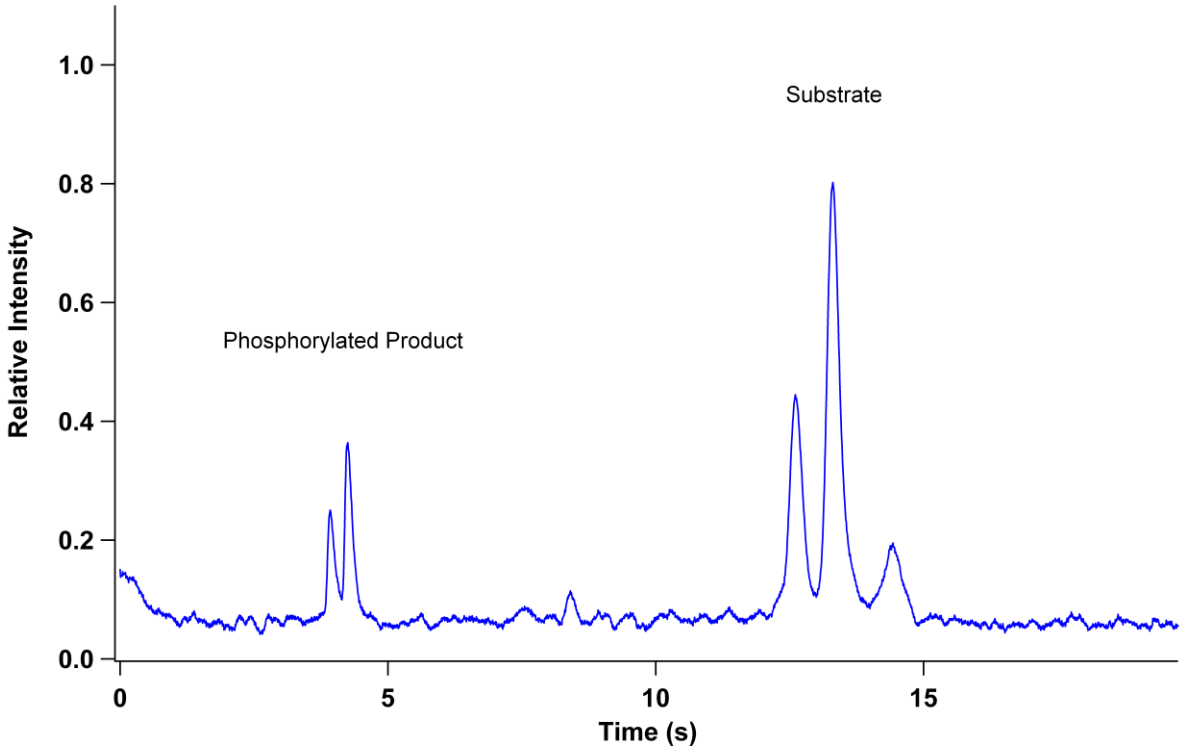

Figure 5.16 Separation of sphingosine kinase substrate and product on an uncoated flow through device

Table 5.11 Separation conditions for sphingosine kinase substrate and product

Separation Conditions	**Figure 5.16**
Channel Coating	uncoated
Buffer	TBE with 5% EOtrol LR and 1% Tween-20
Buffer pH	9.0
Injection Type	Pinch
Electric Field (V/cm)	1292 V/cm
Laser Power (mW)	6
Laser Focus (mm)	10.75

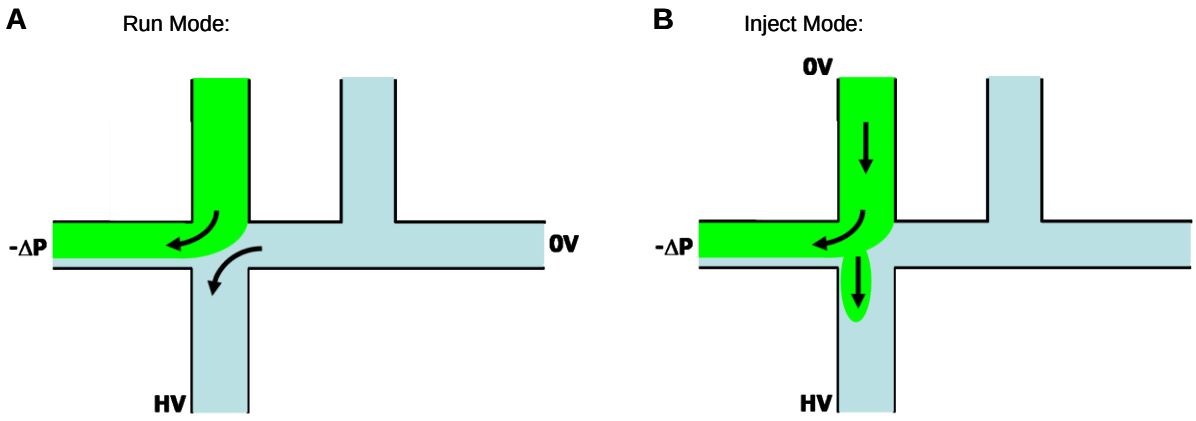

Figure 5.17 High voltage relay switching for simulation of chip operation. In A), the sample is pulled from the SB channel to waste through application of vacuum to the waste reservoir. Simultaneously, an electric field is applied between the CF and analysis channels. In B), a plug of sample is injected into the analysis channel by switching the ground to the SB channel and then quickly back to the CF channel for running.

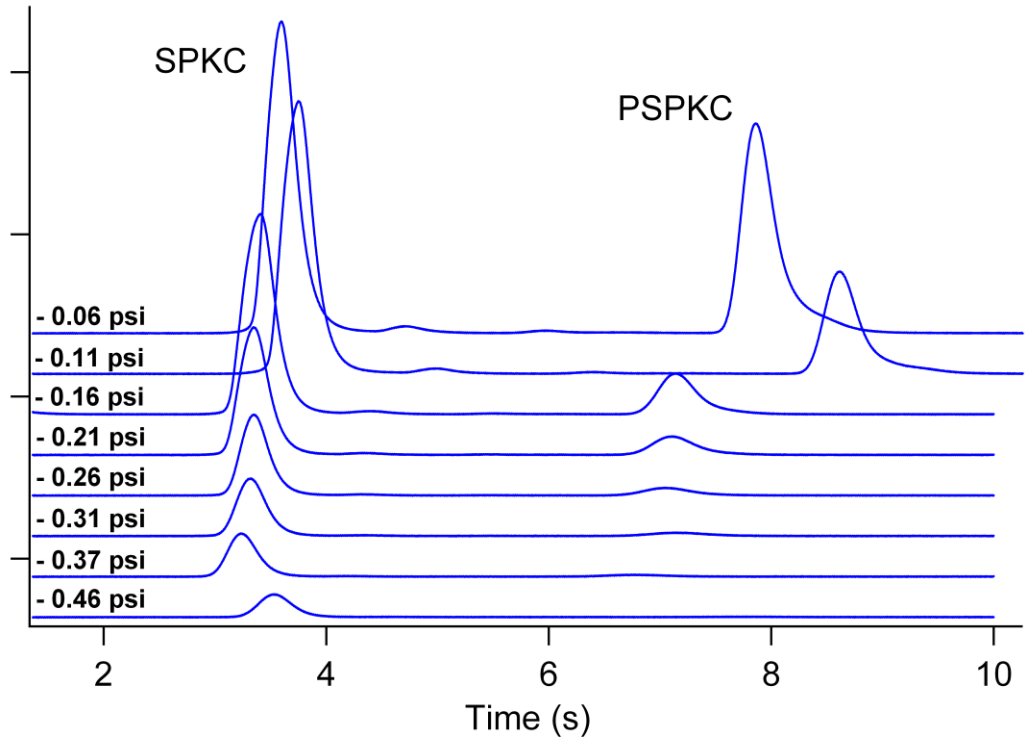

Figure 5.18 Effect of increasing hydrodynamic flow on the separation of SPKC and PSPKC

Table 5.12 Ratio of SPKC to PSPKC peak height for increasing vacuum applied to the waste channel

Applied Pressure (psi)	SPKC/PSPKC peak height ratio
-0.06	1.5
-0.11	2.7
-0.16	5.2
-0.21	7.3
-0.26	11.5
-0.31	18.5
-0.37	23.4
-0.46	34.7

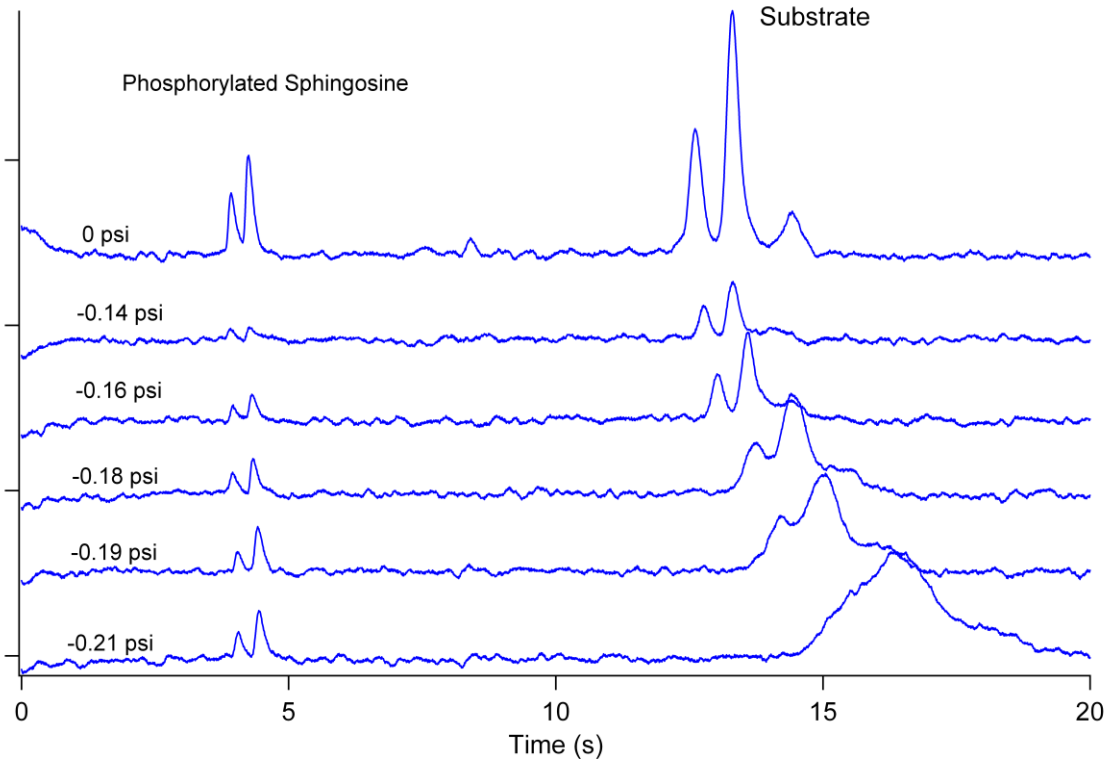

Figure 5.19 Effect of increasing hydrodynamic flow on the separation of the sphingosine kinase and product.

5.6 References

(1) Siow, D. L.; Anderson, C. D.; Berdyshev, E. V.; Skobeleva, A.; Pitson, S. M.; Wattenberg, B. W. *Journal of Lipid Research* **2010**.

(2) Suhaiman, L.; De Blas, G. A.; Obeid, L. M.; Darszon, A.; Mayorga, L. S.; Belmonte, S. A. *Journal of Biological Chemistry* **2010**, *285*, 16302.

(3) McClain, M. A.; Culbertson, C. T.; Jacobson, S. C.; Allbritton, N. L.; Sims, C. E.; Ramsey, J. M. *Analytical Chemistry* **2003**, *75*, 5646.

(4) Li, H.; Wu, H. Y.; Wang, Y.; Sims, C. E.; Allbritton, N. L. *Journal of Chromatography B* **2001**, *757*, 79.

(5) Price, A. K.; Culbertson, C. T. *Analytical Chemistry* **2007**, *79*, 2614.

(6) Rodriguez, I.; Li, S. F. Y. *Analytica Chimica Acta* **1999**, *383*, 1.

(7) Gao, N.; Wang, W. L.; Zhang, X. L.; Jin, W. R.; Yin, X. F.; Fang, Z. L. *Analytical Chemistry* **2006**, *78*, 3213.

(8) Chang, H. T.; Yeung, E. S. *Analytical Chemistry* **1995**, *67*, 1079.

(9) Erim, F. B.; Cifuentes, A.; Poppe, H.; Kraak, J. C. *Journal of Chromatography A* **1995**, *708*, 356.

(10) Cordova, E.; Gao, J. M.; Whitesides, G. M. *Analytical Chemistry* **1997**, *69*, 1370.

(11) Chiu, R. W.; Jimenez, J. C.; Monnig, C. A. *Analytica Chimica Acta* **1995**, *307*, 193.

(12) Legaz, M. E.; Pedrosa, M. M. *Journal of Chromatography A* **1996**, *719*, 159.

(13) Corradini, D.; Rhomberg, A.; Corradini, C. *Journal of Chromatography A* **1994**, *661*, 305.

(14) Woods, L. A.; Roddy, T. P.; Ewing, A. G. *Electrophoresis* **2004**, *25*, 1181.

(15) Borland, L. M.; Kottegoda, S.; Phillips, K. S.; Allbritton, N. L. *Annual Review of Analytical Chemistry* **2008**, *1*, 191.

(16) Hellmich, W.; Pelargus, C.; Leffhalm, K.; Ros, A.; Anselmetti, D. *Electrophoresis* **2005**, *26*, 3689.

(17) Sims, C. E.; Meredith, G. D.; Krasieva, T. B.; Berns, M. W.; Tromberg, B. J.; Allbritton, N. L. *Analytical Chemistry* **1998**, *70*, 4570.

(18) Ros, A.; Hellmich, W.; Regtmeier, J.; Duong, T. T.; Anselmetti, D. *Electrophoresis* **2006**, *27*, 2651.

(19) Greif, D.; Galla, L.; Ros, A.; Anselmetti, D. *Journal of Chromatography A* **2008**, *1206*, 83.

(20) Chao, T. C.; Ros, A. *Journal of the Royal Society Interface* **2008**, *5*, S139.

(21) Gilman, S. D.; Ewing, A. G. *Analytical Chemistry* **1995**, *67*, 58.

(22) Zhang, Z. R.; Krylov, S.; Arriaga, E. A.; Polakowski, R.; Dovichi, N. J. *Analytical Chemistry* **2000**, *72*, 318.

(23) Yi, C. Q.; Zhang, Q.; Li, C. W.; Yang, J.; Zhao, J. L.; Yang, M. S. *Analytical and Bioanalytical Chemistry* **2006**, *384*, 1259.

(24) Huang, W. H.; Ai, F.; Wang, Z. L.; Cheng, J. K. *Journal of Chromatography B-Analytical Technologies in the Biomedical and Life Sciences* **2008**, *866*, 104.

(25) Hogan, B. L.; Yeung, E. S. *Analytical Chemistry* **1992**, *64*, 2841.

(26) Wu, H. K.; Wheeler, A.; Zare, R. N. *Proceedings of the National Academy of Sciences of the United States of America* **2004**, *101*, 12809.

(27) Nelson, A. R.; Borland, L.; Allbritton, N. L.; Sims, C. E. *Biochemistry* **2007**, *46*, 14771.

(28) Lee, T. T.; Yeung, E. S. *Analytical Chemistry* **1992**, *64*, 3045.

(29) Han, F. T.; Lillard, S. J. *Analytical Chemistry* **2000**, *72*, 4073.

(30) Thorsteinsdottir, M.; Beijersten, I.; Westerlund, D. *Electrophoresis* **1995**, *16*, 564.

(31) Lee, K. J.; Mwongela, S. M.; Kottegoda, S.; Borland, L.; Nelson, A. R.; Sims, C. E.; Allbritton, N. L. *Analytical Chemistry* **2008**, *80*, 1620.

(32) Ullsten, S.; Zuberovic, A.; Wetterhall, M.; Hardenborg, E.; Markides, K. E.; Bergquist, J. *Electrophoresis* **2004**, *25*, 2090.

Chapter 6: Cell isolation and lysis for high-throughput single cell analysis

6.1 Introduction

It has been stated that high-throughput single cell chemical cytometry on microfluidic devices is best performed by first isolating and trapping an individual cell.[1-4] After trapping, the cell can be lysed and the contents analyzed. There are several methods for cell manipulation and isolation, the majority of which involve dielectrophoresis, optical tweezers, mechanical trapping or cell trapping in a hydrogel.[1,5-7]

Dielectrophoresis, one of the most common methods for cell trapping, takes advantage of the ability to induce a dipole across a cell using a non-uniform electric field.[6,8] Control of the electric field can then be used to directionally move and position the cell. For trapping, a two dimensional electric field gradient is used to capture cells within a potential well.[7] Several groups have used this method for single cell analysis.[9-11] The technique of using dielectrophoresis for isolating single cells is advantageous in that cells can be deterministically captured and released.[8] There are, however, several drawbacks to this method. First, dielectrophoretic trapping is reliant on the solution flow rate within the microchip channels to bring the cells to the potential wells. It requires sensitive electronics for operation and the fabrication of microfluidic devices containing the appropriate electrodes can be difficult.[12] Finally, the procedure frequently involves the presence of high frequency alternating current (AC) electric fields. These AC fields can cause Joule heating, which places stress on the cells.[1]

The use of optical tweezers is also a common method for trapping and manipulating single cells for analysis. This method uses scattering and gradient forces produced by light to confine particles. Optical trapping has been used on microfluidic devices to capture a single cell and transport it to an analysis region; however, this method of cellular manipulation is labor intensive and the movement of a cell captured in an optical tweezer is slow.[13-15] It has been reported that optical tweezers for CE analysis of individual cells only allows for the analysis of a few cells per hour.[16-17] Like dielectrophoresis, optical trapping also requires sensitive equipment (i.e., optics) to implement.[12] These drawbacks limit the use of optical tweezers for high-throughput single cell analysis applications.

One of the most diverse, and successful, methods for trapping cells is through the use of mechanical obstructions or weirs. In one example, a microchip was designed such that the channels tapered down to dimensions smaller than that of a cell, causing a single cell to become lodged. The microfluidic device was developed with parallel channels to simultaneously capture multiple cells. The trapped cells were then lysed using a detergent and the contents electrophoretically separated.[15] Microwell trapping has also been demonstrated where small wells, with size dependent on cell type, are patterned into the device. The wells are designed to capture a single cell for various measurements.[12,18-19] For example, DiCarlo et al. trapped cells in a microwell array to study carboxylesterases using microscopy.[20] The use of micropatterned weirs or slats to trap individual cells is also highly reported in the literature.[19,21-24] In one example, Hellmich and coworkers used optical tweezers to manipulate cells to an area where vertical posts mechanically trapped the cell. After trapping, the cell was allowed to adhere to the main microchannel wall and subsequent lysis and analysis was performed.[13,25]

Perhaps one of the most promising methods to capture and isolate individual cells is through suction against a narrow aperture. This method is similar to patch clamping techniques where cells are captured against an aperture that is smaller than the dimensions of a cell. In traditional patch clamping, a narrow pipet tip is used to capture a cell and create a highly resistive seal between the cell and the pipet.[26-27] After the seal is formed, small changes in current can be measured that indicate the flow of ions across the cell's membrane. Microfluidic technology has been used to facilitate these transmembrane ion channel studies by providing better control over cell flow paths and positioning for cell trapping. On a microfluidic device, the use of a channel with dimensions smaller than the dimensions of a single cell can be used for trapping. Several good examples of patch clamp measurements on microfluidic devices have been reported.[26-32] In addition to ion channel studies, other examples of using this type of trapping technique to perform single cell experiment can be found in the literature. For instance, Lee's group has trapped cells against narrow apertures fabricated on a microfluidic device in order to study intercellular signaling.[33]

6.1.1 Trapping design for single cell analysis

In order to overcome some of the limitations associated with the flow through chip design, a device utilizing a patch clamp trapping method has been developed. The use of this type of trapping was investigated as a means to eliminate two issues associated with the flow through design. First, on the flow through device there exists the possibility that two or more cells can enter the lysis intersection simultaneously. Using an immobilization strategy, a single cell can be captured to ensure that only one cell is being analyzed at a time. Additionally, on the flow through device, the hydrodynamic cell flow rate must be carefully controlled to simultaneously achieve optimal lysate injection and flow of cellular debris to

waste. Yet, the hydrodynamic flow also causes a bias in the lysate injection for certain analytes, as described in Chapter 5. Use of an immobilization strategy will eliminate these issues because the cell flow rate only needs to be controlled in order to trap a cell. After trapping, the hydrodynamic flow can be reduced to zero prior to cell lysis. Elimination of the constant hydrodynamic flow will also prevent injection bias of intracellular analytes.

In this chapter, the initial development and proof-of-concept for a microfluidic device that incorporates a modified patch-clamping method to trap a single cell for analysis is discussed. On this device, an electroosmotic flow pump is incorporated to control cell trapping and an example of a single cell analyzed on this device is shown. Finally, the potential for parallelization of this design is described.

6.2 Experimental

6.2.1 Chip fabrication

The design for the trapping chip, shown in Figure 6.1, was patterned onto a 50 mm x 50 mm, 0.9 mm thick B270 crown glass substrate using traditional photolithography techniques described in previous chapters. The channels were etched using 10:1 buffered oxide etch (BOE). Channels were etched to approximately 25-30 μm deep which generally left a small bridge, as shown in Figure 6.2A, of approximately 2 to 5 μm width between the trapping channel and the separation channel. Occasionally during the etching process, there was breakthrough at the bridge area such that a small aperture was created. In these instances, when the created aperture had dimensions smaller than the average Jurkat cell (10-15 μm), the chips were bonded and used without the FIB milling step described below. The electroosmotic pump channels (EP1 and EP2) were 85-95 μm wide and approximately 4.2 cm long (each). The cell flow (CF) was 275-285 μm wide and separation (S) and waste (W)

channels were 64-68 μm wide. The bottom, wider section, of the separation channel was 210-220 μm wide. The channel lengths were approximately 8, 12, and 10 mm for the CF, S and W channels, respectively.

After etching, channel access holes were drilled at the end of each channel using aluminum oxide powder blasting (Microblaster, Comco Inc., Burbank, CA). For chips that still had an intact bridge at the trapping site, the photoresist and chrome layers were stripped using acetone and Transene chrome etch (Transene Company, Inc., Danvers, MA). The chip was then recoated with ~10 to 20 nm of chrome using an ion beam sputter system (IBS/E, South Bay Technologies, San Clemente, CA). An approximately 10 μm (width) x 10 μm (depth) trapping aperture was created on each chip using focused ion beam milling (FIB) (Helios Nanolab Dual Beam, FEI, Hillsboro, OR). Scanning electron microscopy (SEM) images of the chip before and after milling are shown in Figure 6.2. The general FIB and SEM settings are listed in Table 6.1.

The multi-trapping chip design is the same as that shown in Figure 6.1 with the exception of the trapping site. Images of the trapping site are shown in Figure 6.10. Channels 1, 2 and 3 were each 25 μm deep and 94, 84 and 72 μm wide, respectively. Each of the trapping channels were FIB milled in the same manner described above. After milling, the chrome layer was then stripped using chrome etch. The microchips were fusion bonded to a 0.9 mm thick B270 cover slip to create a closed channel network. Buffer and sample reservoirs were created by attaching cloning cylinders (Fisher Scientific, 4 mm i.d.) around the access holes using Norland 63 optical adhesive (Norland Products, Inc., Cranbury, NJ). Each reservoir holds a volume of approximately 100 μL.

6.2.2 Channel coatings

To prevent cell adhesion to the cell flow channel, it was coated using the PEG-silane procedure described in Chapter 2. The EP2, S and W channels were also coated with the PEG-silane to reduce the EOF within those channels compared to the EP1 channel. The channels were coated by pulling the PEG-silane from the CF, S, W and EP2 reservoirs to the coating (C) channel reservoir. During this procedure, ethanol was pulled through the EP1 channel to prevent it from being coated with PEG-Silane.

6.2.3 Coating of EOF pumping channels

Two methods for creating an electroosmotic flow pump (EOF pump) were used. In the first case, the EP1 channel was first flushed for ~15 minutes with 1 N NaOH. The 1 N NaOH was pulled to the coating channel and deionized (DI) H_2O was placed in the other channel reservoirs to preserve the PEG-silane coating. Following the NaOH rinse, the EP1 channel was cleansed with a brief rinse of Nanopure H_2O. This left a more negatively charged surface on EP1 compared to the EP2, PEG-silane coated, channel. In the second case, the same procedure as above was followed, except the EP1 channel was then coated with PolyE323 by placing a 7%(w/w) solution of PolyE232 (pH 7) in the EP1 channel reservoir and pulling vacuum on the C channel for approximately 15 minutes. During this procedure, DI water was pulled through all other channels to preserve the PEG-silane coating. All channels were then rinsed with Nanopure H_2O and dried by pulling air through the channels.

After coating, channel C was plugged using wax. Briefly, a small piece of wax was place on the channel access hole and the chip heated on a hotplate to melt the wax. As the wax flowed into the C channel, the chip was quickly cooled by removing it from the heat.

The chip cooling caused the wax to solidify and plug the channel. To later remove the wax plug, the chip reservoirs were filled with 1 N NaOH and the chip was reheated on a hotplate while simultaneously applying vacuum to the C channel access hole.

6.2.4 Cell culture and preparation

Jurkat cells (ATCC TIB-152, American Type Culture Collection, Rockville, MD; obtained from the University of North Carolina Tissue Culture Facility) were used for all experiments. The cell cultures were maintained at 37ºC and 5% CO_2 in RPMI 1640 1X medium (Gibco BRL, Gaithersburg, MD) supplemented with 10% (v/v) fetal bovine serum, 100 μg/mL penicillin and 100 μg/mL streptomycin. The cells were grown in 25-mL polystyrene culture flasks (Nalge Nunc International, Rochester, NY) to densities of $5x10^5$/mL to $1x10^6$/mL before passage.

To load the cells with dye, ~5 x 10^5 cells were pelleted (1000g for 3 minutes) and supernatant discarded. The cells were re-suspended in a solution of 18 μM Oregon Green 488 carboxylic acid diacetate 6-isomer in extracellular buffer (ECB: 135 mM NaCl, 15 mM KCl, 2 mM $MgCl_2$, 2 mM $CaCl_2$, 10 mM HEPES, pH 7.4). Oregon Green in diacetate form is membrane permeable and loading was achieved through simple incubation (~20 minutes) in a centrifuge vial while maintaining the cells at 37ºC. The cells were then washed 3 to 4 times by pelleting and re-suspending in ECB containing 10 mM glucose.

6.2.5 Chip operation and data collection

For operation and data collection, the chip was prepared by filling all channels with an appropriate separation solution such as the Tris/BA buffer described in Chapter 5. The chips were placed on the stage of a Nikon Eclipse (Nikon, Japan) microscope and the trapping channel was observed using a Sony ExwaveHAD color video camera that was

mounted onto the side of the microscope. To observe cell trapping, excitation of the channel intersection was accomplished with a Nikon Intensilight C-HGFIE (Nikon, Japan). The emission light was filtered through a Semrock (Rochester, NY) Brightline FITC-3540B-NTE filter.

To operate the electroosmotic flow pump for cell trapping, platinum electrodes attached to a high voltage supply were placed in the EP1, EP2 and S channel reservoirs. A high voltage switching relay circuit (Figure 6.5) utilizing a 5014YN MOSFET driver, a n-type MOSFET and a Kilovac (CII Technologies, Santa Barbara, CA) 10 kV HV switching relay was used to alternate the applied electric field between the EP1 and EP2 channels for cell trapping and between the EP2 and S channels for cell lysis. The electric field application is shown in Figure 6.4. Electric fields strengths between 175 to 350 V/cm were used for trapping mode and 400 to 1600 V/cm were used for lysis mode.

To collect laser induced fluorescence (LIF) data, an argon ion laser (Melles Griot, Carlsbad, CA) was used at the 488 nm line. The experimental set-up is shown in Chapter 4, Figure 4.3. The laser beam was focused with the appropriate optics from the top of the chip onto the S channel around 10 mm from the trapping aperture. The fluorescence signal was collected using a Hamamatsu H7732-10 photosensor module (PMT) (Hamamatsu Photonics, Japan). The emission was filtered using a 530DF30 filter and a 488 long pass filter. The signal was processed using a Stanford Research Systems SR570 preamplifier (Stanford Research Systems, Sunnyvale, CA) and data collected using a customized Labview program (National Instruments, Austin, TX).

For current measurements, an Axopatch 200B (Molecular Devices, Sunnyvale, CA) was used with the settings listed in Table 6.2. The current measurements were made by placing the microchip in a closed Faraday cage that contained the Axopatch electrodes.

6.3 Results and discussion

The goal of developing this cell trapping device was to eliminate some of the operational issues associated with the flow through device. On the flow through device, there is little control over the number of cells that enter the lysis intersection at the same time. When several cells enter the electric field near the same time point, they also lyse simultaneously and the lysate peaks will co-migrate. This problem can be partially resolved through decreasing the concentration of the cells in the sample reservoir. However, the decreased cell concentration cannot completely ensure that multiple cells do not travel down the cell flow channel together. By creating a method to isolate a single cell, the multi-cell lysis issue can be eliminated.

On the flow through device, it is also necessary to apply a hydrodynamic flow to transport the cells to the lysis region and pull the post-lysis cellular debris to waste. As shown in Chapter 5, this constant hydrodynamic flow can affect the injection of certain analytes that have a near neutral charge, have low electrophoretic mobilities or have electrophoretic mobilities in the opposite direction from the detection point. Because of this hydrodynamic effect, the lysate injection is biased. By first trapping a single cell, hydrodynamice flow on the microchip can be reduced to zero prior to cell lysis. In this way, the separation of the lysate will not be affected by hydrodynamic flow.

To isolate a single cell, a similar technique to patch clamping was employed. In microfluidic patch clamp devices, cells are carefully suctioned against an aperture with

dimensions smaller than that of a single cell. By carefully docking the cell against the aperture, the cell size does not allow it to pass through and a resistive seal can be formed. Using this patch clamp concept, a device was designed to suction an individual cell against a small trapping channel, or trapping aperture. After the cell is captured, it can be electrically lysed and the same electric field used for lysis can be used for the electrophoretic separation of the lysate contents.

To fabricate a channel with dimensions smaller than that of a single cell, it was necessary to use a specialized fabrication technique. Jurkat cells are used for these experiments, which are a line of cancerous T cells with typical diameters around 15 μm. To manipulate the Jurkat cells through the channel network, the chip channels were etched to approximately 25 μm deep. The trapping channel, however, needs to have dimensions smaller than the average diameter of the Jurkat cells. With traditional etching techniques it is difficult to create this narrow channel amongst the larger, 25 μm deep, channels. The mask design was made such that, after etching the channels to an appropriate channel depth, there was still a gap between the top and bottom separation channel as shown in Figure 6.2A. The trapping channel was then created using focused ion beam milling (FIB).

FIB milling uses a stream of gallium ions to sputter material away from the microchip surface. The ion beam is rastered over the chip surface to create a pattern of predefined depth and width. To prepare the chip for FIB milling, the original photoresist and chrome layers were stripped and the chip recoated with a fresh layer of chrome. The reason for the fresh chrome layer was that, after the initial etching, the bottom and sides of the channels were exposed (i.e., bare glass). The Helios Nanolab is a dual beam instrument that provides simultaneous SEM imaging and FIB capabilities. As the electron beam from the SEM

focuses on the chip surface, charging effects can occur on the bare glass surfaces because there is no path for the charge to dissipate. To prevent this charging, it is necessary to coat the microchips with a thin metallic layer. Another reason for stripping the original chrome layer was that, after the initial etching process, there was underetch beneath the chrome layer; thus, the original chrome layer obscured the true size of the remaining gap between the top and bottom of the separation channel. The original chrome layer must be replaced with a fresh chrome layer to accurately see the gap for FIB milling. The trapping aperture was then milled with approximate 10 μm (width) x 10 μm (depth) dimensions across the bridge. These dimensions are smaller than that of the average Jurkat cell yet large enough to allow sufficient fluid flow through to pull a cell from the CF reservoir to the trapping point.

Initially, a syringe pump was attached to the pumping channels of the microchip and used to pull the cells from the sample reservoir and capture a cell against the trapping aperture. There were problems observed when using pressure-driven flow for cell trapping. Once a cell was docked at the trapping aperture, the syringe pump was turned off to prevent the cell from pulling through the trapping channel. It was observed that the on/off switching times of the syringe pump were not sufficient to precisely control the cell flow and docking. Additionally, the loss of some pressure at the chip-to-tubing interfaces made it difficult to control the fluid flow in a reproducible manner. To avoid fluid control problems, an EOF pump was incorporated onto the device. On-chip pressure-driven pumps are created when there are different electroosmotic flow rates between two channels.[34-35] The difference in flow rates between the channels with different EOFs creates a pressure differential at the channel intersection which, in turn, produces field-free pumping in any adjoining channels. The concept of the EOF pump for this chip is shown in Figure 6.3 and was created using a

trident-like channel structure where the center channel (C) was used for coating only. The right channel, as shown in Figure 6.3, was either left uncoated or was coated with a polyamine compound, PolyE323. This polyamine compound was also used in Chapter 2 for reversing the EOF in the flow through device and in Chapter 4 for separation of the SPKC and PSPKC peptides. All of the other chip channels were coated with PEG-silane. The PEG-silane will significantly reduce the EOF in the EP2 channel and also prevent cell adhesion along the CF channel.

During the coating procedure, the solutions were all pulled through the C channel to prevent cross-contamination of the other channels. After preparing the EOF pump channels, the center coating channel was plugged using wax. Wax was used because it can be removed, if needed, to clean and recoat the channels. The reason that the coating channel needs to be plugged is that it is a very short channel and will have lower flow resistance compared to the separation channel containing the trapping aperture. Channel flow resistance is directly proportional to the length of the channel and inversely proportional to the cross-sectional area. The trapping aperture, having a much small cross-sectional area than the rest of the channel network, has a higher flow resistance. When an electric field is applied across the electroosmotic flow pump channels, the pressure-driven fluid will mainly come from the channel with the lower flow resistance (i.e., the unplugged coating channel). With the coating channel plugged, the pressure-driven fluid can only flow through the trapping aperture to pull the cells from the cell flow channel and to the trapping point. The flow through the aperture using the EOF pump is shown in Figure 6.4A. When the electric field is applied across the EOF pump channels, the chip operation is referred to as “trapping mode”.

Once a cell was captured at the trapping aperture it needed to be quickly lysed. Electrical lysis is the most convenient way to lyse the cell because application of an electric field is already required for electrophoretic separation of the cell lysate. In order to lyse the cell, the electric field was switched from between the EOF pump channels to across the trapping aperture and down the separation channel (shown in Figure 6.4B). For example, using an EOF pump created with a PolyE323 coated channel, the EP1 channel was switched from high voltage to floating. The bottom of the separation channel was switched from floating to high voltage. The EP2 channel was left as ground for the duration of the chip operation. When the electric field was applied across the trapping aperture and down the separation channel, the chip operation is referred to as "lysis mode".

When the chip was operated in either the trapping or lysis mode, it was necessary to maintain the third channel (i.e., whichever channel is unused in that particular mode) as floating. If the third channel is left as ground or at high voltage, then an electric field will be applied across that channel, in addition to the required channels. For example, during trapping mode, if the S channel is grounded, rather than floating, then an electric field will exist down the separation channel. This electric field could cause cell lysis prior to trapping. Additionally, for an EOF pump created with PolyE323, if the EP1 pump channel is left as ground during lysis mode, then there will be an additional anodic EOF component towards the positively charged electrode. The other PEG-silane coated channels have a near neutral surface charge with a slightly cathodic EOF upon application of an E-field. Although the opposing EOFs are necessary for trapping mode, when the chip is operated in lysis mode, these opposing EOFs could have a detrimental affect on the lysate separation.

To accomplish the electric field switching between the EOF pump channels and the separation channel a high voltage relay switching circuit was fabricated. This circuit consists of a high voltage relay switch that is run using a MOSFET (metal-oxide-semiconductor field-effect transistor) with a MOSFET driver. A schematic and image for this switching circuit is shown in Figure 6.5.

An image of the chip operation can be seen in Figure 6.6. Here, Jurkat cells were loaded with Oregon Green fluorescent cytosolic dye. Figure 6.6A shows a single cell that was trapped at the aperture using the chip in trapping mode. After the cell was trapped, the chip was switched to lysis mode and the cell can be seen to lyse in Figure 6.6B to F. The cell lysate partially injected into the separation channel and a portion of the lysate flowed back down the cell flow channel. The flow down the cell flow channel was a result of the low flow resistance of this channel.

A Nikon microscope with a Sony video camera was used to observe the trapping of cells. The laser beam was focused on the separation channel, approximately 10 mm from the trapping site, to detect the fluorescent cell lysate components. An example separation from an Oregon Green-loaded cell that was trapped and lysed can be seen in Figure 6.7. In this case, a second laser beam was focused at the trapping point to collect a fluorescent signal that indicated the trapping of a cell. The fluorescent signal could be used for normal chip operation; however, the alignment of two laser beams on-chip is difficult and requires two detection systems with optics.

One benefit of this chip design is that it has the potential to eliminate the need for two LIF detection set-ups. The resistive seal that is created when a cell is captured against the trapping aperture can be used for detection to trigger the electric field switch between

trapping and lysis modes. The resistive seal creation can be detected by monitoring the current across the trapping aperture. A streaming current should be present due to the flow of ions from the separation buffer through the trapping channel. When a cell is trapped, it blocks this streaming current, causing a measurable current drop. To test the current drop when a cell plugs the trapping channel, an Axopatch 200B patch clamp current measuring device was used. Because the current measuring device is very sensitive to noise, it was operated inside of a faraday cage, separate from the normal operational system. Using the faraday cage set-up, the trapping channel could not be simultaneously observed to ensure that a cell was captured. Therefore, cells were pushed through the trapping channel using positive pressure. Pushing cells through the trapping channel should provide a similar current drop to a cell being suctioned against the trapping channel. Examples of the current drop observed as cells were pushed through the trapping channel are shown in Figure 6.8. The current drop measured was similar to that reported in the literature for patch clamping measurements on a microfluidic device where a ~1400 pA current change was noted upon trapping of a cell.[32] While this proof of principle experiment proved the utility of using current measurements for determination of cell trapping, further characterization would be necessary to fully apply this method

One issue that was noted using this device was that debris buildup at the trapping site occurs. Biofouling was discussed in Chapter 2 and is also an issue with this device because over time the trapping channel becomes clogged. As the debris builds up in and around the trapping channel, the flow through the trapping channel decreases until it is no longer strong enough to pull cells from the cell flow channel to the trapping site. An example of this debris buildup is shown in Figure 6.9. A potential solution to resolve this biofouling issue is to

create parallel trapping sites. Initially, three parallel trapping sites were fabricated on a chip. Images of the multi-trapping chip can be seen in Figure 6.10. Each of the channels leading from the EOF pump to the trapping channels were fabricated such that they had decreasing channel widths from the CF side to the W side of the chip. Because channel 1 has the largest width, it has the lowest flow resistance. The flow to this trapping channel will be slightly higher than to trapping channels 2 and 3; therefore, cells will initially be attracted to the first trapping channel. The concept is that cells will flow toward trapping channel 1 until the collection of debris clogs that trapping aperture such that its flow resistance is increased compared to the next trapping channel. The cells will then preferentially flow and trap against the second trapping aperture. The same effect will occur where cells will flow to the second trapping aperture until it becomes too clogged and the resistance becomes higher compared to the third trapping channel. Each trapping channel was designed to feed into the same separation channel so that the laser beam focus for detection does not have to be shifted during chip operation.

Using 10 μm fluorescent beads, trapping at the three trapping channels was observed. Still frames of the video from multi-trapping are shown in Figure 6.11. As a bead was trapped against the first trapping channel, it plugged the flow such that the majority of the flow now fed through the second trapping channel. As the second trapping aperture is plugged with a bead, the flow through the third trapping aperture then becomes highest and a third bead can be trapped. The use of multiple trapping sites has the potential to circumvent the problem of biofouling. More development work with multiple trapping sites needs to be investigated to determine the optimal design for lysing the cells once they have been trapped.

6.4 Conclusion

Trapping of an individual cell before analysis can provide a means to eliminate some of the issues associated with the flow through single cell analysis device. FIB milling of a narrow trapping channel that is smaller than the dimensions of a single Jurkat cell allowed for capture of a single cell. The trapped cell can be held until it is ready to be lysed. Incorporation of an EOF pump onto the chip provided a controllable means to transport a cell from the cell flow channel to the trapping site and to dock the cell against the trapping channel. The trapped cell was then lysed by switching the direction of the electric field. The use of a high voltage switching circuit provided a means for rapidly switching the electric fields necessary for trapping and lysis modes.

Because cell debris buildup at the trapping site is problematic, a multi-trapping site chip was fabricated. As a proof-of-concept, this chip showed that parallelization of the trapping apertures has the potential to eliminate the issue of biofouling and could allow for the analysis of many cells on a single device. The other potential benefit to trapping cells prior to lysis is that the current change that occurs when a cell plugs the trapping aperture can be used as the detection signal to indicate that a cell has been trapped. This signal will simplify the system by eliminating the need for two LIF detection systems.

Additional work needs to be performed to finalize the operation of this device. A chip with more trapping sites must be fabricated to show that high-throughput cell analysis can be achieved.

6.5 Tables and figures

Table 6.1. Helios Nanolab ion beam and electron beam settings

Ion Beam Settings	
Dwell	1 μs
Scan Direction	Bottom to top
Current	2.8 nA
Voltage	30 kV
Electron Beam Settings	
Voltage	20 kV
Current	86 pA

Table 6.2 Axopatch 200B settings for current measurements

ZAP: 0.5 ms	% Compensation: 0
Lag: 1 μs	Whole Cell: off
Series Resistance: 0	Commands: Holding command x 1: off; Ext command: off
Headstage cooled: I	Mode V: Clamp
Config. Whole Cell β: 1	Output Gain: x1
Leak Subtraction: 0.0	

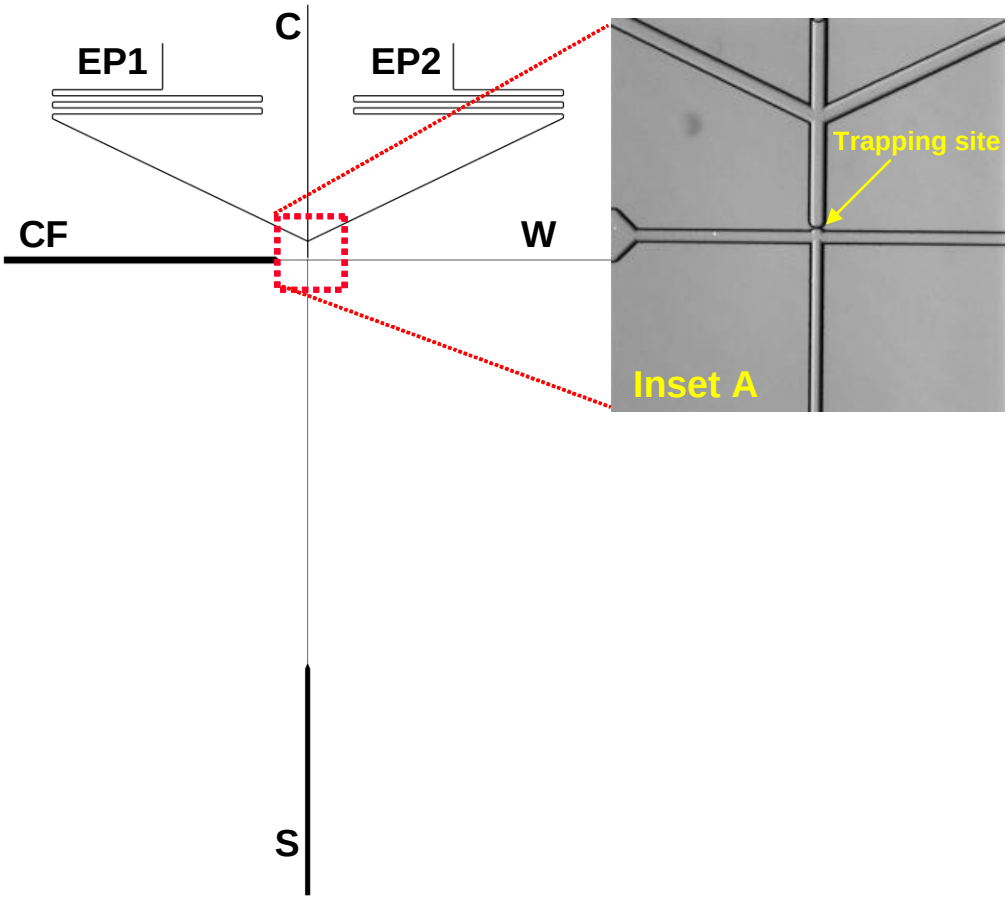

Figure 6.1 Cell trapping chip design with channels labeled. Inset A is a zoom in showing the trident structure for the EOF pump and the trapping site.

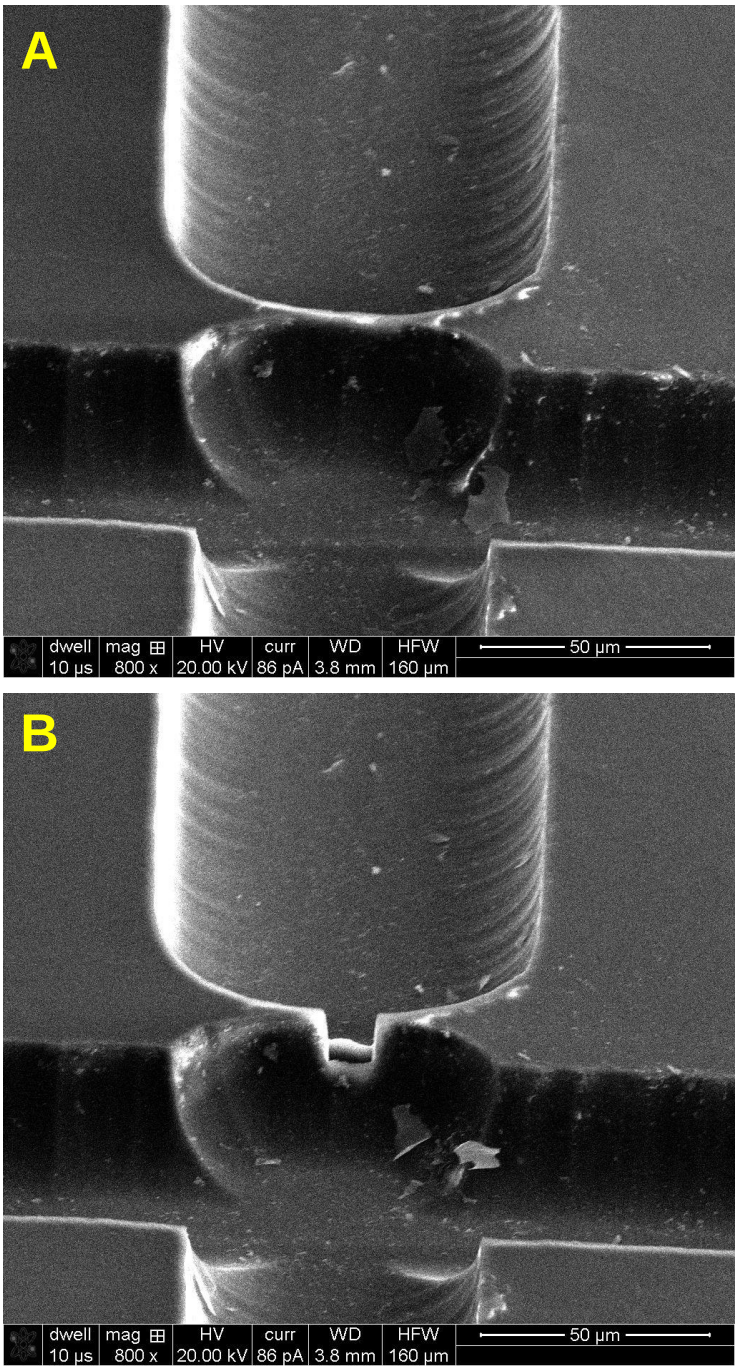

Figure 6.2 SEM images of a cell trapping chip. Image A shows the chip with the gap between the top and bottom of the separation channel prior to milling the trapping aperture. Image B shows the trapping aperture after milling.

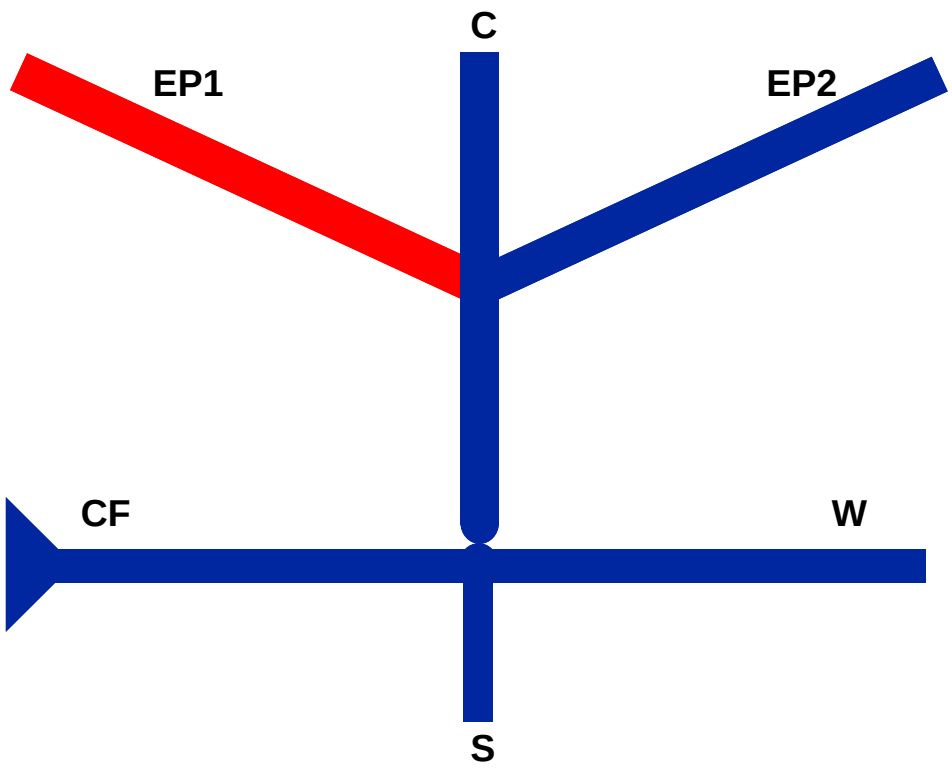

Figure 6.3 Image of channel coatings. EOF pump channel 1 (EP1) is either uncoated or coated with PolyE323 to create a positive surface charge. The EOF pump channel 2 (EP2), separation channel (S), Cell Flow (CF) and Waste (W) channels were coated with PEG-Silane to eliminate the EOF in the EP2 channel and prevent cell adhesion along the CF channel.

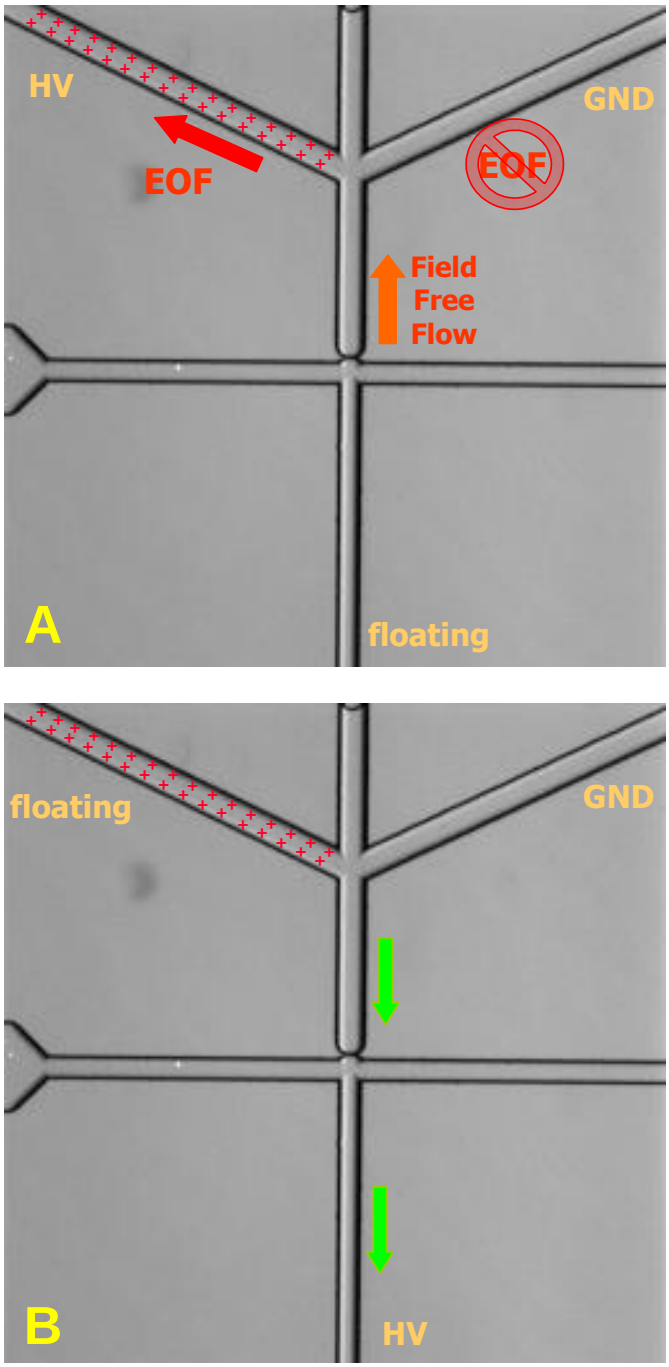

Figure 6.4 Image A indicates the direction of the EOF in each channel for an EOF pump created with PolyE323. The resulting direction of the field free flow through the trapping aperture upon application of voltage to the EOF pump channels is indicated. Image B shows the EOF upon application of ground to the EP2 channel and high voltage (HV) to the bottom of the separation channel. Note: For EOF pumps created using an uncoated EP1 channel, the Electric Field is reversed in Image A.

A

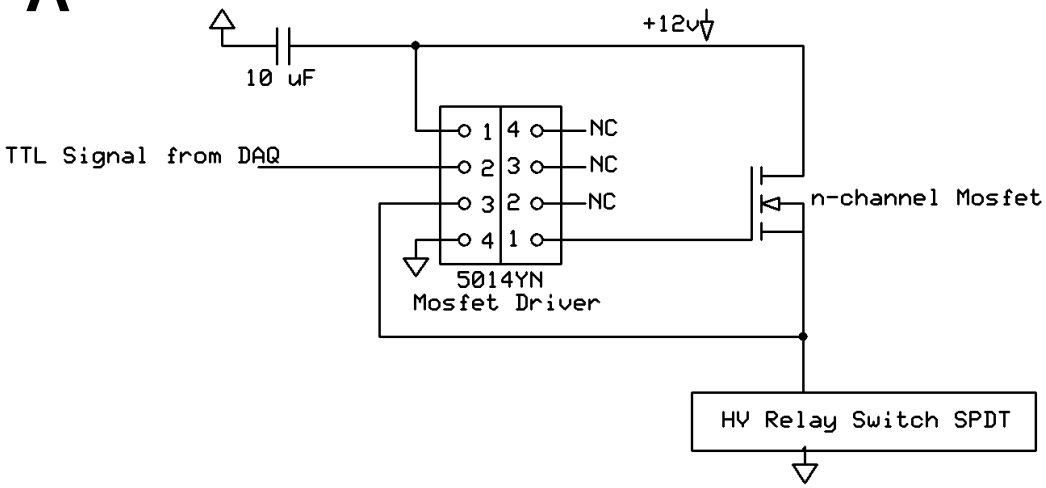

B

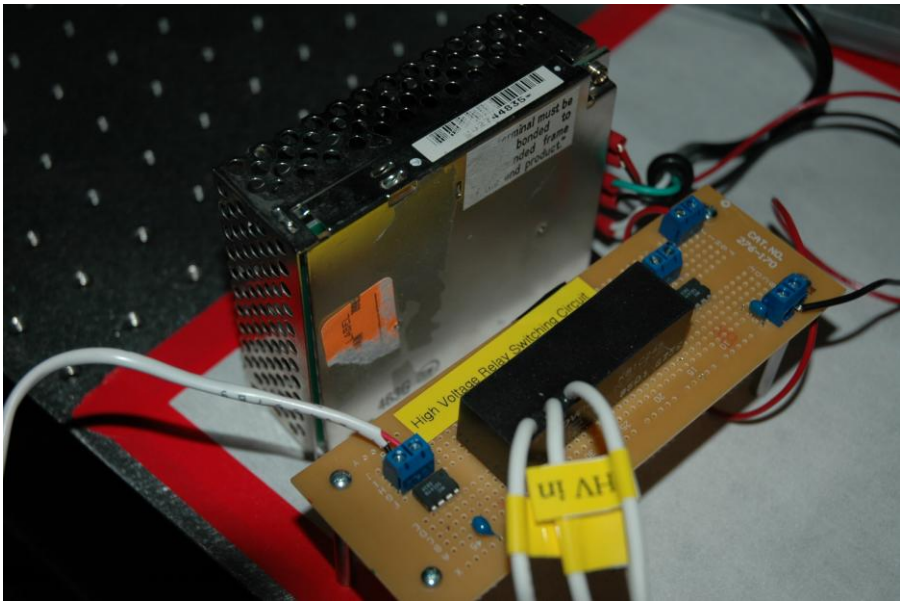

Figure 6.5 Schematic (A) and Image (B) of High Voltage Switching Circuit

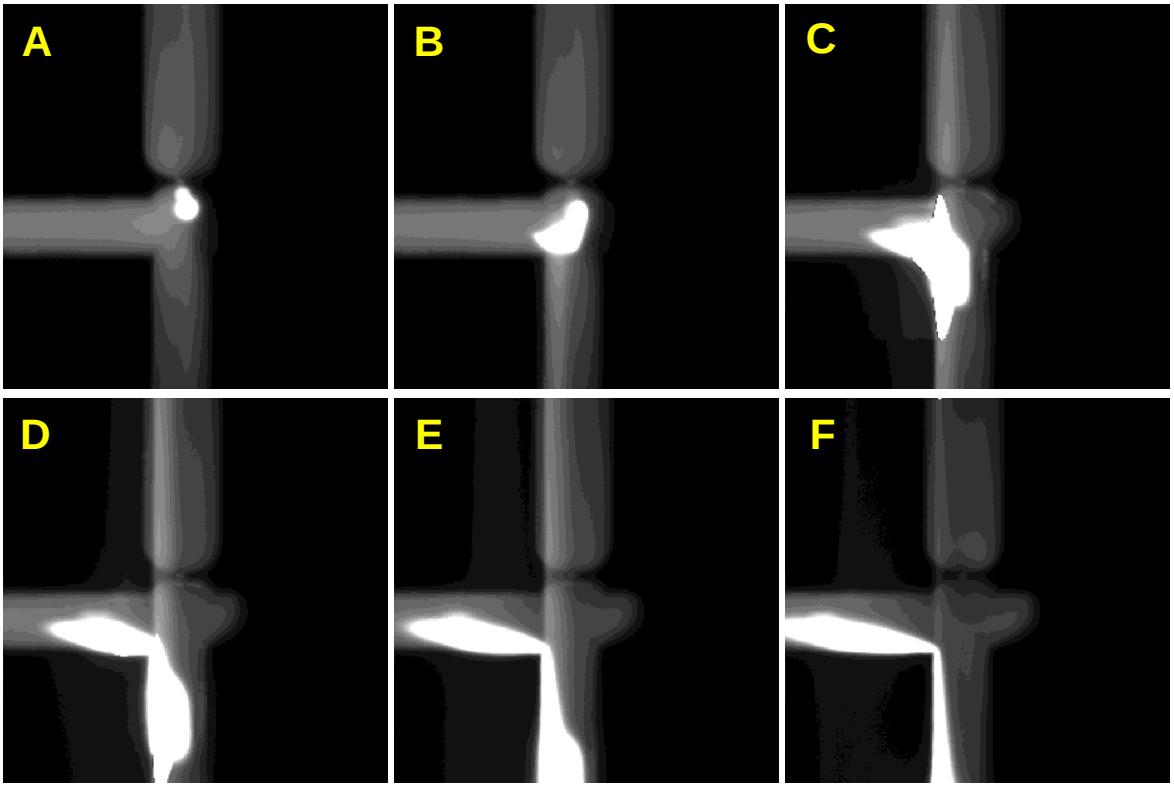

Figure 6.6 Still frames from a video showing cell trapping and lysis modes. In A, a single cell is trapped at the trapping aperture. Images B through F show the voltage switch to Lysis Mode and the subsequent cell lysis and lysate injection.

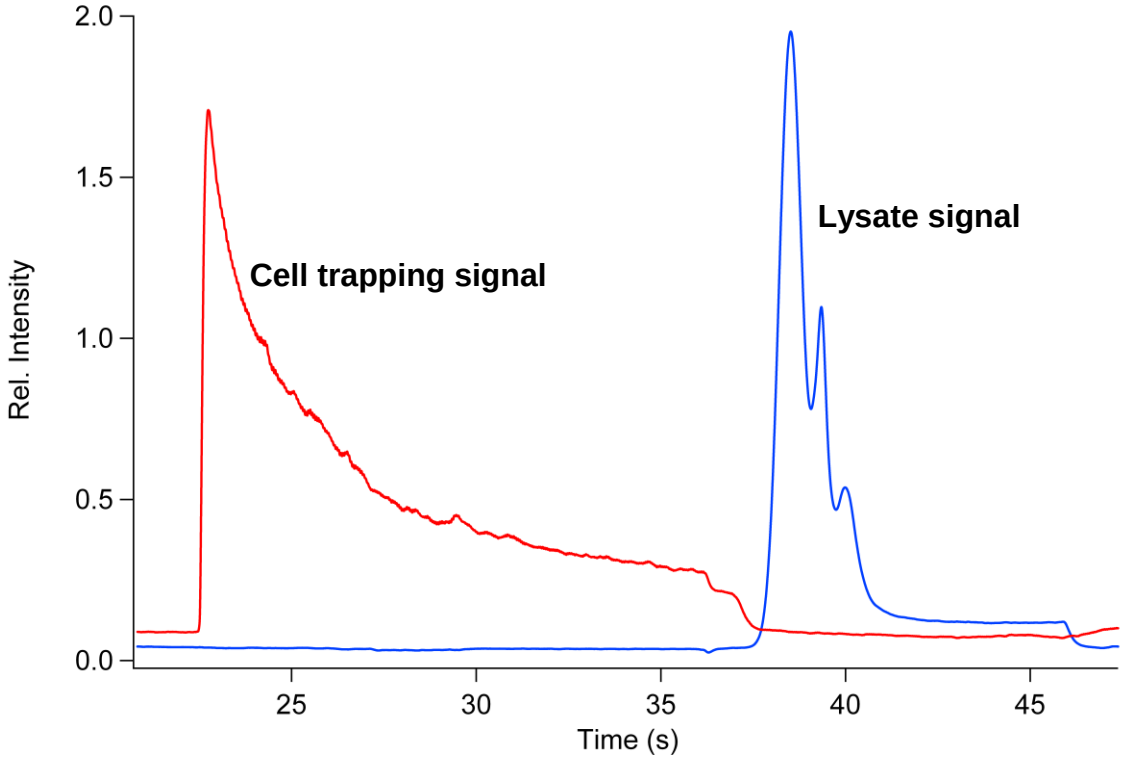

Figure 6.7 Electropherogram showing the signal observed when a single cell was trapped and the resulting lysate peaks detected after lysis.

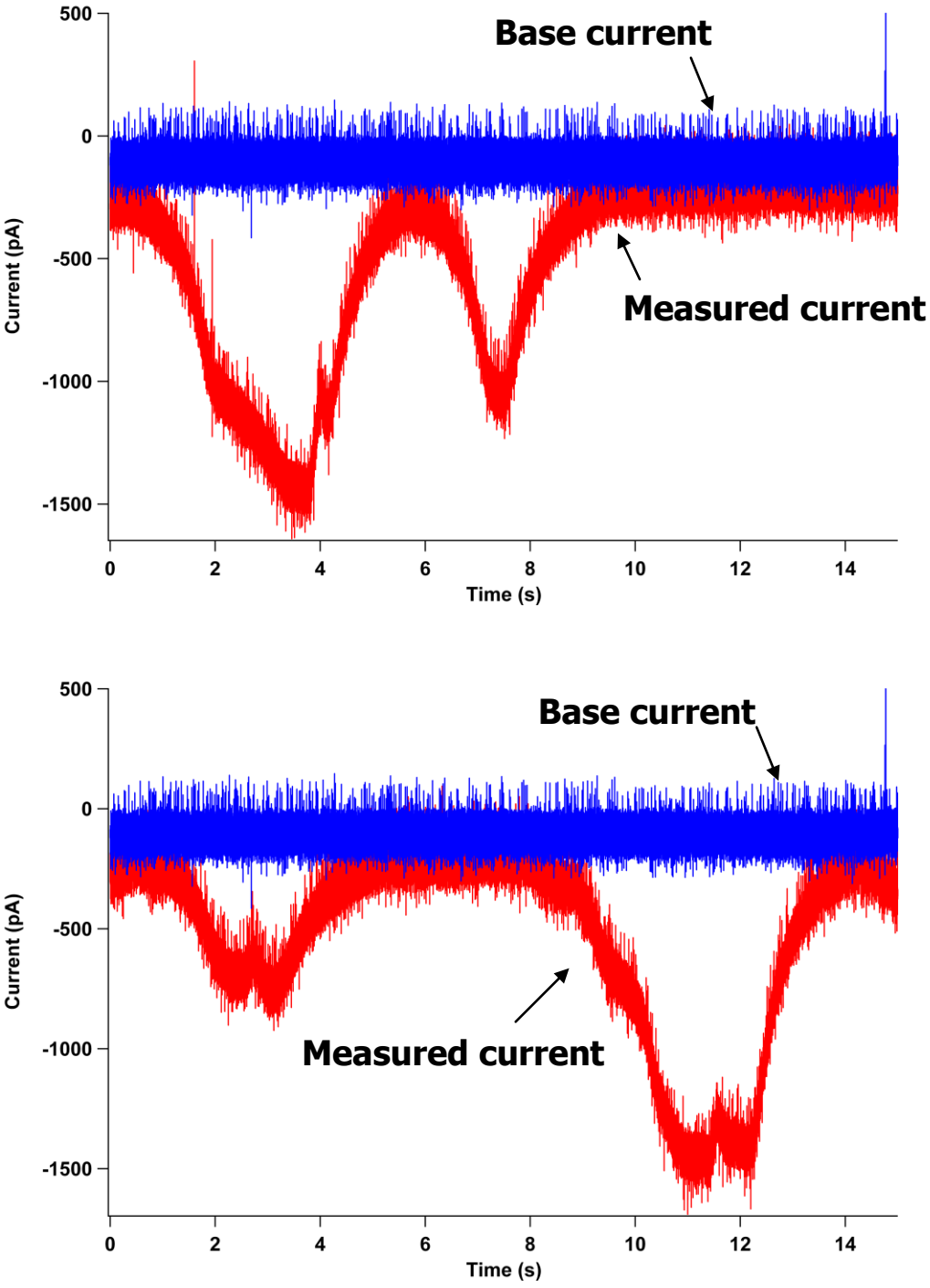

Figure 6.8 Current blockades observed as cells pass through the trapping aperture. The blue traces show the base current, which was offset to zero. The red traces show the current fluctuations as cells are pushed through the trapping channel.

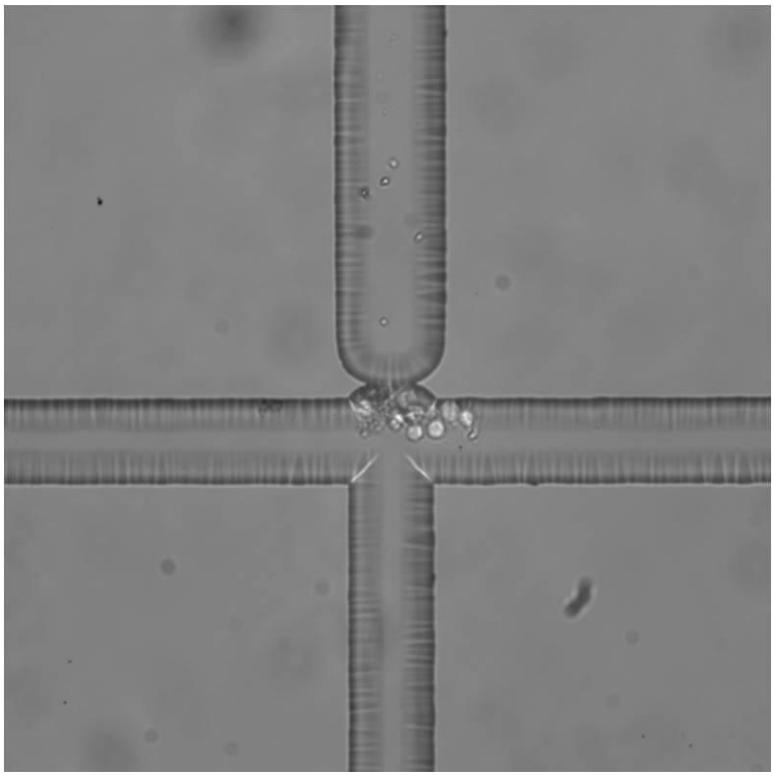

Figure 6.9 Image of debris buildup at the trapping site

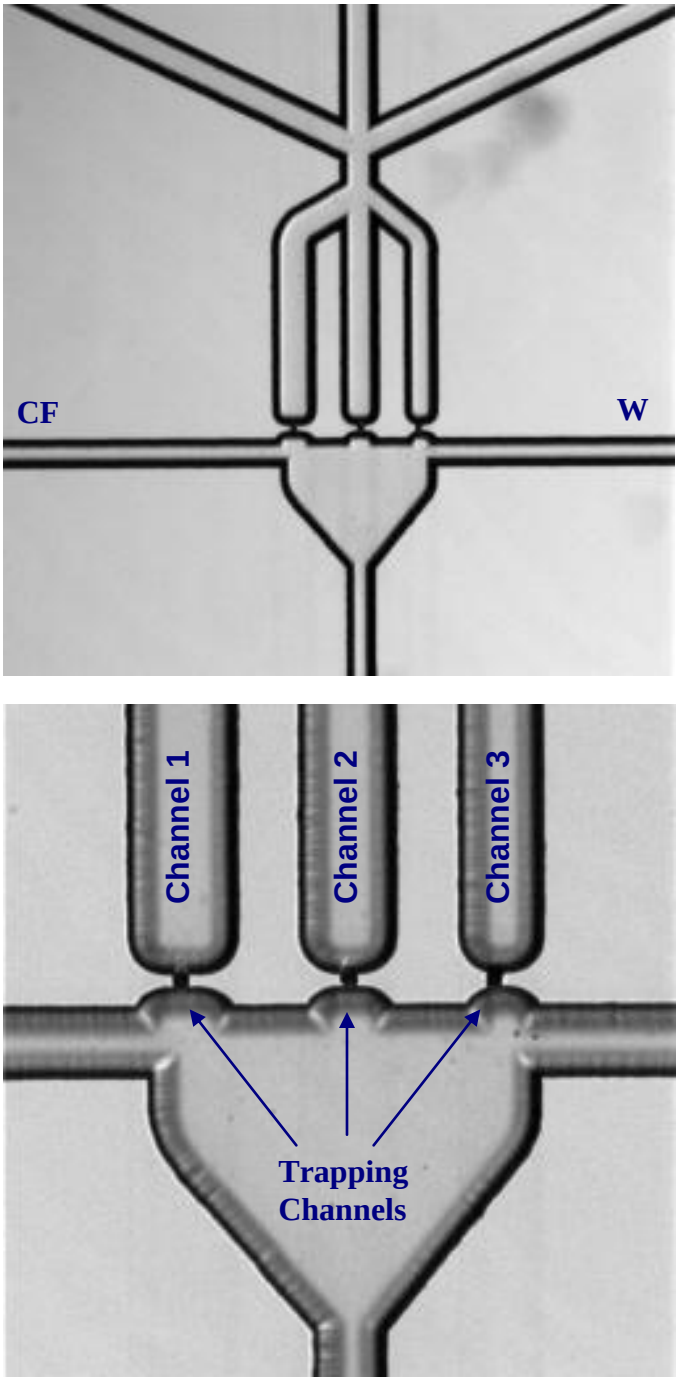

Figure 6.10 Images of a multi-trapping chip showing three FIB milled trapping channels

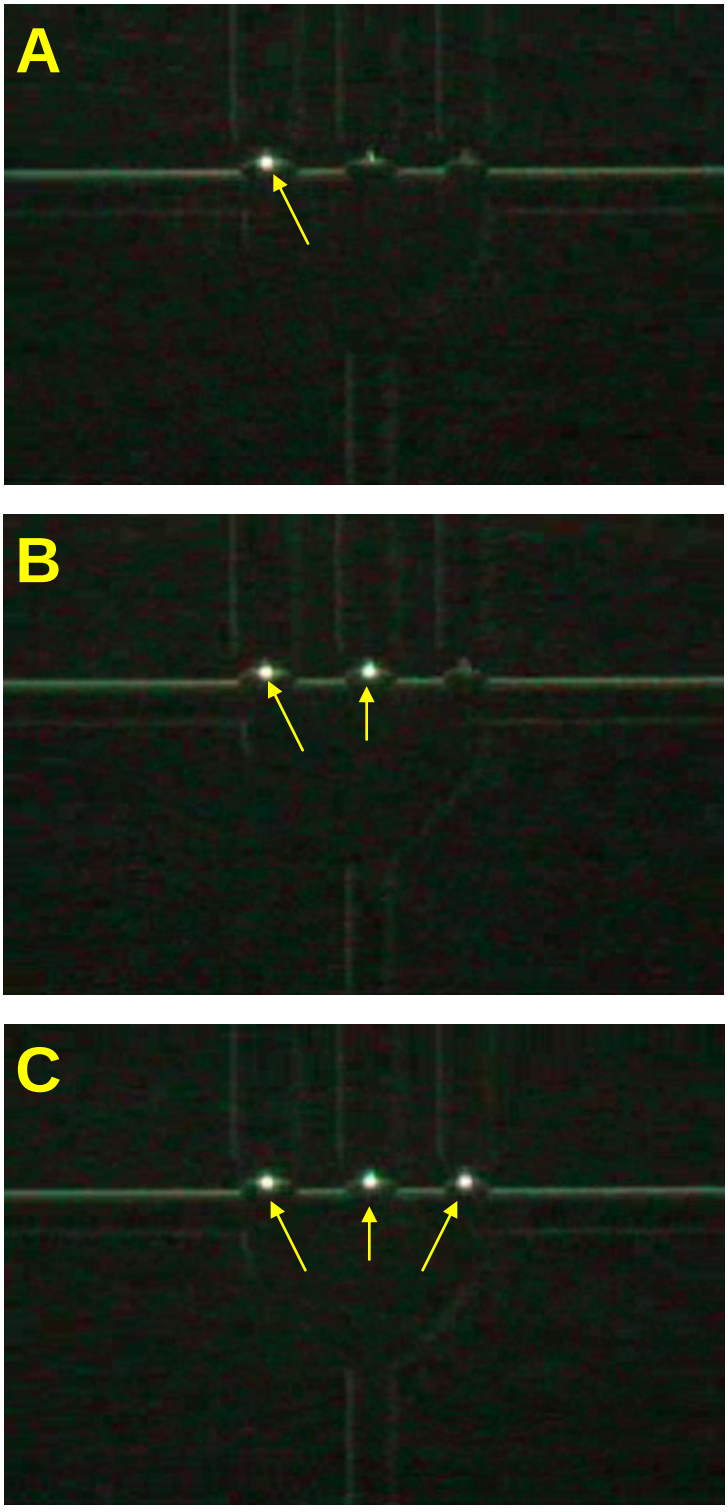

Figure 6.11 Image of sequential capture (A to C) of 10 μm fluorescent beads at the three trapping apertures on a multi-trapping device. The trapped beads are highlighted by the arrows.

6.6 References

(1) Johann, R. M. *Analytical and Bioanalytical Chemistry* **2006**, *385*, 408.

(2) Yang, M. S.; Li, C. W.; Yang, J. *Analytical Chemistry* **2002**, *74*, 3991.

(3) Rettig, J. R.; Folch, A. *Analytical Chemistry* **2005**, *77*, 5628.

(4) Yamaguchi, Y.; Arakawa, T.; Takeda, N.; Edagawa, Y.; Shoji, S. *Sensors and Actuators B-Chemical* **2009**, *136*, 555.

(5) Andersson, H.; van den Berg, A. *Current Opinion in Biotechnology* **2004**, *15*, 44.

(6) Huang, Y.; Ewalt, K. L.; Tirado, M.; Haigis, T. R.; Forster, A.; Ackley, D.; Heller, M. J.; O'Connell, J. P.; Krihak, M. *Analytical Chemistry* **2001**, *73*, 1549.

(7) Li, P. C. H. *Microfluidic lab-on-a-chip for chemical and biological analysis and discovery*; Taylor & Francis/CRC Press: Boca Raton, 2006.

(8) Sims, C. E.; Allbritton, N. L. *Lab on a Chip* **2007**, *7*, 423.

(9) Toriello, N. M.; Douglas, E. S.; Mathies, R. A. *Analytical Chemistry* **2005**, *77*, 6935.

(10) Voldman, J.; Gray, M. L.; Toner, M.; Schmidt, M. A. *Analytical Chemistry* **2002**, *74*, 3984.

(11) Fiedler, S.; Shirley, S. G.; Schnelle, T.; Fuhr, G. *Analytical Chemistry* **1998**, *70*, 1909.

(12) Wheeler, A. R.; Throndset, W. R.; Whelan, R. J.; Leach, A. M.; Zare, R. N.; Liao, Y. H.; Farrell, K.; Manger, I. D.; Daridon, A. *Analytical Chemistry* **2003**, *75*, 3581.

(13) Ros, A.; Hellmich, W.; Regtmeier, J.; Duong, T. T.; Anselmetti, D. *Electrophoresis* **2006**, *27*, 2651.

(14) Greif, D.; Galla, L.; Ros, A.; Anselmetti, D. *Journal of Chromatography A* **2008**, *1206*, 83.

(15) Munce, N. R.; Li, J. Z.; Herman, P. R.; Lilge, L. *Analytical Chemistry* **2004**, *76*, 4983.

(16) Chiu, D. T.; Lillard, S. J.; Scheller, R. H.; Zare, R. N.; Rodriguez-Cruz, S. E.; Williams, E. R.; Orwar, O.; Sandberg, M.; Lundqvist, J. A. *Science* **1998**, *279*, 1190.

(17) Chen, S. J.; Lillard, S. J. *Analytical Chemistry* **2001**, *73*, 111.

(18) Deutsch, M.; Deutsch, A.; Shirihai, O.; Hurevich, I.; Afrimzon, E.; Shafran, Y.; Zurgil, N. *Lab on a Chip* **2006**, *6*, 995.

(19) Li, P. C. H.; de Camprieu, L.; Cai, J.; Sangar, M. *Lab on a Chip* **2004**, *4*, 174.

(20) Di Carlo, D.; Aghdam, N.; Lee, L. P. *Analytical Chemistry* **2006**, *78*, 4925.

(21) Valero, A.; Merino, F.; Wolbers, F.; Luttge, R.; Vermes, I.; Andersson, H.; van den Berg, A. *Lab on a Chip* **2005**, *5*, 49.

(22) Werdich, A. A.; Lima, E. A.; Ivanov, B.; Ges, I.; Anderson, M. E.; Wikswo, J. P.; Baudenbacher, F. J. *Lab on a Chip* **2004**, *4*, 357.

(23) Borland, L. M.; Kottegoda, S.; Phillips, K. S.; Allbritton, N. L. *Annual Review of Analytical Chemistry* **2008**, *1*, 191.

(24) Li, X.; Huang, J.; Tibbits, G. F.; Li, P. C. H. *Electrophoresis* **2007**, *28*, 4723.

(25) Hellmich, W.; Pelargus, C.; Leffhalm, K.; Ros, A.; Anselmetti, D. *Electrophoresis* **2005**, *26*, 3689.

(26) Fertig, N.; Blick, R. H.; Behrends, J. C. *Biophysical Journal* **2002**, *82*, 3056.

(27) Matthews, B.; Judy, J. W. *Journal of Microelectromechanical Systems* **2006**, *15*, 214.

(28) Ionescu-Zanetti, C.; Shaw, R. M.; Seo, J. G.; Jan, Y. N.; Jan, L. Y.; Lee, L. P. *Proceedings of the National Academy of Sciences of the United States of America* **2005**, *102*, 9112.

(29) Pantoja, R.; Nagarah, J. M.; Starace, D. M.; Melosh, N. A.; Blunck, R.; Bezanilla, F.; Heath, J. R. *Biosensors & Bioelectronics* **2004**, *20*, 509.

(30) James, C. D.; Reuel, N.; Lee, E. S.; Davalos, R. V.; Mani, S. S.; Carroll-Portillo, A.; Rebeil, R.; Martino, A.; Apblett, C. A. *Biosensors & Bioelectronics* **2008**, *23*, 845.

(31) Sabounchi, P.; Ionescu-Zanetti, C.; Chen, R.; Karandikar, M.; Seo, J.; Lee, L. P. *Applied Physics Letters* **2006**, *88*.

(32) Seo, J.; Ionescu-Zanetti, C.; Diamond, J.; Lal, R.; Lee, L. P. *Applied Physics Letters* **2004**, *84*, 1973.

(33) Lee, P. J.; Hung, P. J.; Shaw, R.; Jan, L.; Lee, L. P. *Applied Physics Letters* **2005**, *86*.

(34) Culbertson, C. T.; Ramsey, R. S.; Ramsey, J. M. *Analytical Chemistry* **2000**, *72*, 2285.

(35) McKnight, T. E.; Culbertson, C. T.; Jacobson, S. C.; Ramsey, J. M. *Analytical Chemistry* **2001**, *73*, 4045.

Chapter 7： Conclusion and future work

7.1 Research and results summary

In this research, development of a device to perform high-throughput single cell analysis was performed. The main issues, noted in chapter 1, were addressed and improvements made to increase the throughput of the device. Evaluation of the flow through device found that biofouling was a significant issue when using the original coatings, lysate injection efficiency was not optimal because of the variable flow paths through the lysis intersection and the hydrodynamic flow of cells through the chip had the potential to affect the lysate injection.

The first issue, cellular adhesion and the collection of cellular debris at the lysis point, was a key obstacle to the long-term operation of the device. This biofouling affected chip operation and prevented the analysis of more than 20-30 cells at a time. It was found that the covalently bound surface coatings did not provide sufficient surface coverage to prevent cellular adhesion. Other additives and dynamic surface coatings also did not provide long term stability to prevent significant biofouling. The optimal method to prevent biofouling was to use a fetal bovine serum (FBS) channel pretreatment. Incubating the channels with FBS for a short time and also preparing the cells in FBS greatly reduced cellular adhesion and prevented significant cellular debris adhesion to the glass microchannels. The procedure for preparing microchannels with FBS was rapid, taking only 20-30 minutes to prepare a device for data collection. With other coatings tested, the preparation often required hours to days to prepare the chip channels. Using this channel pretreatment, consistent results were

obtained and the throughput was increased to hundreds of cells per operational run of the device.

Because of heat-induced gelation of the FBS proteins at high electric fields, it was necessary to redesign the chip to dilute the FBS prior to cell lysis. This was accomplished by the inclusion of a second focusing channel. The top focusing channel resistance was also decreased to keep the flow path of the cells toward the inlet of the analysis channel. This created a flow path through the lysis intersection that is known to be optimal for good lysate injection efficiency. The two focusing channels dilute the FBS so that high electric fields can be applied along the separation channel for cell lysis and rapid separation of cellular analytes. The flow of the FBS through the intersection along with the addition of surfactant to the focusing channel buffers prevented biofouling. On this device, >1000 cells were lysed and analyzed with no biofouling of the channel surfaces.

Separation conditions for several kinase substrate and product pairs were developed that provide rapid, baseline separation. The injection of some reporters was affected by the constant hydrodynamic flow that is necessary to transport the cells from the sample reservoir to the lysis intersection. In an attempt to eliminate the hydrodynamic flow, a chip was designed that isolates a single cell prior to analysis using a modified patch clamping method. Parallelization of the trapping sites was also demonstrated and has the potential to allow for high-throughput analysis on a single device.

7.2 Future work

There are several aspects of this project that still require development to achieve a fully functioning automated device for single cell kinase analysis. First, the loading of kinase substrates into the cells needs to be optimized. It was found that the stability of the kinase

reporter peptides is problematic. Additionally, because the Myr-ss-SPKC structure has both a polar and nonpolar end, it essentially acts as a surfactant at higher concentrations and causes break down of the cell membranes. Therefore, the overall viability of the cells after loading was often severely decreased from the initial level causing issues with collecting large data sets. The negative effect of the hydrodynamic flow on the injection of the sphingosine kinase substrate, shown in Chapter 5, also proved problematic for detection of the reporter from individual cells. With further evaluation and development of optimal enzyme reporters, high throughput kinase analysis can be achieved. Additionally, further development of the single cell trapping device is necessary to show that multiple cells can be analyzed on a single chip through parallelization of the trapping sites. Finally, development of online sample preparation capabilities is needed.

The ultimate goal of this device is to be completely automated from sample preparation to analysis. The devices discussed in this dissertation all require off-line sample preparation. Some initial work was performed to develop a cell loading station that could be easily incorporated onto the devices described. However, only a few prototype devices were fabricated. The cell loading design and function are shown in Figure 7.1. The basic concept is that a grating-type barrier is created, using FIB milling, to contain cells within a central chamber. Each of the 125 slats of the grating, shown in Figure 7.2, were milled using the same conditions previously described in Chapter 6 but to dimensions of ~1 μm (width) x 5 μm (height). The grating will retain the cells while simultaneously allow fluid flow over the cells. In this way, different solutions for cell loading and washing can be flushed through and the cells can be incubated for any given period of time. After loading, the cells can be washed by exchanging the buffer within the central chamber. The loaded cells can then be

pulled out of the chamber to the cell analysis component of the device. The design is such that either the flow through device or trapping device can be easily connected. Still frames from a video showing cells being loaded on a proof-of-concept device are shown in Figure 7.3.

7.3 Conclusion

In conclusion, a microfluidic device has been developed that can analyze hundreds to thousands of cells from a single sample. Collection of large single cell data sets on a microfluidic device has not previously been reported in the literature. The device developed here can be prepared rapidly for cell analysis and is designed such that essentially any separation channel coating and separation buffer can be employed for the optimal separation of the cell analytes.

7.4 Figures

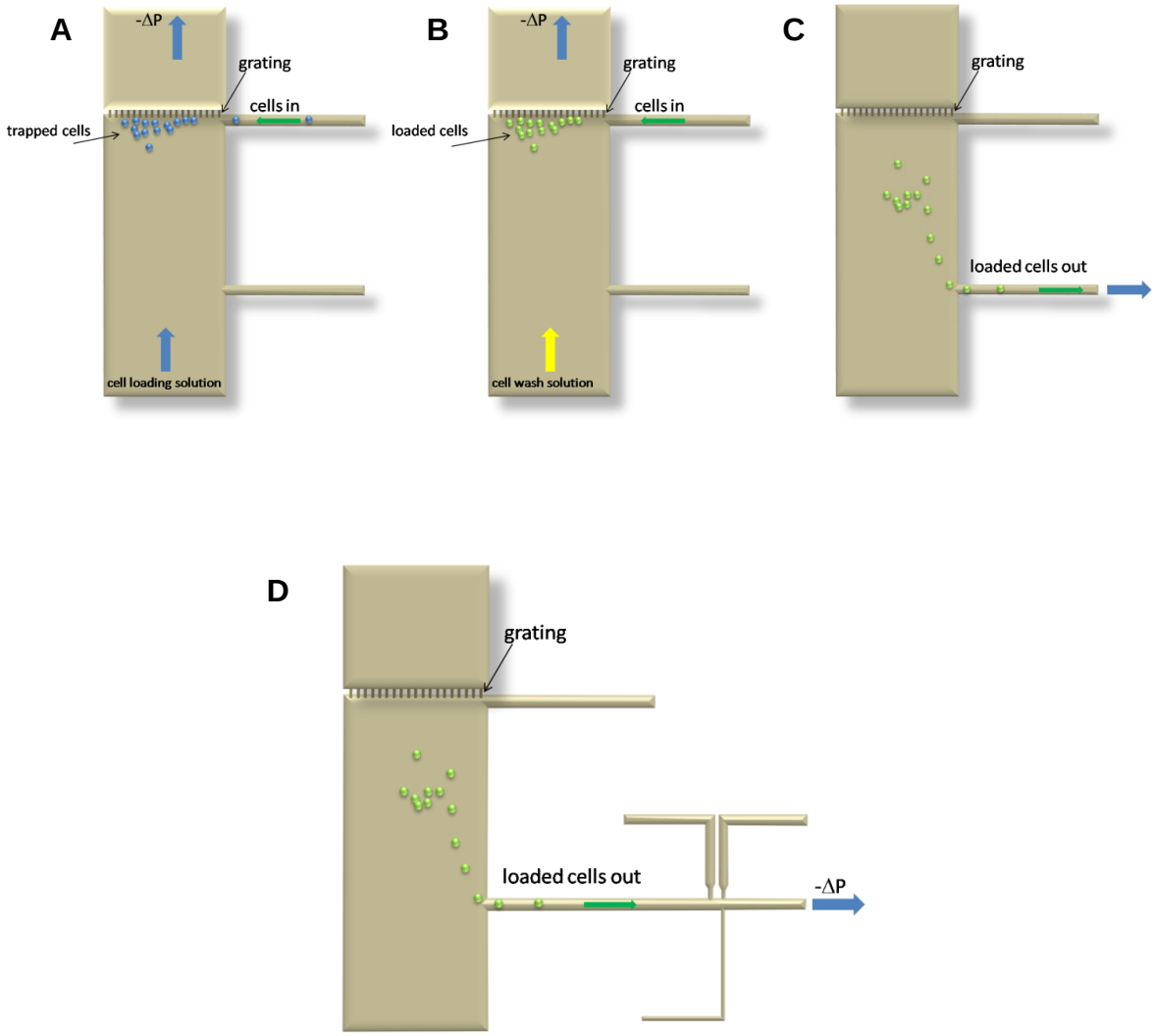

Figure 7.1 Concept for the cell loading station. Cells are pulled from a sample reservoir into the central chamber and retained at a grating (A). Vacuum is applied to the top channel to allow for a continuous flow of loading and wash solutions (B), from the bottom of the main channel, over the cells. After loading, the cells are pulled out of the chamber through application of vacuum to the outlet channel (C). In D, the integration of the cell loading concept with the flow through device is shown.

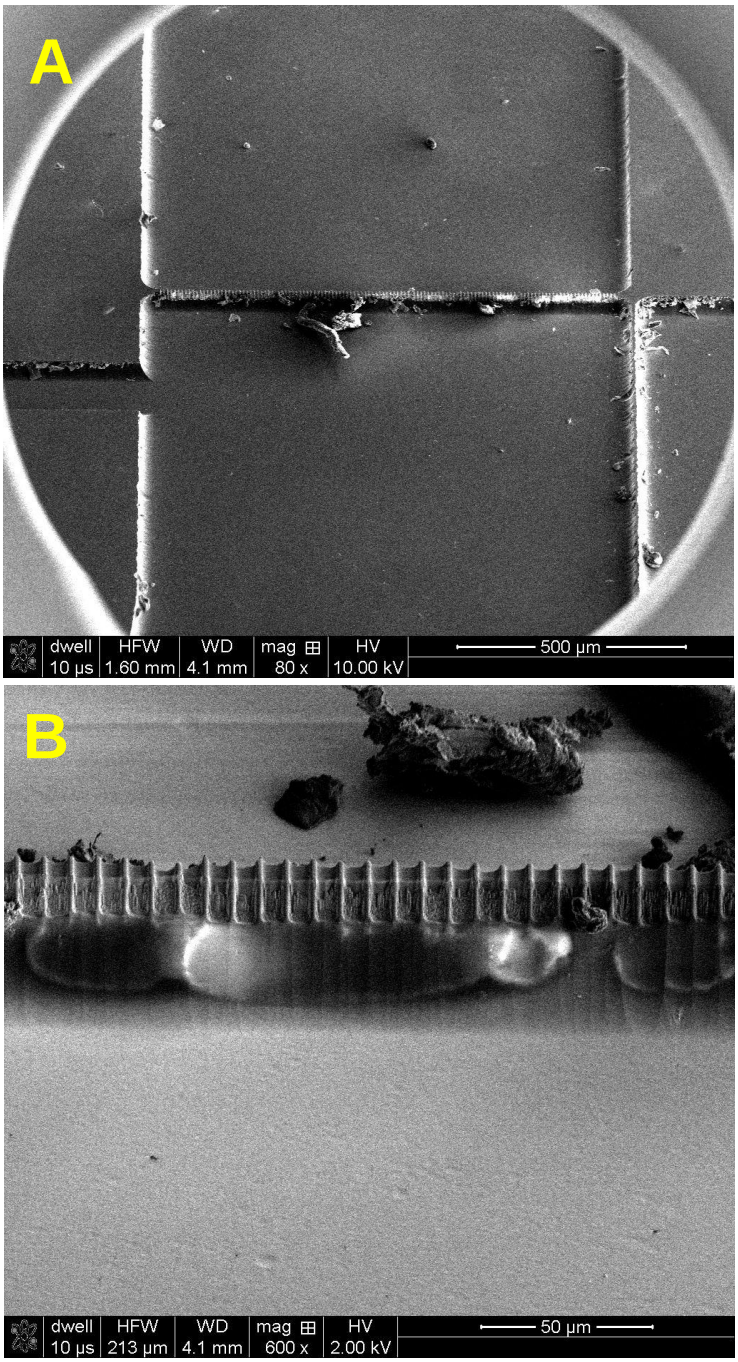

Figure 7.2 SEM images of the grating used to retain cells in the central chamber. The entire chip is shown in A. A zoom in of the FIB-milled retention grating is shown in B.

A) Oregon Green wash and incubation (~5 minutes):

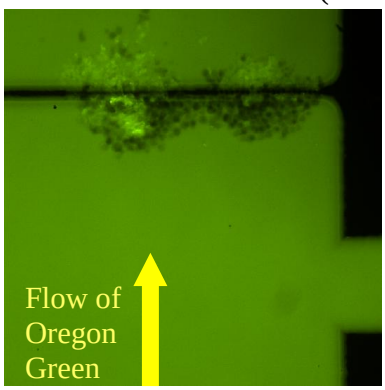

B) Extracellular buffer wash to remove Oregon Green:

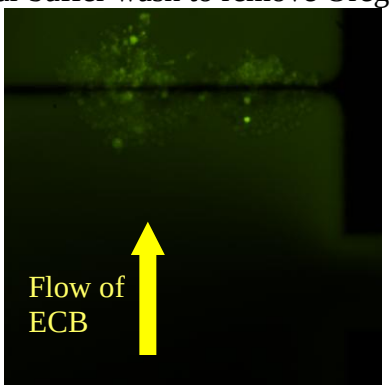

C) Final loaded and washed cells:

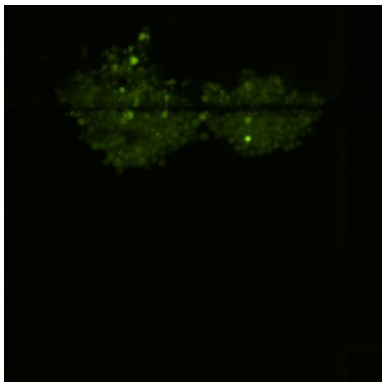

Figure 7.3 Still frame images of cells being loaded with Oregon Green. Cells are retained at the grating and in (A) Oregon Green is pulled across the cells. In (B), the bottom reservoir solution was exchanged for ECB to wash the cells. The final cells loaded with Oregon Green cytosolic dye are shown in (C).